**Title**
Repurposing renin angiotensin pathway inhibitors as disease modifying therapeutics for Parkinson's Disease



**Author**
Kim, Gha-hyun Jeffrey

**Publication Date**
2021

Peer reviewed|Thesis/dissertation

# Repurposing renin angiotensin pathway inhibitors as disease modifying therapeutics for Parkinson's Disease

by
Gha-hyun Kim

THESIS
Submitted in partial satisfaction of the requirements for degree of
DOCTOR OF PHILOSOPHY

in

Pharmaceutical Sciences and Pharmacogenomics

in the

GRADUATE DIVISION
of the
UNIVERSITY OF CALIFORNIA, SAN FRANCISCO

Approved:

DocuSigned by:
Su Guo
607F1205C317481...

Su Guo

Chair

DocuSigned by:
Marina Sirota
DocuSigned by:
Jason Gestwicki
4909848DBB404E5...

Marina Sirota

Jason Gestwicki

Committee Members

To Suk Jeong Kim, fighting against Parkinson's disease

# ACKNOWLEDGEMENTS

"There is still a lot to learn and there is always great stuff out there. Even mistakes can be wonderful." Robin Williams, who also struggled to combat Parkinson's disease, accurately portrayed my PhD journey and thesis work.

First and foremost, I want to thank Dr. Su Guo, my thesis advisor, mentor, and pharmacogenomics class professor. During the time when I was deciding on a lab to conduct my Pharmaceutical Sciences pathway project, Su was very inviting towards me joining the lab that allowed me to develop my PharmD thesis and transition into the PhD program. Without significant experience in molecular biology and neuroscience, Su was very patient and understanding as I have progressed through my experiments. Her mentorship style really ensured me to continue focused on my objectives while at the same time providing me the freedom to explore my interests. I also want to thank Su for providing the resource to necessitate my project and at times reaching out to others to help expand my project.

Next, Dr. Marina Sirota and Dr. Jason Gestwicki have been a substantial part of my thesis progression and development. The guidance of Marina really allowed me to take on the challenge of including clinical informatics work to my project. Jason's scientific curiosity and expertise has provided me with the guidance to progress and better my research. His expertise in screening assays and molecular interactions has helped Su and I to strategize and improve our

research aims. The fruitful discussions during the thesis committee meetings has helped me mentally to have confidence in the work that I was pursuing.

The UCSF PSPG Program emphasizes the importance of exploring different research through the rotation programs and I want to thank Dr. Peter Turnbaugh and Dr. Nadav Ahituv for providing me with new experiences throughout the 10-week rotations where I was able to dive into different fields of research all with the convergence of improving the human health. The PSPG program will be in such great hands with Nadav.

As my project required the collaboration of many expert scientists, I was fortunate to have worked with Dr. Michelle Arkin, Dr. Adam Renslo, Dr. Hao Li, Dr. Bo Huang, Dr. Jiashun Zheng, Dr. Fei Jiang, and Dr. Benjamin Tang. I also want to thank Dr. Deanna Kroetz for being such a wonderful program director of the PSPG program and also allowing me to get hands on experience on her project.

It has been a long journey since I joined the UCSF family and I have much to appreciate including Dr. Esteban Burchard, Dr. Leslie Floren, Dr. Marilyn Stebbins, and Dr. Jaekyu Shin, for the education and mentorship I have received during Pharmacy school and helping me with the transition into the PhD program.

The PhD journey was difficult at times, especially when I wasn't quite able to grasp the big picture or felt like my confidence was going down. For all these moments, I want to thank the

wonderful support from my PSPG family. It is such a wonderful group of close-knit friends that we could reach out to one another. Something I don't think many other schools or programs could offer. I am truly lucky to have this support system.

The Guo lab meetings are one of the most intellectually stimulating meetings that I am able to learn and contribute. I am grateful for all feedback and helpful discussions from the Guo Lab members throughout my time in the lab. It was a pleasure serving as the CFO (Chief Fun Officer). I also want to thank some of the incredible student collaborators and interns that helped throughout my research including Monica Han, Longping Peng, James Shortland, Daryl Nucum, Zachary Baldwin, and Sophie Shen. Their helping hands were greatly appreciated.

Finally, I want to thank my loving family Doman, Myungsuk, and Nahyun. Studying abroad alone imposes many challenges and I want to thank them throughout my education journey to become the scientist I am today. Can't wait to reunite with all of you once I can get on a plane ride.

# CONTRIBUTIONS

Some chapters in this dissertation contain material that is published or manuscripts currently in submission or preparation. Edits of the original manuscript have made accordingly for the preparation of the thesis including inclusion of unpublished data and modification for the purpose of formatting thus do not necessarily represent the final published/submitted form.

Chapter 1 of this dissertation is adapted from two manuscripts including 1) Harrison Liu, Steven Chen, Kevin Huang, Jeffrey Kim et al (2016) "A High-Content Larval Zebrafish Brain Imaging Method for Small Molecule Drug" *PLoS ONE* doi:10.1371/journal.pone.0164645 and 2) Jeffrey Kim, Han Mo, Harrison Liu, Steven Chen, Jiashun Zheng, Hao Li, Michelle Arkin, Bo Huang, Su Guo "In vivo small molecule screen of bioactive compounds with larval zebrafish identifies novel pathways against degeneration of dopamine neurons" currently in preparation for submission. S.G. and G.J.K. conceived the project. G.J.K., H.M., H.L., S.C. performed the experiments. G.J.K., H.M., S.C., H.L., J.Z., analyzed data. H.L., M.A., B.H., and S.G. provided resources, supervision, and funding acquisition. G.J.K. and S.G. wrote the paper with the contributions from all authors.

Chapter 2 of this dissertation is adapted from a current manuscript under review for publication Jeffrey Kim, Han Mo, Harrison Liu, Zhihao Wu, Steven Chen, Jiashun Zheng, Daryl Nucum, James Shortland, Longping Peng, Manuel Elepano, Benjamin Tang, Steven Olson, Nick Paras, Hao Li, Adam R. Renslo, Michelle Arkin, Bo Huang, Bingwei Lu, Marina Sirota, Su Guo (2021)

"A Zebrafish Screen Reveals Renin-Angiotensin System Inhibitors as Neuroprotective via Mitochondrial Restoration in Dopamine Neurons". G.J.K. and S.G. wrote the paper. S.G. and G.J.K. conceived the project. G.J.K., H.M., H.L., Z.W., L.P., S.C., J.S., M.E. performed the experiments. G.J.K., H.M., H.L., Z.W., S.C., J.Z., D.N., B.T., S.O., N.P. analyzed data. H.L., A.R.R., M.A., B.H., B.L., M.S., and S.G. provided resources, supervision, and funding acquisition.

Chapter 3 of this dissertation was modified from a manuscript in preparation: Jeffrey Kim, Adam Melgoza, Fei Jiang, Su Guo (2021) "The effect of renin-angiotensin-aldosterone system inhibitors on organ-specific *ace2* expression in zebrafish and its implications for COVID-19" S.G. and G.J.K. conceived the project. G.J.K. and A.M. performed the experiments. G.J.K. and F.J analyzed data. F.J. and S.G. provided resources, supervision, and funding acquisition. G.J.K. and S.G. wrote the paper with the contributions from all authors.

# Repurposing renin angiotensin pathway inhibitors as disease modifying therapeutics for Parkinson's Disease

Gha-hyun Jeffrey Kim

ABSTRACT

Parkinson's disease (PD), the second most common neurodgenerative disorder, affects millions of people worldwide. With movement-related disabilities and other cognitive impairment as well as psychiatric symptoms, PD not only greatly deteriorates the health and quality of life of patients, but also poses severe burdens on their families. The current drug therapies available for PD provide symptomatic relief but there is yet to be a therapy that can slow disease progression. Spanning across three chapters, the goal of this thesis project involves the notion of the bench-to-bedside approach of identifying promising drug candidates that could provide protective benefits in neurodegenerative disorders and understanding the mechanism behind the neuroprotective effects. Chapter 1 focuses on developing a whole organism based phenotypic screening assay using larval zebrafish and performing high throughput screening of 1403 bioactive compounds. While therapeutic drug discovery has traditionally focused on target-based drug discovery, the implementation of phenotypic drug discovery particularly for neurological diseases allows us to focus on the direct therapeutic impact and bypass the complex biological process of neurodegeneration and in many cases provide leads to novel targets. The transgenic model used in our assay expresses the E. coli nitroreductase (NTR) controlled by the promoter of tyrosine hydroxylase (th), a rate-limiting enzyme in DA synthesis. The NTR converts the pro-drug MTZ to the toxic nitroso radical form in vivo causing DA neuronal loss in the ventral forebrain region. 57 compounds passed the threshold for strictly standardized mean difference (SSMD) and brain

health score (BHS) when compared to the MTZ treatment alone. Pathways implicated in the pathophysiology of PD were shown significant including deubiquination, cyclooxygenase (COX), respiratory electron transport, and mitochondrial biogenesis. Novel pathways were also identified including sleep cycle, cell development, insulin regulation, and blood pressure regulation. In particular, aliskiren, captopril, and olmesartan, which all target the renin angiotensin pathway, showed significant neuroprotection and was validated in a blinded manual counting of DA neurons. In chapter 2, the neuroprotective mechanism of the renin angiotensin pathway was extensively studied by incorporating genetic engineering with conditional CRISPR, RNA-seq, and examining human clinical data. Using conditional CRISPR to knock out the angiotensin receptor type 1 (*agtr1*) in DA neurons, we revealed a cell-autonomous mechanism of neuroprotection through *agtr1* inhibition. DA neuron-specific RNA-seq further identified pathways including the mitochondrial electron transport chain that are significantly perturbed in DA neuron degeneration and is abated by RAAS inhibitor treatment. The neuroprotective effect of RAAS inhibitors was validated with brain imaging and functional analysis in a chemically induced zebrafish Gaucher's disease model and in a Drosophila PD model of *pink1* deficiency. Finally, examination of 308 clinical PD patient data revealed a significant effect of RAAS inhibitors in delaying the onset of levodopa therapy and increasing performance in symptom assessment scores. In the final chapter, the transcriptional modification of RAAS pathway genes were examined at the organ level upon the administration of RAAS inhibitors. This was in light during the recent COVID-19 pandemic in which we tried to address the knowledge gap of whether RAAS inhibitors might affect the expression levels of angiotensin-converting-enzyme-2 (*ace2*), which could impact patient susceptibility to SARS-CoV-2. Upon daily treatment with aliskiren, olmesartan, and captopril for 7 consecutive days, the qRT-PCR analysis of major

RAAS pathway genes in the brain, gill, heart, intestine, kidney, and liver showed organ specific changes in *ace2* expression and the discontinuation of compound treatments for 7 days did not return *ace2* expression to baseline levels. In conclusion, this dissertation work demonstrates the pipeline of accelerated drug discovery in the field of neurodegeneration from the initial drug screening to elucidating the underlying molecular mechanisms and the evaluation of clinical data. The work provided in this thesis hopes to potentially further the development on the therapeutic potential of RAAS inhibitors through the local signaling cascade that could impact diverse physiological functions aside from the classical cardiovascular system.

TABLE OF CONTENTS

# LIST OF FIGURES

# LIST OF TABLES

# LIST OF ABBREVIATIONS

5HT: 5-hydroxytryptamine

DA: Dopamine

HTN: Hypertension

MTZ: Metronidazole

NTR: Nitroreductase

PD: Parkinson’s disease

RAAS: Renin-Angiotensin-Aldosterone System

Tg: Transgenic

TH: Tyrosine hydroxylase

# CHAPTER 1: Identification of neuroprotective compounds with *in vivo* high throughput screening

## 1.1 Abstract

Parkinson's disease (PD) is the second most common neurodegenerative disorder that affects millions of people worldwide but the current therapies are still only limited to the temporary relief of symptoms. As an effort to discover disease-modifying therapeutics to combat the dopaminergic (DA) neuron degeneration, we have conducted a bioactive screen of 1403 bioactive small molecule compounds using an *in vivo* whole organism screening assay using transgenic Tg[fuguth:gal4-uas:GFP; uas-NTRmCherry] larval zebrafish. The transgenic model expresses nitroreductase (NTR) controlled by the tyrosine hydroxylase (th) promotor. The NTR converts the pro-drug MTZ to the toxic nitroso radical form to induce DA neuronal death. 57 compounds passed the threshold for strictly standardized mean difference (SSMD) and brain health score (BHS) when compared to the MTZ treatment alone. The high throughput screening (HTS) data was annotated with the pharmaceutical class, mechanism of action, indication, IC50, target, and the activity information for pathway analysis using the Reactome pathway database. Pathways implicated in the pathophysiology of PD were shown significant including deubiquination, cyclooxygenase (COX), respiratory electron transport, and mitochondrial biogenesis. Novel pathways were also identified including sleep cycle, cell development, insulin regulation, and blood pressure regulation. Non-topology based pathway analysis of the entire screening database additionally identified apoptosis, estrogen hormone, dipeptidyl-peptidase 4,

and opioid receptor Mu 1 to be significant pathways and targets. Leveraging the information obtained from SSMD, BHS, and pathway analysis, a total of 12 compounds were examined with a secondary assay that incorporates the embedding of larvae to take images before and after treatment, reducing the within-sample variability. The z' factor of the assay was determined to be 0.58 indicating an excellent assay. Etodolac, nepafenac, aloperine, protionamide, olmesartan, and captopril showed significant neuroprotection and was validated in a blinded manual counting of DA neurons. Ultimately, the HTS assay and pathway analysis provide a novel approach towards identifying hit-to-lead candidates and previously unknown pathways discovered in this study could provide insight into possible targets for future therapeutics.

## 1.2 Introduction

Neurodegenerative diseases are a major source of disability worldwide that is characterized by the progressive loss of neurons. Parkinson's Disease (PD) is particularly concerning as the prevalence is increasing rapidly without any disease modifying therapies. PD is the second most common disorder that affects more than 10 million people worldwide as of 2020 with an economic burden of $51.9 billion in the United States alone (Yang et al., 2020). While PD is characterized by the cardinal symptoms include bradykinesia, resting tremor, postural instability, and rigidity, many PD patients also experience comorbidities including cardiac disorders and increased infection rates that can significantly impede the quality of life and pose severe burdens on their families and caregivers (DeMaagd and Philip, 2015; Armstrong and Okun, 2020). While there are several therapy options for Parkinson's disease that work by enhancing the

dopaminergic action, decreasing metabolism of dopamine, or replacing the natural form of dopamine with exogenous drugs tailored for each patient, these therapies provide symptomatic relief only (Armstrong and Okun, 2020). Levodopa is considered the gold standard therapy but is associated with significant complications such as the "wearing off" effect, and levodopa induced dyskinesia. The surgical methods with deep brain stimulation has been established as a method for alleviating some of these motor complications and the possibility of neuroprotection in animal models, but the mechanism remains inconslusive (Koprich et al., 2017; Jakobs et al., 2020). In essence, there is an urgent need for identifying disease modifying therapeutics for PD.

While therapeutic drug discovery has traditionally focused on target-based drug discovery, the implementation of phenotypic drug discovery particularly for neurological diseases can impose significant advantages. As phenotypic assays focus on the direct therapeutic impact, it can bypass the need for a complete understanding of neurodegeneration and in many cases provide leads to novel targets (Liu et al., 2016; Moffat et al., 2017). By directly imaging brain and DA neurons which is the hallmark of PD, our phenotypic screen aims to overcome the current challenges in target-based drug discovery including the lack of effective drug discovery in the preclinical stages and difficulty in identifying good targets. Due to an incomplete understanding of the disease process and mechanisms, larval zebrafish impose significant advantages as it possess a high degree of genetic, physiological and morphological similarity with humans. Zebrafish share nearly 87% homology with the disease-associated human genome and the diencephalon region of the zebrafish brain is homologous to the substantia nigra pars compacta in humans which is the region of DA loss in PD patients (Du et al., 2016). The brain development occurs within 3 days post-fertilization (dpf), together with the central nervous system and during this time zebrafish larvae are released from the chorion which can

significantly reduce the amount of handling required thus chosen as our timepoint of drug treatment. In terms of sample preparation, zebrafish can produce large amounts of embryos on a weekly cycle, shows rapid development of organs within days, and is able to grow independently up to 7 dpf without feeding or handling. The transgenic model used in our assay expresses the E. coli nitroreductase (NTR) controlled by the promoter of tyrosine hydroxylase (th), a rate-limiting enzyme in DA synthesis. The NTR converts the pro-drug MTZ (a commonly used antibiotic) to the toxic nitroso radical form in vivo causing DA neuronal loss in the ventral forebrain region.

High-throughput screening (HTS) generates large amounts of data and there are many different approaches towards deciding which compounds to pursue forward. A widely accepted method of estimating the variability and effect size of the data is through the strictly standardized mean difference (SSMD) (Zhang et al., 2007). While using SSMD scores can capture data variability, simply selecting the highest scoring compounds may not be suffice because SSMD is based on the ratio of mean to standard deviation which could lead to high SSMD scores even with a small mean. In this study, we propose a combinatorial approach of using the standard threshold-based method, topology based analysis with the Reactome pathway database, and a non-topology based method of identifying significant pathways within the data obtained from the HTS.

## 1.3 Methods

### 1.3.1 Ethics Statement

The study was reviewed and approved by University of California, San Francisco Institutional Animal Care and Use Committee. The zebrafish system was regularly inspected by the University of California, San Francisco Laboratory Animal Resource Center.

### 1.3.2 Zebrafish husbandry and transgenic lines

For all experiments in the study, homozygous Transgenic Tg[fuguth:gal4-uas:GFP; uas-NTRmCherry] and AB wild type were used. Zebrafish were raised on a 14:10 hr light/dark cycle and maintained in the zebrafish facility according to the University of California San Francisco Institutional Animal Care and Use Committee standards. Embryos were raised in Blue Egg Water (2.4 g CaSO4, 4g IO Salt, 600 µl of 1% Methylene per 20L).

### 1.3.3 High throughput screening of 1403 bioactive compounds

For the *in vivo* high-throughput screening assay we utilized a bioactive compound library from SelleckChem obtained from the UCSF Small Molecule Discovery Center (SMDC). As many of these compounds are FDA approved or validated in preclinical research, the target profiles and pharmacodynamics have been established. The assay was performed on a weekly protocol (Figure 1.1) spanning from the initial collection of Tg[fuguth:gal4-uas:GFP; uas:NTRmCherry] embryos at day 0 and treatment with 200µM 1-phenyl 2-thiourea (PTU) on 1dpf to remove the pigment. On 3dpf, larvae were transferred to round bottom 96-well plates containing 10µM of

screening compounds dissolved in 16mg/100 mL tricaine methanesulfonate blue egg water and treated with 4.5 mM MTZ for 48 hrs. On 5dpf the larvae were imaged to capture the ventral forebrain dopamine (DA) neurons using the InCell 2000 (GE healthcare 28-9534-63) automated microscope with the TexasRed channel and bright field using a 4x 0.2NA objective (Nikon) using the built-in 2.5D deconvolution setting. A total of 5 different poses were acquired by reorienting the larvae with a liquid handler (Biomek FXp) that mixed 40 µL of the solution in each well to change the orientation.

The images were analyzed on a custom generated MATLAB script (Figure 1.2) that allows the manual selection of the best pose and the neurons are automatically extracted using the brightfield images with eyes as landmarks to automatically identify and extract the DA neurons. The analysis was based on a custom CellProfiler (McQuin et al., 2018) pipeline that processes and quantifies the fluorescent intensity and calculates the brain health score (BHS) based on the logarithm of the covariance between the brain image and a reference image generated from multiple healthy brains that was previously described (Liu et al., 2016). All the experiments were performed in a blinded manner from compound treatment to analysis.

### 1.3.4 Topology and non-topology based pathway analysis

The bioactive compound library data was annotated with the Hugo Gene Nomenclature Committee (HGNC) database (Tweedie et al., 2021) and the Therapeutics target database (Wang et al., 2020). For each compound, the pharmaceutical class, mechanism of action, indication, IC50, target, and the activity information was recorded (Figure 1.4). The SSMD and BHS scores were converted to align with the pharmacological activity (i.e. scores of compounds with inducer, agonist, or activators were inversed to match the activity profile of inhibitor or

antagonists). The Reactome pathway analysis was conducted by using the HGNC gene symbols as the identifier and the BHS as the numeric value. The non-topology based pathway analysis was conducted with the entire HTS data. The annotated targets were analyzed with a Wilcoxon ranksum test to determine whether there were significant targets or pathways that had a brain health score that was significantly higher than the average of the entire data set ($p<0.05$, FDR adj$<0.05$).

### 1.3.5 Secondary assay optimization and hit validation

The hit candidates selected from the pathway analysis underwent a secondary assay with greater sample size. The secondary assay was optimized by determining the shape of the well, agarose concentration, and volume of agarose required for embedding. The hit candidates were pretreated in 10μM concentration for 3 hrs prior to the administration of 9mM MTZ. The 5dpf before treatment images were taken on the InCell 6000 (GE healthcare) and subsequently taken again post 24hr incubation. The images were taken with an inverted 20x scope with dsRed and brightfield channels (0.45NA, 7.5 mm working distance). 3μm Z-slices for a total of 40 slices were obtained and the max intensity projection was processed with ImageJ. The BHS was calculated based on the aforementioned Cellprofiler pipeline. The ratio of BHS before treatment and BHS after treatment was used to quantify the neuroprotective effect. For the dose response studies, concentrations of the compounds were prepared from a series of fold dilutions. The candidate compounds were purchased from SelleckChem (NMDA: S7072, Sophocarpine: S2405, IWR Endo: S7086, Etodolac: S1328, Nepafenac: S1255, Aloperine: S2420, SGC-CBP30: S7256, NAC: S1623, AT9283: S1134, Protionamide: S1881, Olmesartan: S1604, Captopril: S2051, Mycophenolate Mofetil: S1501). The manual screening was performed in a blinded

manner by having a single investigator code the compounds and another investigator counting the medium and large DA neurons under the 20x fluorescence stereo microscope.

## 1.4 Results

### 1.4.1 *In vivo* high throughput screening assay identifies neuroprotective compounds

A total of 1403 bioactive compounds (SelleckChem) were screened at 10μM concentration that were obtained from the UCSF Small Molecule Discovery Center (SMDC). The dual flashlight plot was created to visualize the strictly standardized mean difference (SSMD) and the BHS (Figure 1.3). A total of 57 compounds had a BHS score that was significantly greater when compared to MTZ treatment alone (FDR adjusted $P<0.05$) (Table 1.1). 67% of the hit compounds identified were inhibitors while 14% were agonist or activators. The remaining compounds were synthetic hormones or glucocorticoids including prednisolone, budesonide, hexestrol, and mestranol. 4 compounds were natural products from plants including aloperine, matrine, and sesamin. The primary therapeutic class for the compounds consisted of 32% anti-cancer, 31% neurological, 15% infectious diseases, 12% cardiovascular, and 10% endocrinology drugs.

### 1.4.2 Pathway analysis shows mitochondrial and electron transport chain pathways while also identifying previously unknown pathways related to PD

The Reactome pathway analysis identified 24 significant pathways after correcting for false discoveries (Figure 1.5A) ($p<0.05$, FDR=0.01). With PD being highly related to mitochondria

dysfunction, pathways including deubiquination, cyclooxygenase (COX), respiratory electron transport, mitochondrial biogenesis were shown to be significant. Other pathways relevant to PD such as acetylcholine receptors, adrenergic signaling, mitogen activated protein kinase (MAPK) were shown to be significant. Cell cycle and development pathways were also significant including transcriptional regulation by AP-2, G2/M DNA replication checkpoint. Several pathways were previously unknown or under-studied in the context of PD including RAR Related Orphan Receptor (RORA) gene activation, circadian clock, ovarian tumor proteases, PPARα, renin angiotensin system, and insulin regulation. The non-topology based pathway analysis with the Wilcoxon rank-sum test of the entire dataset showed 15 targets and pathways to be significant ($P<0.05$, FDR=0.05) (Figure 1.5B). Apoptosis, estrogen hormone, dipeptidyl-peptidase 4, and opioid receptor Mu 1 were significant in the Wilcoxon rank-sum test but not in the Reactome analysis. A total of 83 compounds were shown to be significant in both the Reactome and Wilcoxon rank-sum test (Table 1.2). 32 compounds were already FDA approved and 20 compounds were in early phase clinical trials. The remaining 31 compounds were in pre-clinical development.

### 1.4.3 Development of secondary assay for hit validation

To validate the hit compounds from the primary screen and pathway analysis results, a medium throughput secondary assay was developed that incorporates larger sample size, higher resolution, and statistical effect size. 5dpf larvae were embedded in 1.2% agarose and imaged before the chemical treatment and 24 hrs after the treatment using the same x,y,z coordinates (Figure 1.6A). The image analysis was conducted by determining the ratio of “after treatment BHS” to “before treatment BHS”. Since the embedding did not necessitate the use of the

multipose from the initial screen, a flat bottom 96 well plate (Griener cat no 655096) was used to provide greater efficiency in embedding and better tracking of well coordinates and resolution. The 40 µl agarose was chosen as it showed a significant difference between the positive control (0.2% DMSO) and negative control (9mM MTZ) without harming or inducing stress of the larvae during the 24 hr incubation period (Figure 1.6B). The calculated z' factor of the secondary assay was 0.58 which is considered an excellent assay with less within-group variation (Figure 1.7A, Supplemental Figure 1.1).

### 1.4.4 Secondary hit validation identifies non-steroidal anti-inflammatory drugs, renin angiotensin system, aloperine, and protionamide to be neuroprotective

Utilizing the secondary hit validation assay, a total of 12 candidate compounds were tested for neuroprotection based on significant pathways, BHS, and SSMD scores. Additionally, NAC (N-Acetyl Cysteine) was used as a reference compound based on previous studies showing significant neuroprotection in other DA models. After treatment with 9mM of MTZ for 48 hrs and comparing the BHS of the before and after images, 10 µM etodolac, nepafenac, aloperine, NAC, protionamide, olmesartan, and captopril showed significant neuroprotection (Figure 1.7B). These compounds were then manually validated in a single blinded design by counting the medium to high intensity dopamine neurons after 24 hrs of MTZ treatment. All compounds except for nepafenac were shown to be significant when comparing to the control ($P<0.05$) (Figure 1.7C). A dose response study of nepafenac showed lower doses (0.04 µM and 2.0 µM) to be neuroprotective (Supplemental Figure 1.2). Drugs that were found to be significantly neuroprotective were then administered in combination to determine the possible drug pairs that could provide additive or synergistic effects on neuroprotection. The combination of etodolac-

nepafenac, etodolac-protionamide, and etodolac-aloperine showed a greater BHS compared to the administration of either compound alone (Figure 1.7D).

### 1.4.5 Statistical Analysis

The SSMD and BHS data from high throughput screening studies were analyzed by unpaired t-test using the R program and expressed as means ± SEM unless otherwise stated. The pathway analysis with Reactome was conducted with an over-representation (hypergeometric) test. The non-topology based pathway analysis was tested with the Wilcoxon rank-sum test to identify significant targets from the entire screen. All the secondary hit validations were conducted with an unpaired t-test between the sample and negative control (MTZ treatment).

## 1.5 Discussion

By developing a whole organism screening assay that can directly image the DA neurons of larval zebrafish at a high throughput scale, we have established a new method of identifying compounds that can protect against dopamine degeneration. The secondary hit validation assay that utilizes the embedding technique to image the before and after treatment images showed an excellent z' factor score. Using a threshold or certain percentage cutoff for high throughput screens may not always translate to success in secondary analysis. This could be attributed to batch or plate effects, systematic errors such as liquid handling, or incubation time differences. While normalization efforts and quality control systems are put into effect, the nature of our assay involved larval zebrafish which could result in larvae-to-larvae reporter expression differences or differences in image quality due to incorrect poses. Thus by utilizing not only the

SSMD and brain health score cutoff, but also employing pathway analysis we were able to narrow the amount of hit compounds tested with the secondary screen to a manageable number. For example, dimesna, SB590885, or teniposide during the initial screen was shown to be significantly different in DA neuron intensity compared to MTZ alone. However, they were not significant in the pathway analysis with Reactome and the Wilcoxon test, so priority was given to test other compounds.

The pathway analysis revealed mitochondrial dysfunction and respiratory transport chain pathways which are known to be closely tied to the etiology of PD (Park et al., 2018) and strengthens our small molecular screening assay for DA neurodegeneration to have relevance to PD. Etodolac and nepafenac identified in the screen are known as COX-2 selective inhibitors which have been previously been studied as potential PD therapeutics with its anti-inflammatory properties. Particularly COX-2 is known to be involved in microglia activation, production of radicals, and has shown to protect against DA neuron loss in 6OHDA rat models (Sánchez-Pernaute et al., 2004; Bartels and Leenders, 2010).

Pathways that are novel to PD could provide new insight to therapeutics. Several genes and pathways relating to the circadian rhythm were significant from the Reactome pathway including the BMAL1:CLOCK:NPAS2 circadian gene expression. Sleep disturbances is a common nonmotor complaint in PD but the etiology is not well understood (Breen et al., 2014). The circadian clock gene BMAL1 is important in sleep control and leukocytes of PD patients have shown to have altered expression that also correlates with PD severity (Cai et al., 2010). Furthermore, mice studies have shown that cholinergic neurons of the basal forebrain are more active in Bmal1 muscle-overexpressed mice(Ehlen et al., 2017). Insulin regulation and glucose control was also significant in the pathway analysis. It is known that hyperglycemia increases the

production of reactive oxygen species from the mitochondrial electron transport chain and type 2 diabetes is associated with an increased risk of Parkinson's disease (Hu et al., 2007).

The natural product aloperine showed strong neuroprotective effects from both the initial screen and subsequent validations. Aloperine is a quinolizidine-type alkaloid that is known to have antioxidant properties through suppression of NF-κB signaling(Xu et al., 2014), the activation of nuclear factor erythroid-related factor 2 (Song et al., 2018), and showed to inhibit apoptosis in amyloid induced mouse cells in a mitochondria dependent pathway (Zhao et al., 2018). The potential of natural compounds and its secondary metabolites are increasing interest in neurodegeneration but further establishment of pharmacokinetic and pharmacodynamic are needed (Sharifi-Rad et al., 2020).

The initial screen had a relatively low sample size of n=3 which could have led to variability and potential false errors. However, this was mitigated by calculating the SSMD score and evaluating not only single compounds, but a group of compounds based on pharmacological targets for pathway analysis. Furthermore, the secondary validation was conducted with greater sample size along with a confirmation with a blinded manual screen. As the assay is based on a chemical induced damage of the inactive metronidazole being converted to the toxic nitroso radical form, it is also possible that the compounds could be inhibitors of nitroreductase. However, none of the hit compounds selected are shown to have evidence of NTR inhibition. Further validation of the hit compounds with other DA degeneration models would be useful.

## 1.6 Figures

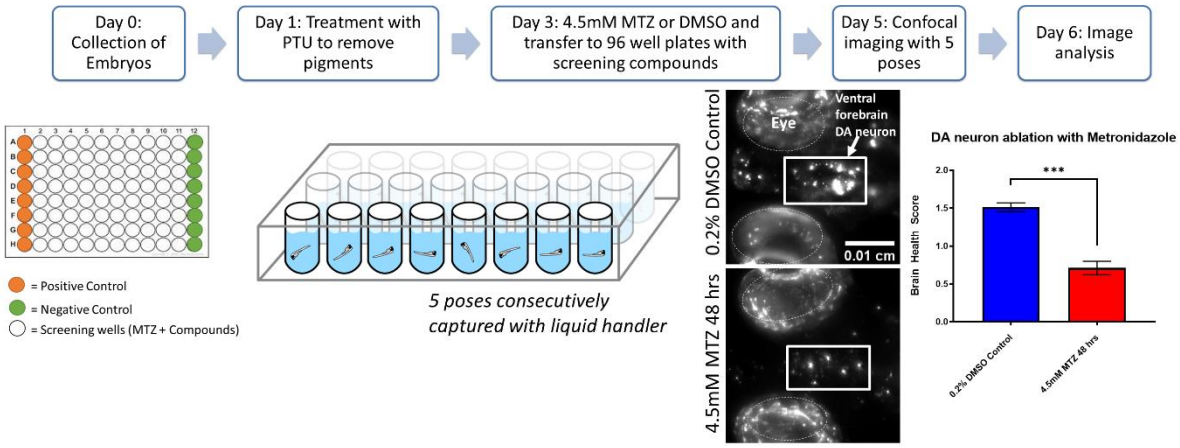


**Figure 1.1 Overview of the in vivo high throughput screening assay with larval zebrafish.** 3dpf larvae are transferred to 96 well plates with 10μM screening compounds. DMSO (positive control) or 4.5mM MTZ (negative control) was treated for 24hrs and the ventral forebrain DA neurons of larvae were imaged with brightfield and TexRed channels. Images were analyzed with a custom generated Cellprofiler pipeline. The robust z' factor of the assay was determined to be 0.58 (n=48 for each group; $p<0.001$, unpaired t test).

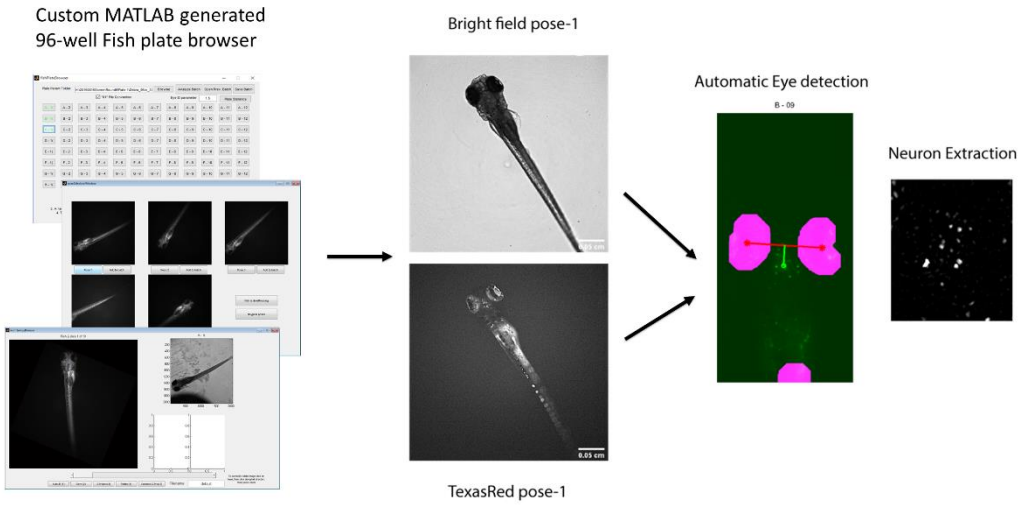


**Figure 1.2 Schematic of the image processing conducted with the custom generated MATLAB "fishplatebrowser" and Cellprofiler.** The custom MATLAB program was used to identify the best pose of the zebrafish to be used for analysis. The brightfield and TexRed images were used to automatically detect the eye and diencephalon region of the brain to quantify DA neurons with the Cellprofiler program.

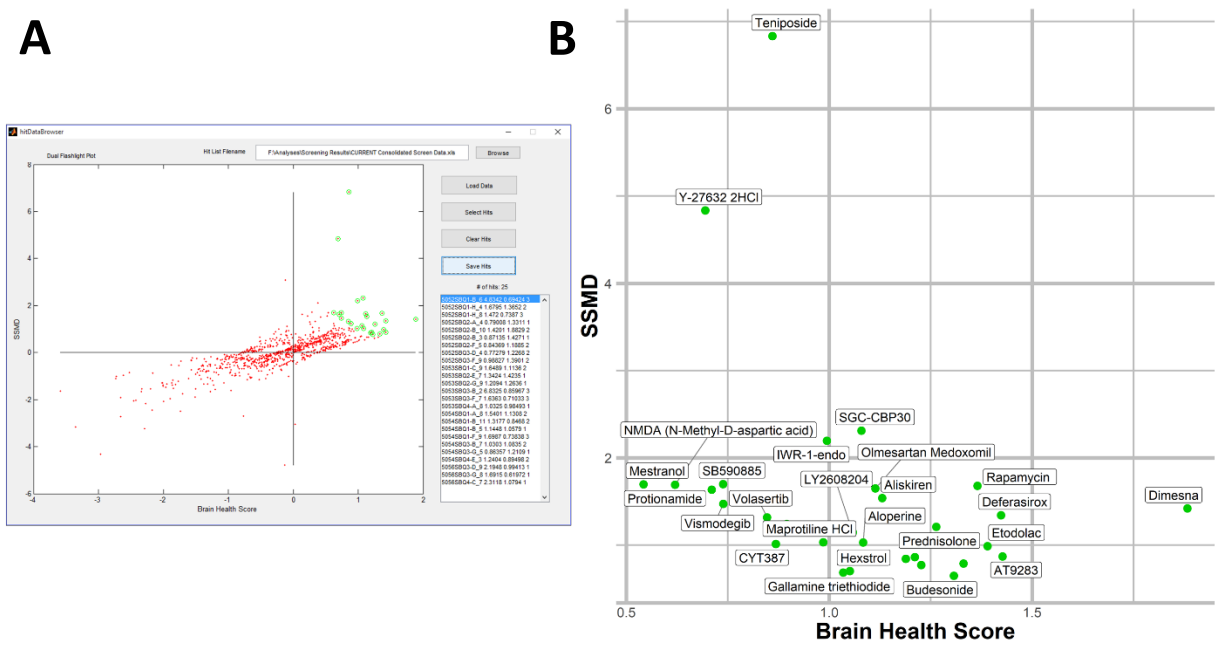


**Figure 1.3 Identification of top hit candidates with high brain health score and SSMD. (A)** Dual flashight plot generated from custom made GUI "HitDataBrowser" with MATLAB. Compounds can be selected and exported with SSMD, BHS, and corresponding sample number. **(B)** First quadrant compounds showing the highest BHS and SSMD scores based on manual selection. Details of the compounds are shown in table 1.

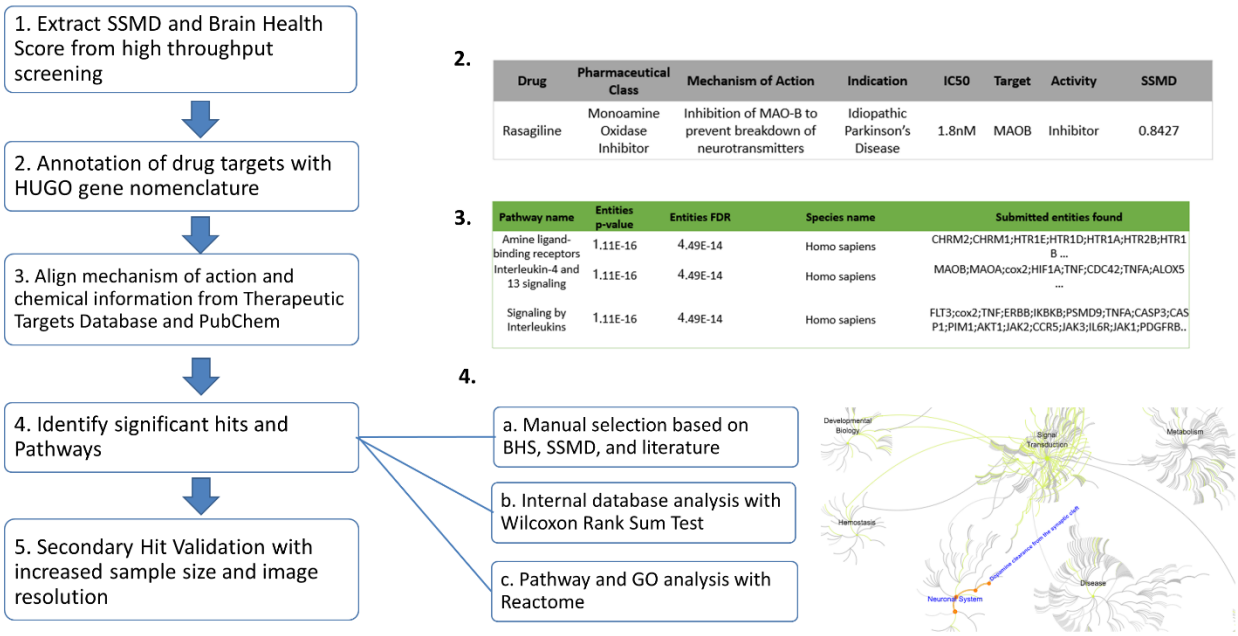


**Figure 1.4 Pathway analysis pipeline for the high throughput screening data.** Pipeline of processing the screening data and conducting pathway analysis. The example output of the annotations are shown on the right side with the corresponding numbers of each step. Deciding the significant hits were based on three categories including manual selection with good BHS and SSMD score, Wilcoxon rank sum test, and Reactome pathway analysis.

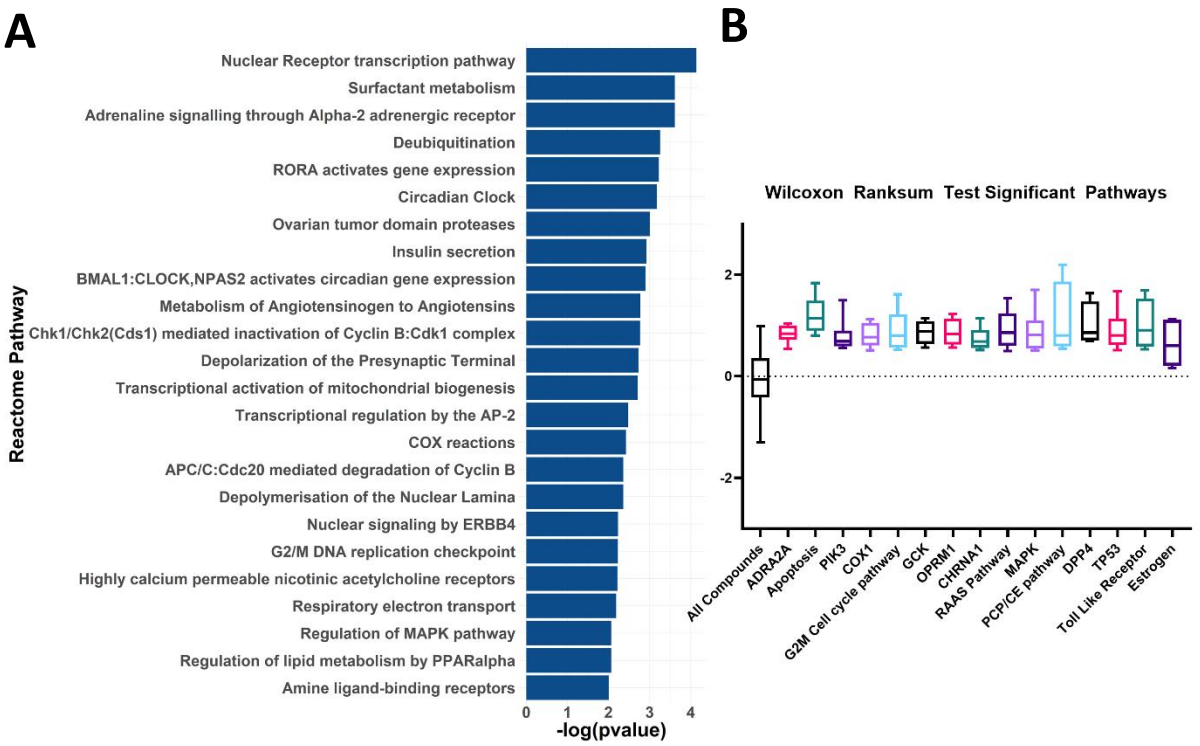


**Figure 1.5 Pathway analysis of high throughput screening data identifies novel mechanisms of neuroprotection. (A)** List of significant pathway sorted from highest to lowest significance (Padj <0.01). **(B)** Significant pathways from the Non-topology based pathway analysis of the entire high throughput screening database. The BHS of the drug targets were compared against the BHS distribution of all the compounds in the first column. (n=5 to 13; Padj <0.05, Wilcoxon rank sum test). ADRA2A: Alpha-2A adrenergic receptor, PIK3: Phosphoinositide 3-kinase, COX1: Cytochrome c oxidase subunit I, OPRM1: Mu type opioid receptor, CHRNA1: Cholinergic Receptor Nicotinic Alpha 1 Subunit, RAAS: Renin angiotensin system, MAPK: Mitogen-activated protein kinase, PCP/CE: Planar cell polarity and convergent extension, DPP4: Dipeptidyl peptidase-4, TP53: Tumor protein P53

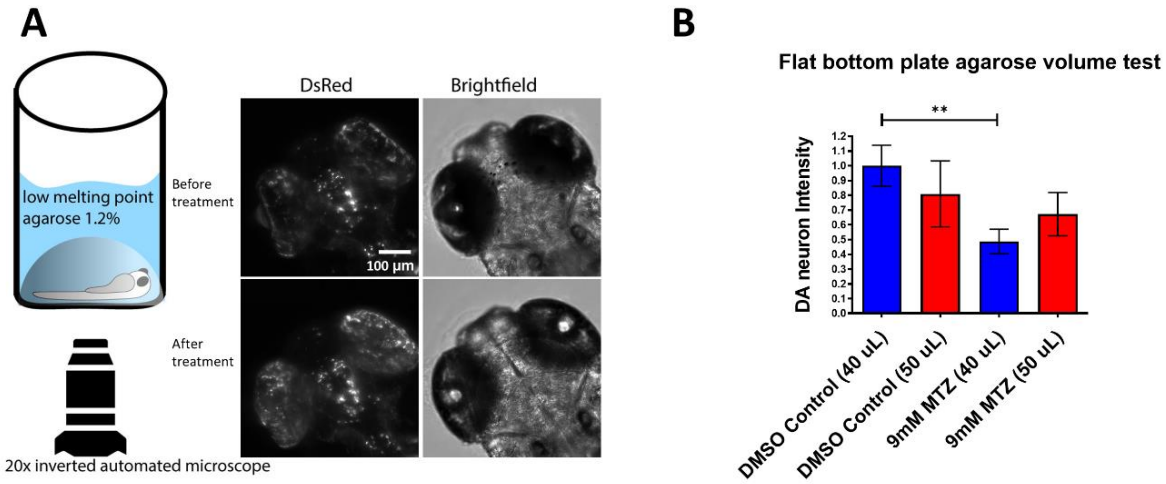


**Figure 1.6 Development of a robust medium throughput assay for secondary hit validation of pathway analysis candidates. (A)** Schematic of the secondary hit validation assay using automated imaging. At 5dpf, larvae were embedded in 1.2% agarose and imaged under brightfield and DsRed channel. The larvae were treated with 0.2% DMSO or 9mM MTZ with or without the hit compounds. At 6dpf, larvae were again imaged with the same x,y,z coordinates. Image shown is an example of a 0.2% DMSO control. **(B)** Comparison of 40 µl and 50 µl low melting point agarose 1.2% for embedding. 40 *µl* agarose showed significant difference in between DMSO control and 9mM MTZ (n=8; $P<0.05$, unpaired t test).

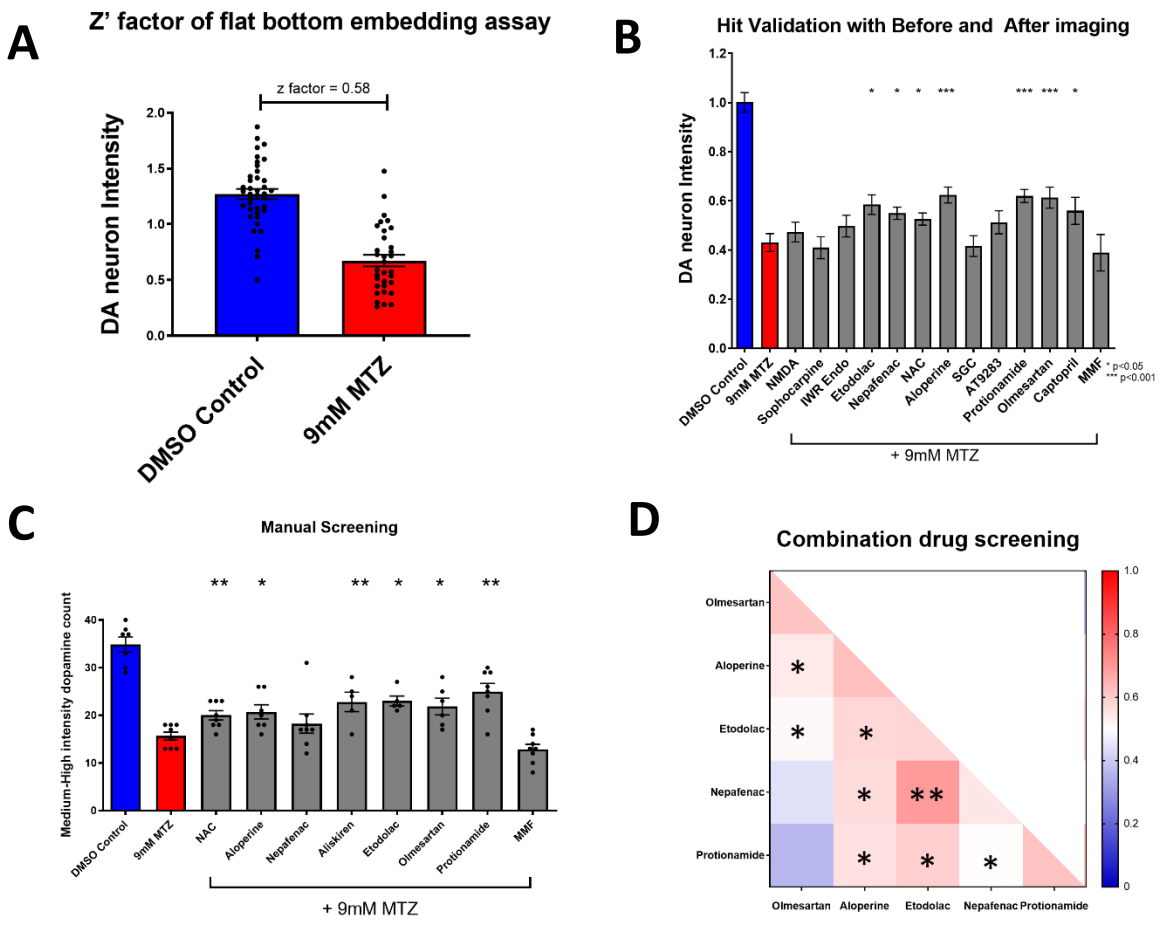


**Figure 1.7 Secondary hit validation with before and after treatment images and manual validation. (A)** Evaluation of the Z'-factor for the secondary hit validation assay. The 0.2% DMSO control and 24 hrs of 9mM MTZ treatment showed a significant difference in DA neuron intensity with a z'factor of 0.58. **(B)** Secondary hit validation of compounds with the embedding assay. 10µM of the candidate compounds were treated with 9mM MTZ for 24 hours. Etodolac, nepafenac, NAC, aloperine, Protionamide, Olmesartan, and Captopril showed significantly greater "BHS After treatment" to "BHS before treatment" ratio compared to the negative control (9mM MTZ) (n=22 to 30; *P<0.05, ***P<0.001, unpaired t test). **(C)** Manual screening of the significant compounds identified from the secondary hit validation assay. All compounds were treated and examined after 24hrs. (n=7 to 8; *P<0.05, **P<0.01, unpaired t-test). **(D)** Heatmap matrix showing the BHS for the testing of administering two hit compounds in combination. All candidate compounds were 10µM in concentration. The combination of etodolac-nepafenac, etodolac-protionamide, and etodolac-aloperine showed greater BHS compared to the administration of either alone. 0.2% DMSO for positive control and 9mM MTZ for negative control. (n=12 to 16; *P<0.05, **P<0.01, unpaired t test).

# Supplemental Figures

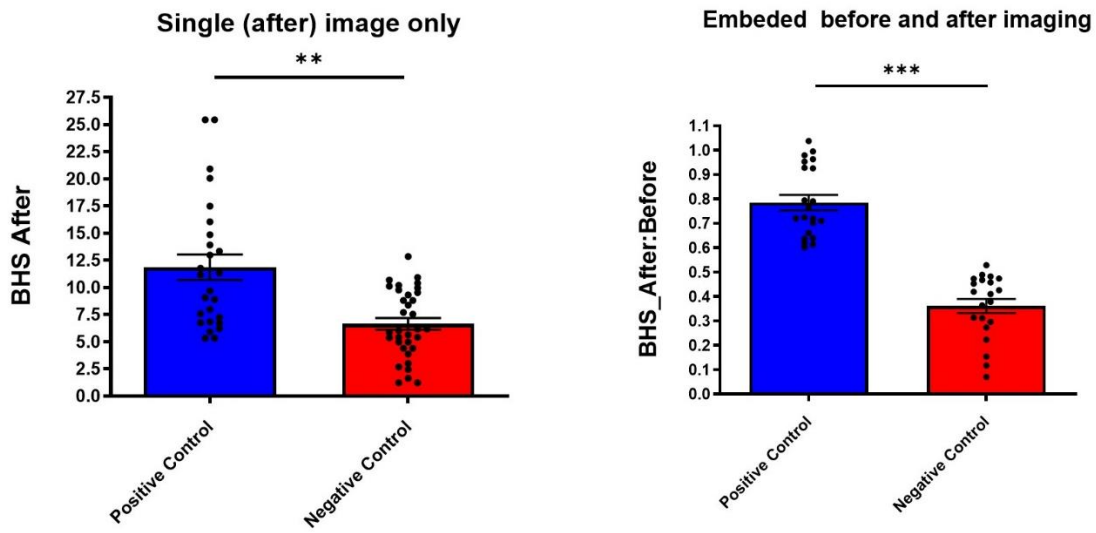


**Supplemental Figure 1.1 Medium throughput assay with agarose embedding and taking before/after images significantly decreases sample variability.** Transgenic Tg[fuguth:gal4-uas:GFP; uas:NTRmCherry] 5dpf larvae were treated with 0.2% DMSO (positive control) or 9mM MTZ (negative control) for 24 hrs. The left graph indicates the BHS of the after image only. The right graph is the BHS ratio between the before and after treatment images. (n=16; *P<0.05, **P<0.01, unpaired t test)

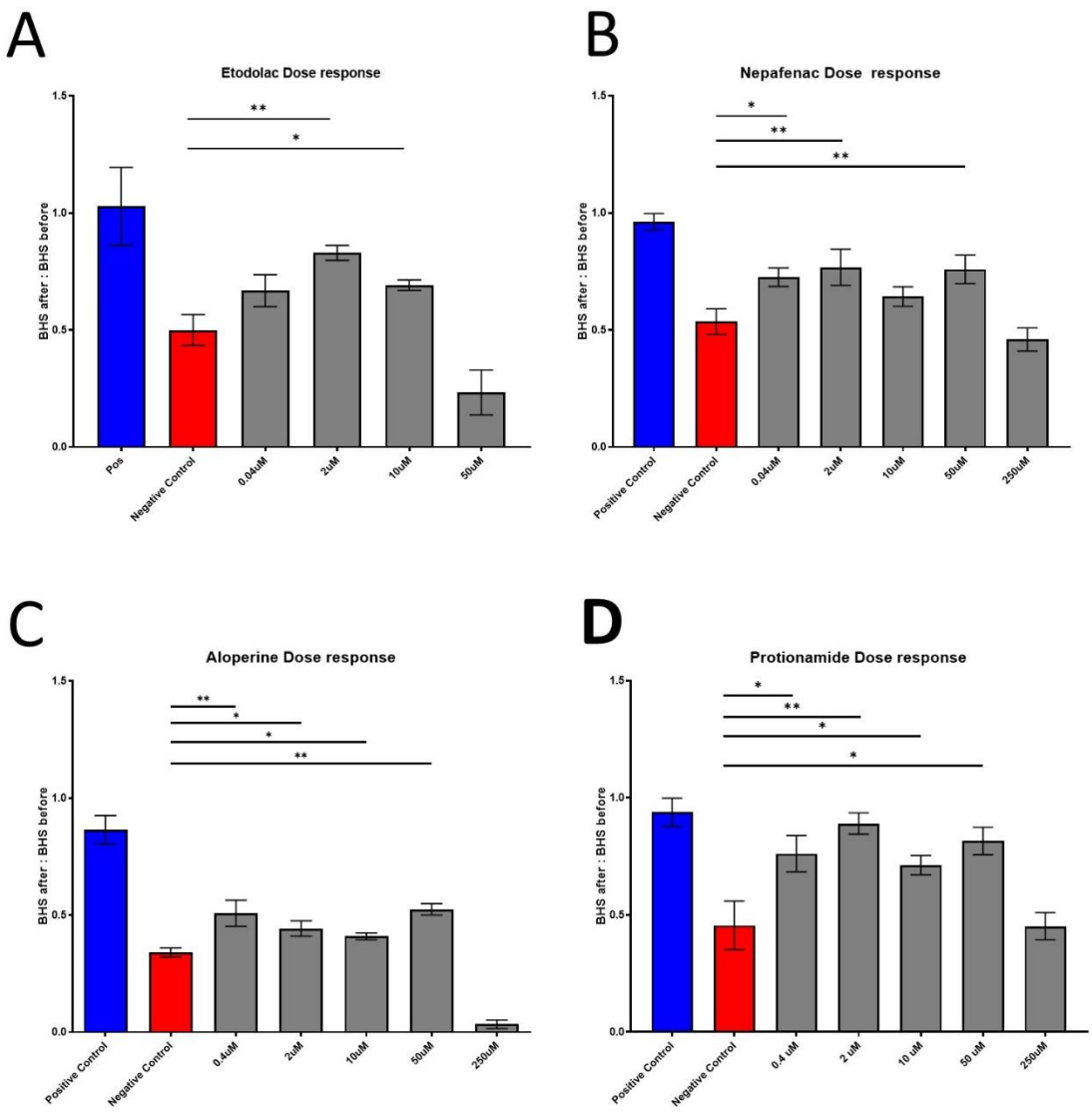


**Supplemental Figure 1.2. Dose response curve of hit candidates using medium throughput assay. (A-D)** The hits candidates that showed significant in the secondary hit validation were tested with serial fold dilutions for dose response **(A)** Etodolac, **(B)** Nepafenac, **(C)** Aloperine, **(D)** Protionamide. 9mM of MTZ was administered with the compounds for 24hrs at 5dpf. For 250nM of aloperine, larvae showed lethality. (n=10 to 12; *P<0.05, **P<0.01, unpaired t test)

# 1.7 Tables

## Table 1.1. Top 30 hit compounds from the bioactive high throughput screen with high SSMD and BHS scores

| Compound Name | SSMD | Brain Health Score | P-value | Selleckchem ID | Mechanism of Action |
|---|---|---|---|---|---|
| **Dimesna** | 1.4201 | 1.8829 | 0.0120 | S1201 | Inactivation of acrolein |
| **AT9283** | 0.8713 | 1.4271 | 0.0134 | S1134 | JAK2/3 kinase inhibitor |
| **Deferasirox** | 1.3424 | 1.4235 | 0.0152 | S1712 | Iron chelator |
| **Etodolac** | 0.9883 | 1.3901 | 0.0155 | S1328 | COX inhibitor |
| **Rapamycin** | 1.6795 | 1.3652 | 0.0165 | S1039 | mTOR inhibitor |
| **AG-490 (Tyrphostin B42)** | 0.7901 | 1.3311 | 0.0167 | S1143 | EGFR inhibitor |
| **Budesonide** | 0.6488 | 1.3074 | 0.0170 | S1286 | Glucocorticoid steroid |
| **Prednisolone** | 1.2094 | 1.2636 | 0.0171 | S1737 | Glucocorticoid steroid |
| **Nepafenac** | 0.7728 | 1.2268 | 0.0176 | S1255 | COX inhibitor |
| **Sophocarpine** | 0.8636 | 1.2109 | 0.0176 | S2405 | Tetracyclic quinolizidine alkaloid |
| **Ganetespib (STA-9090)** | 0.8437 | 1.1885 | 0.0203 | S1159 | HSP90 inhibitor |
| **Aliskiren Hemifumarate** | 1.5401 | 1.1308 | 0.0205 | S2199 | Direct renin inhibitor |
| **Olmesartan Medoxomil** | 1.6489 | 1.1136 | 0.0208 | S1604 | Angiotensin II receptor blocker |
| **Aloperine** | 1.0303 | 1.0835 | 0.0210 | S2420 | PI3K/Akt inhibitor |
| **SGC-CBP30** | 2.3118 | 1.0794 | 0.0222 | S7256 | CREBBP inhibitor |
| **LY2608204** | 1.1448 | 1.0579 | 0.0238 | S2155 | Glucokinase activator |
| **Hexstrol** | 0.7018 | 1.0509 | 0.0241 | S2473 | Nonsteroidal estrogen |
| **Gallamine triethiodide** | 0.6848 | 1.0341 | 0.0336 | S2471 | Cholinergic receptor blocker |
| **IWR-1-endo** | 2.1948 | 0.9941 | 0.0342 | S7086 | Wnt inhibitor |
| **Cyproterone Acetate** | 1.0325 | 0.9849 | 0.0365 | S2042 | Androgen receptor antagonist |
| **Maprotiline HCl** | 1.2404 | 0.8950 | 0.0375 | S2517 | Noradrenalin reuptake inhibitor |
| **CYT387** | 1.0129 | 0.8683 | 0.0430 | S2219 | JAK1/2 kinase inhibitor |
| **Teniposide** | 6.8325 | 0.8597 | 0.0403 | S1787 | DNA topoisomerase II inhibitor |
| **Volasertib (BI 6727)** | 1.3177 | 0.8468 | 0.0411 | S2235 | Plk1 inhibitor |
| **Vismodegib** | 1.4720 | 0.7387 | 0.0417 | S1082 | Hedgehog inhibitor |
| **SB590885** | 1.6987 | 0.7384 | 0.0423 | S2220 | B-raf inhibitor |
| **Protionamide** | 1.6363 | 0.7103 | 0.0432 | S1881 | Class 1A anti-arrhythmic, Sodium Channel Blocker |
| **Y-27632** | 4.8342 | 0.6942 | 0.0433 | S1049 | ROCK1 inhibitor |
| **NMDA (N-Methyl-D-aspartic acid)** | 1.6915 | 0.6197 | 0.0436 | S7072 | NMDA agonist |
| **Mestranol** | 1.6959 | 0.5421 | 0.0447 | S2125 | Estrogen receptor activation |

## Table 1.2. Significant compounds and pathways identified from the Reactome and Wilcoxon Ranksum test

| *Compound* | *Pathway name* | *SSMD* | *Target* | *Activity* | *FDA Status* | *Clinical Trial Status* |
|---|---|---|---|---|---|---|
| *Dexmedetomidine* | Adrenaline signalling through Alpha-2 adrenergic receptor | 1.040 | ADRA2A | AGONIST | Approved | |
| *Guanabenz Acetate* | Adrenaline signalling through Alpha-2 adrenergic receptor | 0.984 | ADRA2A | AGONIST | Approved | |
| *Noradrenaline* | Adrenaline signalling through Alpha-2 adrenergic receptor | 0.855 | ADRA2A | STIMULATOR | Approved | |
| *Phentolamine Mesylate* | Adrenaline signalling through Alpha-2 adrenergic receptor | -0.818 | ADRA2A | INHIBITOR | Approved | |
| *Medetomidine* | Adrenaline signalling through Alpha-2 adrenergic receptor | 0.777 | ADRA2A | AGONIST | Approved | |
| *Ivabradine HCl* | Adrenaline signalling through Alpha-2 adrenergic receptor | -0.539 | ADRA2A | INHIBITOR | Approved | |
| *Y-27632 2HCl* | Apoptosis | 4.834 | ROCK1 | INHIBITOR | | Phase 2 |
| *Oprozomib* | Apoptosis | 1.558 | PSMB8 | INHIBITOR | | Phase 1 |
| *Apoptosis Activator 2* | Apoptosis | -1.291 | CASP3 | ACTIVATOR | | |
| *Evodiamine* | Apoptosis | -1.150 | BCL2 | INDUCER | | |
| *RKI-1447* | Apoptosis | 1.124 | ROCK1 | INHIBITOR | | |
| *Dynasore* | Apoptosis | 0.913 | DNM1 | INHIBITOR | | |
| *PF-573228* | Apoptosis | 0.891 | PTK2 | INHIBITOR | | |
| *Carfilzomib (PR-171)* | Apoptosis | -0.801 | PSMD9 | AGONIST | Approved | |
| *ZSTK474* | Cell surface interactions at the vascular wall | 1.500 | PIK3CA | INHIBITOR | | Phase 1 |
| *Dactolisib (BEZ235, NVP-BEZ235)* | Cell surface interactions at the vascular wall | 0.904 | PIK3CA | INHIBITOR | | Phase 2 |
| *RepSox* | Cell surface interactions at the vascular wall | 0.746 | TGFB1 | INHIBITOR | | |
| *Dasatinib* | Cell surface interactions at the vascular wall | 0.690 | SRC | INHIBITOR | Approved | |
| *ML347* | Cell surface interactions at the vascular wall | 0.625 | TGFB1 | INHIBITOR | | |
| *CAL-101 (Idelalisib, GS-1101)* | Cell surface interactions at the vascular wall | 0.590 | PIK3CA | INHIBITOR | | Phase 2 |
| *Bosutinib (SKI-606)* | Cell surface interactions at the vascular wall | 0.558 | SRC | INHIBITOR | Approved | |
| *Ibuprofen (Dolgesic)* | COX reactions | 1.124 | COX | INHIBITOR | Approved | |
| *Mefenamic acid* | COX reactions | 1.074 | COX | INHIBITOR | Approved | |
| *Etodolac (Lodine)* | COX reactions | 0.988 | COX | INHIBITOR | Approved | |
| *Bromfenac* | COX reactions | 0.778 | COX | INHIBITOR | Approved | |
| *Nepafenac* | COX reactions | 0.773 | COX | INHIBITOR | Approved | |
| *Diclofenac Sodium* | COX reactions | 0.694 | PTSG2 | INHIBITOR | Approved | |
| *Ketorolac (Ketorolac tromethamine)* | COX reactions | 0.577 | COX | INHIBITOR | Approved | |
| *Suprofen(Profenal)* | COX reactions | 0.510 | COX | INHIBITOR | Approved | |
| *Enzastaurin (LY317615)* | Depolymerisation of the Nuclear Lamina | 0.522 | Prkcb | INHIBITOR | | Phase 3 |
| *JTC-801* | G-protein activation | -1.223 | OPRM1 | ANTAGONIST | | |
| *Matrine((+)-Matrine)* | G-protein activation | 0.800 | OPRM1 | AGONIST | | Post marketing |
| *Naloxone HCl* | G-protein activation | 0.564 | OPRM1 | AGONIST | Approved | |
| *Tenovin-1* | G2/M DNA damage checkpoint | -1.612 | TP53 | ACTIVATOR | | |
| *VE-821* | G2/M DNA damage checkpoint | 0.923 | ATM | INHIBITOR | | |
| *VE-822* | G2/M DNA damage checkpoint | 0.781 | ATR | ANTAGONIST | | |
| *LY2608204* | Glycolysis | 1.145 | GCK | INHIBITOR | | Phase 0 |
| *Clorsulon* | Glycolysis | 0.907 | GPM1 | INHIBITOR | | |
| *Vismodegib (GDC-0449)* | Hh mutants that don't undergo autocatalytic processing are degraded by ERAD | 1.472 | SHH | INHIBITOR | Approved | |
| *PNU-120596* | Highly calcium permeable nicotinic acetylcholine receptors | 1.142 | CHRNA1 | AGONIST | | |

| *Compound* | *Pathway name* | *SSMD* | *Target* | *Activity* | *FDA Status* | *Clinical Trial Status* |
|---|---|---|---|---|---|---|
| *Tropicamide* | Highly calcium permeable nicotinic acetylcholine receptors | 0.952 | CHRNA1 | INHIBITOR | Approved | |
| *Darifenacin* | Highly calcium permeable nicotinic acetylcholine receptors | 0.869 | CHRNA1 | INHIBITOR | Approved | |
| *Pancuronium dibromide* | Highly calcium permeable nicotinic acetylcholine receptors | 0.860 | CHRNA1 | INHIBITOR | Approved | |
| *Gallamine triethiodide(Flaxedil)* | Highly calcium permeable nicotinic acetylcholine receptors | 0.685 | CHRNA1 | INHIBITOR | Approved | |
| *Adiphenine* | Highly calcium permeable nicotinic acetylcholine receptors | 0.671 | CHRNA1 | INHIBITOR | | |
| *Bethanechol chloride* | Highly calcium permeable nicotinic acetylcholine receptors | 0.570 | CHRNA1 | AGONIST | Approved | |
| *Atropine sulfate monohydrate* | Highly calcium permeable nicotinic acetylcholine receptors | 0.551 | CHRNA1 | INHIBITOR | Approved | |
| *Cytisine* | Highly calcium permeable nicotinic acetylcholine receptors | 0.520 | CHRNA4 | AGONIST | | |
| *Aliskiren hemifumarate* | Metabolism of Angiotensinogen to Angiotensins | 1.540 | REN | INHIBITOR | Approved | |
| *Imidapril HCl* | Metabolism of Angiotensinogen to Angiotensins | 0.938 | ACE | INHIBITOR | | Phase 3 |
| *Clinofibrate* | Metabolism of Angiotensinogen to Angiotensins | 0.860 | ACE | INHIBITOR | | |
| *Quinapril hydrochloride (Accupril)* | Metabolism of Angiotensinogen to Angiotensins | 0.707 | ACE | INHIBITOR | Approved | |
| *Ramipril* | Metabolism of Angiotensinogen to Angiotensins | 0.498 | ACE | INHIBITOR | Approved | |
| *SB590885* | Negative feedback regulation of MAPK pathway | 1.699 | RAF1 | INHIBITOR | | |
| *Selumetinib (AZD6244)* | Negative feedback regulation of MAPK pathway | 1.098 | MEK1 | INHIBITOR | | Phase 2 |
| *RAF265 (CHIR-265)* | Negative feedback regulation of MAPK pathway | 0.886 | RAF1 | INHIBITOR | | Phase 2 |
| *SL327* | Negative feedback regulation of MAPK pathway | 0.812 | MEK1 | INHIBITOR | | |
| *Vemurafenib (PLX4032, RG7204)* | Negative feedback regulation of MAPK pathway | 0.625 | BRAF | INHIBITOR | Approved | |
| *Tanshinone IIA* | Negative feedback regulation of MAPK pathway | 0.547 | MAP2K1 | INHIBITOR | | Phase 3 |
| *PD0325901 (PD325901)* | Negative feedback regulation of MAPK pathway | 0.511 | MEK1 | INHIBITOR | | Phase 2 |
| *IWR-1 (endo-IWR 1)* | PCP/CE pathway | 2.195 | WNT1 | INHIBITOR | | |
| *EHop-016* | PCP/CE pathway | 0.879 | RAC1 | INHIBITOR | | |
| *XAV-939* | PCP/CE pathway | 0.544 | WNT1 | INHIBITOR | | |
| *Protionamide* | Peptide hormone metabolism | 1.636 | INHA | INHIBITOR | | Phase 1 |
| *Alogliptin* | Peptide hormone metabolism | 0.988 | DPP4 | INHIBITOR | Approved | |
| *TAK-875* | Peptide hormone metabolism | 0.733 | gpr40 | ANTAGONIST | | Phase 3 |
| *SGC-CBP30* | Regulation of Hypoxia-inducible Factor (HIF) | 2.312 | DOT1L | INHIBITOR | | |
| *Rapamycin* | Regulation of TP53 Activity | 1.679 | MTOR | INHIBITOR | Approved | |
| *P22077* | Regulation of TP53 Activity | 1.145 | USP7 | INHIBITOR | | |
| *ETP-46464* | Regulation of TP53 Activity | 1.085 | MTOR | INHIBITOR | | |
| *Ridaforolimus* | Regulation of TP53 Activity | 1.078 | MTOR | INHIBITOR | | Phase 3 |
| *PP242* | Regulation of TP53 Activity | 0.896 | MTOR | INHIBITOR | | |
| *KU-0063794* | Regulation of TP53 Activity | 0.618 | MTOR | INHIBITOR | | |
| *PHT-427* | Regulation of TP53 Activity | 0.616 | AKT1 | INHIBITOR | | |
| *Entinostat (MS-275)* | Regulation of TP53 Activity | 0.574 | HDAC1 | INHIBITOR | | Phase 2 |
| *AZD1152-HQPA (Barasertib)* | Regulation of TP53 Activity | 0.517 | AURKB | INHIBITOR | | Phase 1 |
| *Carprofen* | Respiratory electron transport | 0.697 | cox2 | INHIBITOR | Approved | |
| *Cilengitide* | Smooth Muscle Contraction | 0.718 | ITGA1 | INHIBITOR | | Phase 1 |
| *(-)-Huperzine A* | Synthesis of PC | 1.320 | ACHE | INHIBITOR | | Phase 2 |
| *Odanacatib (MK 0822)* | Toll-Like Receptors Cascades | -1.054 | CTSK | AGONIST | | Phase 1 |
| *EUK 134* | Toll-Like Receptors Cascades | 0.529 | APP | INHIBITOR | | |
| *NMDA* | TP53 Regulates Metabolic Genes | 1.691 | NMDA | AGONIST | | |
| *BAM 7* | TP53 Regulates Transcription of Genes Involved in G2 Cell Cycle Arrest | 0.763 | BAX | INDUCER | | |

## 1.8 References


1. Yang, W. *et al.* Current and projected future economic burden of Parkinson's disease in the U.S. *npj Park. Dis.* **6**, 15 (2020).

2. DeMaagd, G. & Philip, A. Parkinson's Disease and Its Management: Part 1: Disease Entity, Risk Factors, Pathophysiology, Clinical Presentation, and Diagnosis. *P T* **40**, 504–532 (2015).

3. Armstrong, M. J. & Okun, M. S. Diagnosis and Treatment of Parkinson Disease: A Review. *JAMA - J. Am. Med. Assoc.* **323**, 548–560 (2020).

4. Koprich, J. B., Kalia, L. V & Brotchie, J. M. Animal models of α-synucleinopathy for Parkinson disease drug development. *Nat. Rev. Neurosci.* **18**, 515–529 (2017).

5. Jakobs, M., Lee, D. J. & Lozano, A. M. Modifying the progression of Alzheimer's and Parkinson's disease with deep brain stimulation. *Neuropharmacology* **171**, 107860 (2020).

6. Liu, H. *et al.* A high-content larval zebrafish brain imaging method for small molecule drug discovery. *PLoS One* **11**, 1–14 (2016).

7. Moffat, J. G., Vincent, F., Lee, J. A., Eder, J. & Prunotto, M. Opportunities and challenges in phenotypic drug discovery: An industry perspective. *Nat. Rev. Drug Discov.* **16**, 531–543 (2017).

8. Du, Y. *et al.* Spatial and Temporal Distribution of Dopaminergic Neurons during Development in Zebrafish. *Front. Neuroanat.* **10**, 115 (2016).

9. Zhang, X. D. *et al.* The use of strictly standardized mean difference for hit selection in

primary RNA interference high-throughput screening experiments. *J. Biomol. Screen.* **12**, 497–509 (2007).

10. McQuin, C. *et al.* CellProfiler 3.0: Next-generation image processing for biology. *PLOS Biol.* **16**, e2005970 (2018).

11. Tweedie, S. *et al.* Genenames.org: the HGNC and VGNC resources in 2021. *Nucleic Acids Res.* **49**, D939–D946 (2021).

12. Wang, Y. *et al.* Therapeutic target database 2020: enriched resource for facilitating research and early development of targeted therapeutics. *Nucleic Acids Res.* **48**, D1031–D1041 (2020).

13. Park, J.-S., Davis, R. L. & Sue, C. M. Mitochondrial Dysfunction in Parkinson's Disease: New Mechanistic Insights and Therapeutic Perspectives. *Curr. Neurol. Neurosci. Rep.* **18**, 21 (2018).

14. Bartels, A. L. & Leenders, K. L. Cyclooxygenase and neuroinflammation in Parkinson's disease neurodegeneration. *Curr. Neuropharmacol.* **8**, 62–68 (2010).

15. Sánchez-Pernaute, R. *et al.* Selective COX-2 inhibition prevents progressive dopamine neuron degeneration in a rat model of Parkinson's disease. *J. Neuroinflammation* **1**, 6 (2004).

16. Breen, D. P. *et al.* Sleep and circadian rhythm regulation in early Parkinson disease. *JAMA Neurol.* **71**, 589–595 (2014).

17. Cai, Y., Liu, S., Sothern, R. B., Xu, S. & Chan, P. Expression of clock genes Per1 and

Bmal1 in total leukocytes in health and Parkinson's disease. *Eur. J. Neurol.* **17**, 550–554 (2010).

18. Ehlen, J. C. *et al.* Bmal1 function in skeletal muscle regulates sleep. *Elife* **6**, e26557 (2017).

19. Hu, G., Jousilahti, P., Bidel, S., Antikainen, R. & Tuomilehto, J. Type 2 Diabetes and the Risk of Parkinson{\textquoteright}s Disease. *Diabetes Care* **30**, 842–847 (2007).

20. Xu, Y.-Q. *et al.* Aloperine attenuated neuropathic pain induced by chronic constriction injury via anti-oxidation activity and suppression of the nuclear factor kappa B pathway. *Biochem. Biophys. Res. Commun.* **451**, 568–573 (2014).

21. Song, S. *et al.* Aloperine activates the Nrf2-ARE pathway when ameliorating early brain injury in a subarachnoid hemorrhage model. *Exp Ther Med* **15**, 3847–3855 (2018).

22. Zhao, J. *et al.* Neuro-protective effects of aloperine in an Alzheimer's disease cellular model. *Biomed. Pharmacother.* **108**, 137–143 (2018).

23. Sharifi-Rad, M. *et al.* Impact of Natural Compounds on Neurodegenerative Disorders: From Preclinical to Pharmacotherapeutics. *J. Clin. Med.* **9**, 1061 (2020).

# CHAPTER 2: Understanding the neuroprotective mechanism of the renin angiotensin pathway

## 2.1 Abstract

Parkinson's disease (PD) is the second most common neurodegenerative disorder for which no disease-modifying therapeutics are available. Here we report the neuroprotective action of Renin-Angiotensin-Aldosterone System (RAAS) inhibitors identified from an *in vivo* whole organism small molecule screen employing transgenic zebrafish. First, we established a chemo-genetic dopamine (DA) neuron ablation model that suffers from mitochondrial dysfunction and is suitable for high content screening. Second, we performed an *in vivo* DA neuron imaging-based screen of >1400 bioactive compounds that identified RAAS inhibitors to be significantly neuroprotective. Third, using conditional CRISPR to knock out the angiotensin receptor type 1 (*agtr1*) in DA neurons, we revealed a cell-autonomous mechanism of neuroprotection through *agtr1* inhibition. DA neuron-specific RNA-seq further identified pathways including the mitochondrial electron transport chain that are significantly perturbed in DA neuron degeneration and is abated by RAAS inhibitor treatment. Fourth, the neuroprotective effect of RAAS inhibitors is validated with brain imaging and functional analysis in a chemically induced zebrafish Gaucher's disease model and in a Drosophila PD model of *pink1* deficiency. Finally, examination of 308 clinical PD patient data revealed a significant effect of RAAS inhibitors in delaying the onset of levodopa therapy and increasing performance in symptom assessment scores. Taken together, from establishing a high throughput screening model and elucidating the underlying molecular mechanisms to the evaluation of clinical data, our findings uncover the

therapeutic potential of targeting the RAAS pathway for neuroprotection and demonstrate a salient approach that bridges basic science to translational medicine.

## 2.2 Introduction

As the most common movement disorder and the second most common neurodegenerative disorder, Parkinson's Disease (PD) affects 0.3% of the general population, with a majority of cases being sporadic [1,2]. The hallmark of PD is a loss of substantia nigra dopamine (DA) neurons accompanied by a variety of motor and non-motor features. Cardinal symptoms of PD include bradykinesia, resting tremor, postural instability, and rigidity [3,4]. With movement-related disabilities and other cognitive impairment as well as psychiatric symptoms, PD not only deteriorates the health and quality of life of patients, but also poses severe burdens on their families and caregivers. The economic cost of PD is estimated to be at least $14.4 billion a year in the United States [5] and PD is increasing at a greater rate compared to other neurodegenerative disorders [6].

The current drug therapies available for PD provide only symptomatic relief by enhancing the dopaminergic action, decreasing metabolism of DA, or replacing the natural form of DA with exogenous drugs [7,8]. However, there is yet to be a therapy that can halt or slow down disease progression. The current gold standard treatment for the management of PD is levodopa coupled with peripheral decarboxylase inhibitor such as carbidopa [9,10]. While it provides benefits in improving motor symptoms in the short term, chronic therapy can result in motor fluctuations

and dyskinesias. Furthermore, many patients experience a wearing-off effect where levodopa loses its efficacy even with dosing adjustments.

In recent years, the drug discovery pipeline for neurological diseases has been stagnant, with a phase I to approval rate being only 8.4% from 2006 to 2015 [11,12] which is lower than other therapeutic areas such as hematology or infectious diseases and lower than the average approval rate of all therapeutic indications. One of the reasons for such lack of success can be attributed to the fact that conventional approach of target-based drug discovery is difficult in the setting of neurological diseases because of the complex etiology and biological pathways involved [13–15]. Phenotypic screening provides a promising opportunity. In particular, the whole organism-based drug discovery as a renaissance approach has been successfully applied to model organisms including yeast, *C. elegans*, zebrafish, and mice [16–19]. Larval zebrafish, being a vertebrate that can fit in 96-well plates, offers multiple advantages including genomic and anatomical conservation in addition to high throughput capabilities. Screens have uncovered therapeutic leads that are currently in clinical testing and/or shed light on biological mechanisms [20,21].

Here, we report a DA neuron-based neuroprotective drug discovery pipeline for PD, from assay development to small molecule screening, hit target validation, mechanisms, and ultimately, evolutionary conservation of neuroprotection across species including humans. Due to the late onset and variable phenotypic expressivity of genetic PD models and the highly toxic nature of neurotoxins (e.g., MPTP) to researchers, no good *in vivo* assay systems exist that are suitable for high content screening of neuro-protectives. We therefore first established an inducible chemo-genetic DA neuron ablation model in larval zebrafish. This model expressed the *E. coli* nitroreductase (NTR) controlled by the promoter of tyrosine hydroxylase (*th*), a rate-limiting enzyme in DA synthesis. Addition of the commonly used and safe-to-handle antibiotic,

metronidazole (MTZ), caused robust DA neuron loss. By showing that DA neuron loss is preceded by mitochondrial DNA damage and ensuing mitochondrial dysfunction, we demonstrated the validity and relevance of this model to PD for small molecule screening purpose. Using this model to screen >1400 bioactive small molecules, we uncovered a series of compounds that protected against DA neuron loss by inhibiting different proteins in the renin-angiotensin-aldosterone system (RAAS), a pathway classically known for regulating vasoconstriction and water homeostasis [22]. Genetic validation and molecular characterization further revealed that the angiotensin receptor 1 (AGTR1) acted cell autonomously in DA neurons, the inhibition of which restored the expression of mitochondrial pathway genes disrupted by neurotoxic insults. Furthermore, we showed that RAAS inhibitors were neuroprotective in a zebrafish model for Gaucher's disease, a lysosomal storage disorder with strong comorbidity of PD [23]. They were also protective in a *Drosophila pink1*-deficient PD model [24]. Finally, utilizing the Parkinson's Progression Marker Initiative (PPMI) database [25], we performed a clinical informatics analysis to uncover that RAAS inhibitors significantly slowed down PD progression. Together, our results delineate a powerful approach for neuroprotective small molecule drug discovery that leverages whole organism screening and cross-species validation.

## 2.3 Methods

### 2.3.1 Study design

This study was designed to identify neuroprotective small molecules for Parkinson's disease (PD). A chemo-genetic DA neuron degeneration model employing the NTR-MTZ system was first characterized to uncover mitochondrial dysfunction as a plausible cause of cell death. A whole organism DA neuron imaging-based small molecule screen employing such transgenic zebrafish was then carried out. By screening 1403 bioactive small molecule compounds, the RAAS pathway inhibitors were identified to be significantly neuroprotective. Their neuroprotective actions were further validated in multiple animal models and in human PD patients. Cell type-specific CRISPR and RNA-seq revealed a DA neuron-autonomous regulation of mitochondrial function as a mechanism underlying the neuroprotective effects of RAAS inhibitors. *In vivo* studies employing zebrafish were approved by the Institutional Animal Care Use Committee at University of California, San Francisco. Use of patient data in the PPMI database was approved by the Michael J Fox Foundation PPMI Data and Publications Committee. No statistical methods were used to predetermine sample size. The sample size (*n*) for each experimental group was indicated in the figure legends. The compound treatment, image collection, and data analysis, for the compound screening, manual counting for secondary hit validation of RAAS inhibitors, western blot of morpholino injections, mass spectrometry of adult fish brains, and adult zebrafish behavior studies were performed in a blinded manner. For all other experiments, the investigators were not blinded to allocation during experiments and outcome assessment. All the experiments were replicated at least two independent times.

### 2.3.2 Zebrafish husbandry and transgenic lines

Zebrafish were raised on a 14:10 hr light/dark cycle and maintained in the zebrafish facility according to the University of California San Francisco Institutional Animal Care and Use Committee standards. Embryos were raised in Blue Egg Water (2.4 g CaSO4, 4g IO Salt, 600 µl of 1% Methylene per 20L).

The following transgenic lines were used: *Tg[fuguth:gal4-uas:GFP; uas-NTRmCherry]*(for *in vivo* drug screening, hit validation, MO injection, and behavioral assessment); *Tg[UAS:mtPAGFP:mtDsRed2]* (for imaging mitochondrial dynamics, kindly provided by Dr. Edward Burton's lab [89]); *Tg[th1:gal4; uas:NTRmCherry]*(for CBE double immunofluorescence staining of TH and 5HT, conditional CRISPR knockout of *agtr1a* and *agtr1b*, DA neuron specific RNA-seq). Tg[*th1-gal4*] was kindly provided by Dr. Jiulin Du's lab [90].

### 2.3.3 *Agtr1a* and *agtr1b* morpholino knockdown and western blot validation of knockdown

Morpholino (MO) antisense oligonucleotides that inhibit protein translation were designed for *agtr1a* and *agtr1b* (Supplemental Figure 2.3A) and purchased from Gene Tools, LLC. 0.5mM *agtr1a* and *agtr1b* MO working solution was mixed with 1% phenol red and micro-injected into 1-cell stage embryos (estimated 1-4 nls per embryo). At 5 dpf, control and morphants were treated with 9 mM MTZ for 24 hrs and confocal imaging was performed with brightfield and DsRed channel at 6dpf. 8-bit images were cropped to isolate the diencephalic region of the brain and the DA neuron intensity was quantified with ImageJ.

For western blotting, the 6dpf larvae with DMSO or MTZ treatment were collected after performing confocal imaging. 30 larvae for each group were homogenized in 150uL of SDS sample buffer and boiled for 10 minutes at 99°C and transferred to ice. The samples were centrifuged for 1 min at 12,000 rpm and the supernatant was transferred to a new tube with 5x SDS protein loading buffer. The samples were loaded into Mini-PROTEAN® TGX™ Gels (cat# 4561083) and run at 180V for 50 mins. Transblotting was done using the Trans-Blot® Turbo™ Transfer System (cat# 1704150) and washed with PBS. Primary antibodies were incubated at 4°C overnight. For the anti-rabbit *agtr1* antibody (Proteintech 25343-1-AP), 1:500 was used; for the anti-mouse beta actin control (Sigma A5441), 1:2000 dilution was used. Horseradish Peroxidase conjugated secondary antibodies were used (Abcam ab6721 and ab6728) with 2hr incubation. After washing off the secondary antibodies with PBS, the western blot was visualized with the iBright CL750 Imaging System (Invitrogen A44116). The expected bands of 37kda for anti-beta actin and 50kda for anti-AGTR1 were identified and analyzed with imageJ using the "Mean Grey Value" measurement tool.

### 2.3.4 *In vivo* whole organism imaging-based high-throughput screening assay and secondary validation

The drug screening was performed in 96-well plates with the bioactive compound library from SelleckChem obtained from the UCSF Small Molecule Discovery Center (SMDC). 10µM of compounds were dissolved in blue egg water containing 0.2% DMSO for a total volume of 200µL. *Tg[fuguth:gal4-uas:GFP; uas:NTRmCherry]* were treated with 200µM 1-phenyl 2-thiourea (PTU) on 1dpf and at 3dpf, larvae were transferred to 96-well plates containing the screening compounds. 0.2% DMSO (positive control) or 4.5mM MTZ (negative control).

Treatment lasted for 48hrs. At 5dpf, the larvae were imaged with brightfield and TexRed channels. The multi-pose method [38] was used to image DA neurons *in vivo* using In Cell Analyzer 2000. The images were analyzed using a custom CellProfiler [91] pipeline that masks the eye and auto-detects the DA neurons to calculate the Brain Health Score (BHS) and SSMD score as previously described [38].

For the secondary hit validations, 40µL of 1.5% agarose was added to ensure that the larvae were embedded in a dorsal down position for confocal imaging before and after MTZ treatment. The live confocal imaging was conducted in the In Cell Analyzer 6000 with DsRed and FITC channels with 200ms exposure time. For the dose response studies, concentrations of the RAAS inhibitors were prepared from a series of fold dilutions. The Renin angiotensin pathway inhibitors used in the study including olmesartan, aliskiren, captopril, were purchased from Sigma-Aldrich (cat #144689-63-4, 62571-86-2, 173334-58-2). Metronidazole and NAC were purchased from Selleck Chemicals (cat# S1907, S1623). CBE was purchased from Sigma Aldrich (cat# 6090-95-5).

### 2.3.5 Adult and larval zebrafish locomotor behavior assay

For all adult and larval behavior assays, animals were individualized and incubated in their home tanks in a $26^0$C behavior room overnight for habituation. Six-well plates were used to house individual larva in each well with 5mL of total volume per well. The wells were placed on a lightbox and the videos were recorded from a top-down view. For the adult behavior experiments, the fish were individually housed in their home tank with 500mL of system water. For the 2-week duration of the adult behavior test, they were fed with flakes in the morning and

replaced with fresh water containing the test compounds daily. The recordings were taken from the top view for 5 minutes. The total distance moved for the 5-minute duration was analyzed through the EthoVision XT® software using the dynamic subtraction algorithm with detection limits between 10 to 100 pixels. For larval fish, the static subtraction algorithm was used with detection limits between 10 to 40 pixels.

### 2.3.6 Assessment of nuclear and mitochondrial DNA integrity

*Tg[fuguth:gal4-uas:NTRmCherry]* were treated with PTU (1:100)(200µM) on 1dpf. At 5dpf, the larvae were treated with 4.5mM MTZ for 8hrs and immediately transferred to HBSS (Ca/Mg Free) Buffer (Gibco 14170120) and the brains were dissociated with TrypLE (Gibco 12604013) for 30 minutes. DA neurons were collected via mouth pipetting and the genomic DNA was extracted using extraction buffer (10 mM Tris pH 8.2, 10 mM EDTA, 200 mM NaCl, 0.5% SDS, 200 µg/ml proteinase K). The nuclear DNA was PCR amplified using the primer sequences: Forward 5’ to 3’ AGAGCGCGATTGCTGGATTCAC, Reverse 5’ to 3’ GTCCTTGCAGGTTGGCAAATGG and the mitochondrial DNA was PCR amplified using the primer sequences: Forward 5’ to 3’ TTAAAGCCCCGAATCCAGGTGAGC, Reverse 5’ to 3’ GAGATGTTCTCGGGTGTGGGATGG. The target base pair sizes are 10.7kb and 10.3kb respectively. The PCR was performed with the QIAGEN Long-Range PCR Kit (cat# 206402) optimized for long-range amplification of genomic DNA. The PCR was performed with an initial denaturation step at 94 °C for 1 min, 24 cycles (nuclear DNA) or 19 cycles (mitochondrial DNA) of 94 °C for 15 s, 69 °C for 45 s, and 72 °C for 30 s, with final extension at 72 °C for 10 min. The DNA integrity was evaluated by gel electrophoresis (2% agarose) and the bands were

analyzed with ImageJ using the “Calibrate” function to determine the optical density of the molecular weight standard, the nuclear DNA, and mitochondrial DNA bands.

### 2.3.7 *In vivo* imaging of mitochondrial dynamics

Transgenic zebrafish *Tg[th1:gal4; uas:NTRmCherry]* were crossed with *Tg[UAS:mtPAGFP:mtDsRed2]* and treated with PTU (1:100) (200µM) at 1dpf. The larvae were screened for *th1-NTRmCherry* on 4dpf and were treated with either 0.2% DMSO (control) or 4.5mM MTZ for 16 hrs. The larvae were embedded with 1% low melting point agarose (Sigma 39346-81-1)(1:100 tricaine added,0.168ug/mL) in 35mm glass bottom dishes (Corning). The PA-GFP was activated with the Nikon 40x WI objective DAPI channel for 1 min. Upon successful activation, the mitochondria were observable under GFP. Live imaging was performed with 10s intervals for a total of 10 mins. The imaging movies were processed with ImageJ and IMARIS software (version 9.7) where the xyz coordinates of the mitochondria movements were obtained. The values were exported to a custom MATLAB script to calculate total displacement, velocity, and direction.

### 2.3.8 Mass spectrometry of adult zebrafish for olmesartan detection

Zebrafish were treated with 10 µM of olmesartan medoxomil (Sigma Aldrich cat# 144689-63-4, the pro-drug form of olmesartan) for 14 days. The drug was freshly dissolved in the system water and administered daily. On day 14, adult zebrafish were dissected to collect the body and the brain which were then pooled to obtain approximately 125mg per sample (n=10 males, 10

females). The samples were homogenized, and mass spectrometry was performed with olmesartan, the active form of the compound, as a reference (Sigma Aldrich cat# 144689-24-7).

### 2.3.9 Drug treatment in the chemically induced Gaucher's disease model in larval zebrafish

Zebrafish treated with CBE (a chemical inhibitor of GBA) and the RAAS inhibitor olmesartan were tested for both locomotor behavior and confocal imaging of DA neurons. Initially, CBE concentrations ranging from 100 mM, 500 mM, and 1 mM were used to treat embryonic and larval zebrafish from 1dpf to 5dpf with fresh compounds dissolved in Blue Egg Water changed daily to determine that 500 mM is the optimal concentration for the study (Supplemental Figure 2.5). Prior to treatment with CBE, olmesartan, or levodopa, 5dpf larvae were embedded in 96-well glass bottom plates with 1.5% agarose and blue egg water and imaged using a 20x objective under the InCell 6000 confocal microscope. CBE (500 mM), olmesartan (10 mM) or levodopa (500 mM) were added to the agarose-embedded larvae. 24 hrs later, the 6dpf larvae were again imaged and the before vs. after TH intensity was quantified using ImageJ. For behavioral recording, 5dpf larvae were treated with CBE, olmesartan, or levodopa for 24 hrs in 6-well plates and behavior was analyzed using Ethovision XT® using the methodologies described above.

### 2.3.10 Drug treatment in the Drosophila *pink1*-deficient model

Newly eclosed *PINK1$^{B9}$; TH-Gal4>UAS-mito-GFP* male flies were raised on instant fly food (Carolina) or instant fly food containing 100 μM olmesartan. Flies were transferred to fresh vials daily. After two weeks, the flies were scored for wing posture or examined under dissecting microscope for thoracic indentation. Afterwards, flies were dissected for DA neuron staining. At

least 7 individuals were examined for each condition. Dissected brain tissue samples were briefly washed with 1x PBS and fixed with 4% formaldehyde in 1x PBS containing 0.25% Triton X-100 for 30 minutes at room temperature. Fixed samples were subsequently blocked with 1x PBS containing 5% normal goat serum and incubated for 1 hour at room temperature followed by incubation with primary antibodies at 4°C overnight. The primary antibodies used were: chicken anti-GFP (1:5,000, Abcam), and rabbit anti-TH (1:1000, Pel-Freez). After three washing steps with 1x PBS/0.25 % Triton X-100 each for 15 minutes at room temperature, the samples were incubated with Alexa Fluor® 594- and Alexa Fluor® 488-conjugated secondary antibodies (1:500, Molecular Probes) for 3 hrs at room temperature and subsequently mounted in SlowFade Gold (Invitrogen). Samples were observed under a Leica SP8 confocal microscope and fluorescent confocal images were processed using Photoshop.

### 2.3.11 FACs, qPCR, and RNA Sequencing

FACs was performed on the BD FACSaria III Cell Sorter with 488nm, 561nm and 638nm channels. To ensure high accuracy of cell sorting, DA neurons were sorted with both 488 and 561nm channels from *Tg[fuguth:gal4-uas:GFP; uas:NTRmCherry]*. The dead cells stained with DAPI (1ng/mL) were sorted with the 405nm channel. The FACs-sorted cells were immediately processed for RNA extraction (Ambion) and converted to cDNA for qPCR. The primers were designed with NCBI primer blast and validated with gel electrophoresis prior to the qPCR run. The Ct values were compared relative to *ef1a1* as a housekeeping gene (Table 2.1).

For RNA-seq, approximately 500 DA neurons were collected per sample with biological triplicates using the FACs procedure described above. RNA was extracted using the Lexogen

SPLIT RNA extraction kit (cat 008) and the quality was assessed in the Agilent 2100 Bioanalyzer (cat# G2939BA). The library was prepared using the Lexogen QuantSeq 3' mRNA-Seq Library Prep Kit FWD for Illumina (cat# 015). The libraries were quality controlled using Agilent 2100 Bioanalyzer and pooled at 20mL of 3ng/mL concentration. The RNA-seq was performed on the Illumina HiSeq 4000 (cat SY-401-4001), with single end 50bp, generating 350 million reads per lane. FastQC was performed for quality check and all sequences showed high per base sequence quality with greater than 75% uniquely mapped reads aligned against GRCz11 (Supplemental Figure 2.7A). The count normalization was performed using the DESeq2's median of ratios method which accounts for sequencing depth and RNA composition. This normalization method allows for gene count comparisons between samples, which is suitable for comparing differential gene expression across different sample groups with high sensitivity and specificity [92,93]. To visualize the similarity of our samples, initially a sample-level QC was performed using Principal Component Analysis (PCA) as shown in Supplemental Figure 2.7B. Each dot represents a sample from the respective group. The raw counts for each gene were modeled and the log2 fold changes were shrunken and differential gene expression analysis was performed using DESeq2 in R with an α level of 0.05 and FDR of 0.1. The gene set was then annotated and converted from the zebrafish ensemble gene (ENSG) to homo sapiens ENTREZ gene ID with gProfiler. The pathway analysis was conducted on DAVID for the KEGG pathway maps and Metascape for enriched ontology clusters.

### 2.3.12 Antibody Staining of 5HT and DA neurons in larval zebrafish

6dpf larvae were fixed in 4% PFA overnight, washed with PBS, and their brains were dissected. After 24hrs of dehydration in 100% methanol overnight followed by rehydration, the samples

were incubated in primary antibodies for 72hrs at 4°C with the rabbit anti-5HT (Immunostar cat#20080) and mouse anti-TH (Immunostar cat#22941) primary antibodies. The brains were then subjected to secondary antibody labeling, using Alexa Fluor 488 anti-mouse (cat A-11001) and Alexa Fluor 568 anti-rabbit (cat A-11036). The brains were stored in 75% Glycerol and mounted for confocal imaging. The confocal imaging was taken on the Nikon Ti inverted fluorescence microscope with CSU-W1 large field of view using Apo LWD 40x/1.15 water immersion lens under GFP and RFP channels.

### 2.3.13 Conditional CRISPR

The sgRNA sequences were predicted and designed based on the CHOPCHOP and CRISPRscan database (Supplemental Figure 2.6A). The sgRNAs were synthesized and co-injected with Cas9-LS protein (UC Berkeley, https://qb3.berkeley.edu/facility/qb3-macrolab/) into 1-cell stage embryos. The genomic DNAs were extracted and sequenced. Upon different designs of sgRNAs (8 for each gene), a maximal knockout efficiency of 58% and 65% were obtained for *agtr1a* and *agtr1b* respectively, based on the analysis with the Synthego ICE software (version 2.0, https://ice.synthego.com/#/). The plasmid backbone used for the conditional knockout construct was the Tol2-pUAS:Cas9T2AGFP;U6:sgRNA1;U6:sgRNA2, in which UAS elements drive the expression of Cas9 and GFP linked via the T2A peptide and two sgRNA targets can be simultaneously used. The BsaI and BsmBI restriction sites were used for the sgRNA target sequence cloning as previously described [49]. After cloning, the obtained plasmid construct was co-injected with Tol2 transposase mRNA into 1-cell stage embryos derived from *Tg[th1:gal4; UAS:NTRmCherry]*. To validate successful knockout of the genes, after live imaging of DA neurons under both GFP and RFP channels, the zebrafish brains were dissociated with TrypLE

Express for 30 mins and mouth-pipetting was used to collect the $GFP^{+}NTRmCherry^{+}$ DA neurons for PCR and sequencing (Supplemental Figure 2.6C).

### 2.3.14 Parkinson's Progression Markers Initiative Data Analysis

The PPMI is an observational clinical study providing a comprehensive database for clinical, imaging, and biological data. The PPMI repository contains clinical data with subject demographics, comprehensive medication history, UPDRS motor assessments, and non-motor assessments. The data were downloaded and accessed in May 2019. Initially 423 *de novo* PD patients, defined as subjects with a diagnosis of PD with two years or less who are not taking any PD medications, were identified, in which 115 patients had missing information or withdrew from the study making the total included subjects to be 308 patients. Among the 308 patients, 96 patients were taking either ACE inhibitors or ARBs (RAAS group) while 212 patients were not taking ACE inhibitors or ARBs (no RAAS group). Based on the medication history, the average Time-to-Levodopa was compared between the two groups. Among the 212 patients, 42 patients had a diagnosis of hypertension (ICD code R03.0) and were taking other medications for the management of their hypertension. 170 patients were neither hypertensive nor taking other blood pressure medications. For the patient cohorts, propensity score matching was used to match the covariates including age, gender, race, smoking, caffeine consumption, alcohol consumption, and history of head injury (Supplemental Figure 2.8A-C) between the cohorts taking RAAS inhibitors (RAAS group) and not taking RAAS inhibitors (no RAAS group). For the UPDRS motor assessment analysis, a subset of patients from each cohort not taking levodopa for at least three years from their initial PPMI enrollment were selected to remove the possible confounding effects of levodopa on motor improvement. Part 1 (non-motor experiences of activities of daily

living), part 2 (motor experiences of activities of daily living), and part 3 (motor examination) were assessed (Supplemental Figure 2.8 E-F).

### 2.3.15 Statistical analysis

The imaging data from screening studies and behavior studies were analyzed by unpaired t-test using R program and Graphpad Prism software and expressed as means ± SEM unless otherwise stated. Wilcoxon rank sum test was used for the analysis of the high throughput screening database. Differential gene expression analysis of the RNA-seq data was done using the DESeq2 package in R and the fold changes of gene expressions were evaluated with Wald test at an $\alpha$ of 0.05 and FDR 0.1. Clinical data analysis of the PPMI database on Time-to-Levodopa was conducted with a Log-rank Mantel-cox test; the UPDRS motor scores were analyzed with nonparametric one-way analysis of variance (ANOVA) and post-hoc Tukey Test.

## 2.4 Results

### 2.4.1 The Nitroreductase-Metronidazole (NTR-MTZ) chemo-genetic DA neuron degeneration model shows mitochondrial damage prior to neuronal loss and is scalable for small molecule screening

No currently available models are suitable for neuro-protective small molecule screening. Genetic models have weak variable and late onset degeneration phenotypes [26]. Neurotoxins such as MPTP are highly toxic to experimenters and not scalable for high content screening. We have therefore used an inducible chemo-genetic DA neuron degeneration model, employing the nitroreductase-metronidazole (NTR-MTZ) system [27–29]: NTR was expressed as a transgene in tyrosine hydroxylase ($TH^+$) DA neurons to convert the pro-drug MTZ (a commonly used antibiotic) to the toxic nitroso radical form *in vivo*. 24 hours (hrs) after adding MTZ, we observed robust DA neuronal loss in the ventral forebrain region (Figure 2.1), the homologous group to mammalian substantia nigra DA neurons [30].

Although the NTR-MTZ system has been previously used for cell ablation [27–29] and noted to induce apoptotic cell death [31], the underlying mechanisms of cell death are not well understood. Previous reports suggest that MTZ as an antibiotic targets bacterial DNA [32]. In vertebrate cells, two organelles containing DNA are the nucleus and the mitochondria. A qPCR assay based on the notion that DNA lesions block DNA polymerase progression [33,34], was used to detect nuclear versus mitochondrial DNA lesions. Total DNAs were extracted from purified DA neurons in DMSO control and 4.5 mM MTZ-treated transgenic larvae (8 hrs after MTZ treatment, when DA neurons are morphologically intact). PCR of equal long-length nuclear or mitochondrial DNA products was carried out using primers as previously described [33,34]. This

data uncovered a significant damage of mitochondrial DNA but not nuclear DNA in MTZ-exposed individuals (Figure 2.2). The nuclear DNA was unaffected possibly due to protection by nucleosomes; this observation also supports the notion that the time of our assessment precedes that of overt neurodegeneration.

We next performed *in vivo* time-lapse imaging, which uncovered mitochondrial dysfunction in morphologically intact DA neurons after MTZ treatment. These include reduced mitochondrial number, increased mitochondrial length, decreased motility and velocity. Interestingly, in MTZ-treated DA neurons, mobile mitochondria moved exclusively in retrograde direction toward neuronal soma, suggesting that they are targeted for repair and/or mitophagy (Figure 2.3B-F). Together, mitochondrial defects are observed prior to DA neurodegeneration in the NTR-MTZ model, suggesting that mitochondrial DNA damage and ensuing mitochondrial dysfunction is likely a cause rather than a consequence of DA neuron degeneration.

Given the observed mitochondrial deficits prior to neurodegeneration in the NTR-MTZ model, we next wondered whether enhancing the activity of genes functioning in mitochondrial quality control would protect against neurodegeneration in the model. Homozygous *parkin* mutations account for the majority of early onset autosomal recessive PD [35]. The *parkin* gene encodes a conserved E3 ubiquitin ligase that promotes mitochondrial quality control [36]. The zebrafish Parkin protein is approximately 80% identical to the human counterpart in functionally relevant domains. We therefore synthesized mRNAs encoding full-length human *parkin* gene or EGFP (control) and micro-injected them into 1-cell stage *Tg[fuguth:gal4-uas:NTRmCherry]* embryos. Because of the short-lived nature of microinjected mRNAs, we treated control or *parkin* mRNA-injected embryos with MTZ at an earlier stage, 30 hrs post fertilization (hpf), and subsequently imaged at 50 hpf. This regimen of MTZ administration similarly led to DA neuron loss.

Moreover, increased expression of Parkin significantly protected DA neurons (Figure 2.4A). Remarkably, increased expression of *pink1* and *DJ-1*, two other genes associated with mitochondrial quality control [37], was also neuro-protective (Figure 2.4B-C). In the case of *pink1*, the kinase dead mutant form failed to show protective effects, further validating the specificity of our assay system (Figure 2.4B). Human a-synuclein, associated with a dominant form of PD, did not show any protection, consistent with its toxic rather than neuroprotective nature (Figure 2.4D-E). These results suggest that DA neuron degeneration in the NTR-MTZ model can be alleviated by enhancing the activity of mitochondrial quality control genes.

### 2.4.2 A whole organism DA neuron-imaging based chemical screen identifies inhibitors of RAAS signaling as neuroprotective

We have previously described a high throughput *in vivo* brain imaging method using zebrafish larvae [38]. Using this method and the established DA neuron degeneration model as described above, we screened >1400 bioactive compounds (SelleckChem) that are part of the UCSF Small Molecule Discovery Center (SMDC) bioactive screening set. Many have validated biological and pharmacological activities, with demonstrated safety and effectiveness in preclinical and clinical research, and some are FDA-approved therapeutics. A dual-flashlight plot of Brain Health Score (BHS) and strictly standardized mean difference (SSMD) score were generated to quantitatively document the effects of each compound on DA neuron integrity (Figure 2.5). Compounds were then manually selected based on high BHS and SSMD scores for secondary hit validation. Olmesartan, captopril, and aliskiren, all of which inhibit the RAAS pathway (Supplemental Figure 2.1), were found to be strong neuroprotective hits that are more efficacious than N-acetyl cysteine (NAC) (Supplemental Figure 2.2, Figure 2.6), an available over-the-counter supplement

with substantial anti-oxidant properties that works primarily by restoring body's natural antioxidant glutathione [39]. Additionally, a Wilcoxon rank-sum test comparing all 13 RAAS pathway inhibitors from the primary screen with the entire screening library uncovered a significantly higher SSMD score for RAAS Inhibitors (Figure 2.7).

In our primary screen and secondary validations, prophylactic dosing was used (i.e., screening compounds were added earlier than MTZ). In order to determine whether the neuroprotective benefits of RAAS inhibitors can be observed after MTZ treatment (i.e., mimicking therapeutic dosing), we carried out MTZ ablation 8 hrs or 24 hrs prior to administering olmesartan (Supplemental Figure 2.4A). In both cases, olmesartan showed significant neuroprotection, suggesting that RAAS inhibitors can be beneficial even after the onset of neurotoxic insults (Supplemental Figure 2.4B).

With PD being highly associated with motor symptoms and occurring mostly in adult populations, we next determined whether RAAS inhibitors are capable of restoring motor function in adult *Tg[fuguth:gal4-uas:NTRmCherry]* zebrafish treated with MTZ. Prolonged treatment of MTZ with or without RAAS inhibitors was performed over the period of two weeks in adult transgenic zebrafish accompanied by locomotor behavioral tracking (Figure 2.8A). As a positive control, we used levodopa, a gold standard symptomatic drug that can restore motor function in PD patients by increasing DA release from surviving neurons [3,6]. Compared to vehicle controls, MTZ-treated animals showed a progressive decline of locomotive ability for the first 5 days post MTZ treatment and then reached steady low levels. Co-administration of levodopa one day after MTZ did not prevent initial locomotor decline, but was able to subsequently restore locomotor function, and interestingly, a hyper-locomotor state was reached at Day 14. The chronic use of levodopa leading to hyperactivity is previously reported in mouse

studies [40,41]; also, uncontrolled involuntary muscle movement such as dyskinesia is a common side effect of chronic levodopa use in humans [42]. In contrast to levodopa, administration of the RAAS inhibitor olmesartan one day after MTZ fully ameliorated locomotor defects (Figure 2.8B). The bioavailability of RAAS inhibitors in the brain and their ability to cross the blood brain barrier (BBB) are not well understood [43,44]. In particular, whether olmesartan enters the brain and the conversion of the pro-drug to its active carboxylate form is not known. Upon 14 days of treating with olmesartan medoxomil, the pro-drug form of olmesartan, mass spectrometry was performed, which detected the presence of active olmesartan in the adult zebrafish brain (Figure 2.8C).

Finally, to verify whether the chemical inhibitors indeed target RAAS signaling components to exert their neuroprotective effects in zebrafish, we knocked down the angiotensin receptor 1 (*agtr1*) gene activity. Two genes (*agtr1a* and *agtr1b*) encode *agtr1* in vertebrates including zebrafish. We designed morpholino (MO) antisense oligonucleotides that inhibited protein translation (ATG MO) (Supplemental Figure 2.3A), and micro-injected them into 1-cell stage embryos. Using an *agtr1* antibody, we verified the protein knockdown in *agtr1a and 1b* double morphants (Supplemental Figure 2.3C). The morphants appeared morphologically normal. At 5 dpf, control and morphants were treated with 9 mM MTZ for 24 hrs. Significant DA neuron protection was observed in *agtr1b* and *agtr1a&1b* double morphants, the extent of which was comparable to Olmesartan treatment (Figure 2.9, Supplemental Figure 2.3B). These data suggest that inhibition of *agtr1* protects against DA neuron degeneration.

### 2.4.3 *agtr1* inhibition in DA neurons is neuroprotective

The RAAS pathway as a peptidergic system is composed of ligands and G-protein coupled receptors (GPCRs) classically known to regulate blood pressure and salt retention [45,46]. RAAS inhibitors are widely used drugs for treating high blood pressure. In recent years, RAAS signaling expression is detected outside vasculature and in the central nervous system [47,48]. To understand the potential contribution of neuronal RAAS to DA neuron degeneration, we first performed qPCR on DA neurons purified by Fluorescence-Activated Cell Sorting (FACS) from the anterior brains of 5-day old *Tg[fuguth:gal4-uas:GFP; uas:NTRmCherry]* larvae. qPCR results uncovered enriched expression of pro-renin receptor, angiotensinogen, *agtr1a*, *agtr1b*, and Angiotensin Converting Enzyme (*ace*), whereas the expression of *renin* and *ace2* was undetectable in DA neurons compared to the rest of non-DA cells (Figure 2.10).

To address the role of neuronal RAAS, we performed CRISPR-mediated conditional knockout [49,50] of *agtr1a* and *agtr1b* in DA neurons (Figure 2.11). Eight different sgRNAs for each gene were designed and screened to identify those with high knockout efficiency (Supplemental Figure 2.6A-B). The Gal4-UAS system was used to selectively express the Cas9 enzyme under the control of tyrosine hydroxylase promoter. DNA constructs containing both the UAS-Cas9 and U6 promoter-driven sgRNAs were delivered into one-cell stage *Tg[th1:gal4; uas:NTRmCherry]* embryos, followed by quantification of DA neuronal integrity. We found that larvae conditionally expressing Cas9 and effective *agtr1a* and *agtr1b*-targeting sgRNAs (Supplemental Figure 2.6B) preserved greater DA neuron intensity than those expressing control scrambled sgRNAs following MTZ treatment (Figure 2.12). These results suggest that inhibition of *agtr1* in DA neurons is neuroprotective.

### 2.4.4 RAAS inhibitors are neuroprotective for DA neurons in a chemically induced Gaucher's Disease model

Given that NTR-MTZ-induced DA neuron degeneration does not occur in human patient settings, we next tested whether RAAS inhibitors are neuroprotective in other models relevant to human PD. Mutations in the *glucocerebrosidase* (*gba*) gene causing Gaucher's disease (GD) are the most common genetic risk factor for PD [23]. Chemical inhibition of GBA has been successfully used to model the disease in both mice [51] and zebrafish [52], whereas the zebrafish genetic model for GD has a much weaker and later-onset DA neurodegeneration phenotype [53].

We first observed that the GBA inhibitor conduritol B-epoxide (CBE) dose-dependently reduced DA neuron integrity and locomotor activity in larval zebrafish, with 500 mM in the medium yielding significant results (Supplemental Figure 2.5). We next tested whether olmesartan exerts a protective effect against CBE-induced DA neuron loss and locomotor deficit. Levodopa was used in comparison. While both levodopa and olmesartan were able to ameliorate locomotor deficits induced by CBE (Figure 2.13), only olmesartan was able to rescue TH immunoreactivity deficits induced by CBE treatment (Figure 2.14). Furthermore, CBE preferentially damaged TH neurons as revealed by the double immunofluorescent staining of TH and 5HT (serotonin) (Figure 2.14). Together, these results demonstrate that RAAS inhibitors are not only neuroprotective in the synthetic NTR-MTZ model but is also neuroprotective in a Gaucher's disease model. They also reinforce the validity of the NTR-MTZ synthetic model for neuroprotective small molecule screening.

### 2.4.5 DA neuron-specific RNA-seq reveals that the AGTR1 inhibitor olmesartan restores the expression of mitochondrial electron transport pathway genes disrupted by neurotoxic insults

To further understand the molecular basis underlying the neuroprotective effects of RAAS inhibitors, we carried out DA neuron-specific RNA-seq (Figure 2.15A). *Tg[th1:gal4; uas:NTRmCherry]* larvae were treated with vehicle, CBE, MTZ, olmesartan, CBE+olmesartan, or MTZ+Olmesartan for a defined time window, followed by FACs purification of DA neurons from anterior brains and cell type-specific RNA-seq. MTZ and CBE models were theretofore referred to as neurotoxic models. Upon annotating the sequence reads with the GRCz11 genome assembly, normalizing the read counts, and plotting all the significant gene expression changes ($\alpha$=0.05, FDR=0.1), we noted that the two neurotoxic models shared significant overlap and formed distinct clusters compared to the DMSO- or olmesartan alone control groups. Furthermore, co-treatment with olmesartan in both neurotoxic models restored transcriptomic expression to levels that were similar to controls, especially on the transcriptomes up-regulated in the neurotoxic models (Figure 2.15B). Pathway enrichment analysis with the Reactome and KEGG pathway database showed 28 significantly altered pathways in the neurotoxic models when compared to the vehicle controls, with many of these pathways relating to the mitochondrial electron transport chain ($P<0.01$). Interestingly, the differential gene expression common to both neurotoxic models in comparison to vehicle controls also showed high significance (LogP =-2.55) for the PD KEGG pathway (ID: hsa05012). These results further reinforce the notion that the neurotoxic models used in this study are highly relevant to PD.

Cluster analysis of the gene ontology and pathways using g:Profiler, DAVID (version 6.8)[54], and Metascape [55] GO enrichment revealed distinct ontology clusters that were commonly altered in both neurotoxic models compared to controls. Importantly, several pathways related to

the mitochondrial function such as ATP synthesis, oxidative stress, and electron transport chain showed the highest significance values (Figure 2.16A). Moreover, the addition of olmesartan to the neurotoxic models most significantly affected the clusters related to mitochondrial function, including respiratory electron transport, oxidative phosphorylation, ATP metabolic process, and inorganic cation transport, when compared to the neurotoxic models (Figure 2.16B).

Given the prominence of mitochondrial pathway gene alterations in the neurotoxic models and by olmesartan, we further examined the molecular nature of these genes. As described earlier, preferential mitochondrial DNA damage was observed in DA neurons of the NTR-MTZ model prior to neuronal loss (Figure 2.1). There is also a strong link to mitochondrial dysfunction in lysosomal storage diseases [56] . Thus, disruption of mitochondrial gene expression is possibly causal to DA neuron degeneration in these models. The expression of 1248 genes were commonly altered in the two neurotoxic models compared to vehicle controls (Figure 2.17A), while the expression of 507 genes were commonly altered by olmesartan co-treatment in comparison to each of the neurotoxic insult alone ($\alpha$=0.05, FDR=0.1) (Figure 2.17B). The differentially expressed genes related to mitochondrial function were divided into up-regulated and down-regulated categories. 14 genes that were significantly up-regulated in the neurotoxic models behaved oppositely upon olmesartan treatment. They function in the mitochondrial electron transport chain (e.g., Complex I, III, IV, and V) and TOM-TIM complex critical for protein translocation through the mitochondrial membrane. One gene, *trim3*, which was significantly down-regulated in the neurotoxic models, was up-regulated by olmesartan co-treatment (Figure 2.17). Trim3 (Tripartite motif containing 3), with reported ubiquitin ligase activity, is found to be down-regulated in PD patient plasma [57] and can attenuate apoptosis via activating PI3K/AKT signaling pathway in PD models [58]. Many of these mitochondrial

pathways were no longer significantly altered when comparing the olmesartan+CBE or olmesartan+MTZ groups to the vehicle control group (Table 1.2). Taken together, these findings suggest that active AGTR1 receptor is necessary for upregulating the expression of mitochondrial electron transport pathway genes and down-regulating *trim3* upon neurotoxic insults. Inhibiting its activity can help restore normalcy of these pathways, leading to neuro-protection.

### 2.4.6 The AGTR1 inhibitor olmesartan rescues the phenotypes of *pink1*-deficient *Drosophila*

*Drosophila* offers a plethora of genetic PD models in which DA neuronal loss is evident [59,60]. The conserved PINK1-Parkin pathway that directs mitochondrial quality control (MQC) has been originally delineated in flies [24,61–64]. These models have been used in genetic and pharmacological testing for genes and agents that offer neuroprotection [65].

Although the RAAS pathway similar to vertebrates has not been fully described in *Drosophila*, genes encoding the angiotensin converting enzymes are detected in this species [66]. Recently, it has also been reported that RAAS inhibitors rescue memory defects in a *Drosophila* Alzheimer's disease model [67]. We therefore tested olmesartan in the *Drosophila pink1* model, which recapitulates key features of PD including mitochondrial dysfunction, aberrant mitochondrial morphology, DA neuron and muscular degeneration [24,63,64]. The most robust phenotype of the *pink1* mutant flies is the degeneration of their indirect flight muscle caused by the accumulation of dysfunctional and morphologically aberrant mitochondria. This results in flies with collapsed thorax (thoracic indentation) and abnormal wing posture, manifested as

droopy or held-up wings as opposed to the straight wings in control animals. Treatment of *pink1* mutant flies by feeding them with food containing 100 mM olmesartan resulted in significant rescue of wing posture (Figure 2.18A-C) and the thoracic indentation (Figure 2.18D-F). The abnormal mitochondrial morphology and neuronal loss phenotypes in DA neurons were also rescued (Figure 2.18G-J). Collectively, these results suggest that olmesartan's protective effect is conserved across species.

### 2.4.7 RAAS inhibitors slow down disease progression in human PD patients

Since RAAS inhibitors are commonly used anti-hypertensives, this provided us with an opportunity to ask whether the neuroprotective benefits of RAAS inhibitors shown in zebrafish and *Drosophila* can be observed in human PD patients. We used the Parkinson's Progression Markers Initiative (PPMI) database, which includes a total of 423 *de novo* PD patients, 308 of which had complete data (accurate medication and medical history records for each visit throughout the longitudinal study, no missing records on age, gender, duration of PD, and high visit compliance with no more than 3 missing records for motor assessment score). The *de novo* PD patients refer to subjects who have a diagnosis of PD for two years or less and are not taking any PD medications at the time of enrollment. Among them, 96 patients were on RAAS inhibitors (RAAS) while 212 patients were not (non-RAAS). Among the non-RAAS cohort, 42 patients were hypertensive and taking other medications such as calcium channel blockers or diuretics for the management of hypertension (Figure 2.19A).

Using this dataset, we sought to compare PD progression in patients on RAAS inhibitors to those who were not. At present, there are no accepted progression biomarkers for PD [68]. The

Unified Parkinson's Disease Rating Scale (UPDRS), while widely utilized, suffers from limitations including subjectivity and ambiguities in the written text [69]. Because of the wear-off and debilitating side effects of levodopa after prolonged use [70,71], clinicians delay the prescription of levodopa to PD patients until absolutely necessary (i.e., at the onset of debilitating motor symptoms). Studies have shown that early initiation of levodopa does not impact disease progression [10] and late levodopa administration can also be a strategy to prolonging the levodopa-induced dyskinesia-free period [72]. Therefore, we used the Time-to-Levodopa as a quantifiable and objective parameter to measure disease progression. Our analysis uncovered that patients on RAAS inhibitors had a significantly delayed onset of levodopa therapy compared to the patients not on RAAS inhibitors (difference, -5.8; 95% CI -11.26 to -0.4254; P=0.035) (Figure 2.19B). To control for hypertension as a variable, we compared patients on RAAS inhibitors to those on other classes of anti-hypertensive medications. This analysis also uncovered a significant effect of RAAS inhibitors in delaying the onset of levodopa therapy as shown in the Kaplan Meier curve (P=0.032) (Figure 2.19C).

The UPDRS scores part I, II, and III were also examined for a subset of patients within each cohort whom were levodopa-naïve for at least 3 years; this subset of patients was chosen since levodopa use can significantly influence the UPDRS scores. The UPDRS part I score, which examines the mentation, behavior, and mood, showed a significantly lower score in the cohort on RAAS inhibitors compared to the cohorts not on RAAS inhibitors or those taking other hypertensive medications over the course of 5 years (difference: NO RAAS vs RAAS=0.289, Other HTN vs RAAS=0.266, P=0.017) (Figure 2.19D). The UPDRS part 2 and part 3 did not show significance in patients taking RAAS inhibitors when compared to other cohorts (P=0.82)

(Supplemental Figure 2.8F). Taken together, these data suggest that inhibition of RAAS signaling slows down disease progression in human PD patients.

## 2.5 Discussion

For most neurodegenerative disorders, there exist no disease-modifying therapeutics [73]. Here we validated the NTR-MTZ-based chemo-genetic DA neuron degeneration model in zebrafish by showing that DA neuronal loss is preceded by preferential mitochondrial DNA damage and ensuing mitochondrial dysfunction. We then used this system to conduct a whole organism imaging-based chemical screen and identified the inhibitors of Renin-Angiotensin (RAAS) system to be significantly neuroprotective. The RAAS system is a G-protein coupled receptor (GPCR) signaling pathway well known for salt homeostasis and vasoconstriction [74] but not for neurodegeneration. Using cell type-specific CRISPR-mediated genome editing, we uncovered that disruption of the angiotensin receptor 1a and 1b (*agtr1a* and *agtr1b*) in DA neurons is significantly neuroprotective. Dopamine neuron-specific RNA-seq further revealed the molecular action of RAAS signaling in regulating the expression of genes important for mitochondrial function. Inhibition of RAAS signaling was also neuroprotective in a zebrafish model of Gaucher's disease (GD), a *Drosophila pink1* model, and human PD patients. Together, this study identifies RAAS inhibitors as promising therapeutics for slowing down PD progression and highlights a new approach composed of high content screening in zebrafish, cross-species validation, and examination of human clinical data to uncover previously unrecognized neuro-protective agents and underlying mechanisms.

Since its introduction, the NTR-MTZ-mediated cell ablation has been used for a wide array of studies including tissue regeneration and developmental biology [75,76]. Although MTZ has historically been widely prescribed as an antibiotic through its effective coverage of gram-negative bacteria, the underlying mechanism of cell death in vertebrates has however remained elusive. By investigating the integrity of mitochondrial and nuclear DNAs, performing live imaging of mitochondria, and DA neuron-specific RNA-seq, we link the mode of NTR-MTZ-mediated cell death to mitochondrial dysfunction for the first time to our knowledge. This property, together with its safe and scalable nature, makes the NTR-MTZ-mediated cell ablation model in larval zebrafish a valuable small molecule drug discovery tool for a variety of disorders where mitochondrial dysfunction is a prevalent underlying pathophysiological mechanism. Given the synthetic nature of the model, it is advisable that additional validation in etiologically relevant models as we have done in this study are to be carried out.

Our unbiased small molecule screen together with cross-species validation and mechanistic characterizations has revealed that inhibition of RAAS signaling is significantly neuroprotective for DA neurons in the context of animal PD models and moreover human PD patients, through a plausible mechanism of regulating mitochondrial function. Hits that target different components of the RAAS pathway (e.g., renin, ACE, and *agtr1*) were initially uncovered from the primary screen and were validated in secondary screening. The AGTR1 inhibitor olmesartan was further shown to be effective in adult zebrafish, in a zebrafish Gaucher's disease (GD) model, and *Drosophila pink1*-deficient model. The GD model was created by inhibiting the disease-causing GBA protein with a chemical inhibitor CBE, previously shown to be effective in both mice and zebrafish [51,52]. This chemically induced GD model presents several advantages over the genetic model of GD [53]: First, it shows significant DA

neuronal loss at larval stages, whereas the genetic GD model only exhibit weak and variable deficit of DA neurons at adult stages. Second, it can be conveniently combined with transgenic lines that label DA neurons. Also, its conditional nature allows us to have temporal control and gain access to DA neurons prior to degeneration at desired and controllable stages. Cell type-specific RNA-seq has revealed a close link between GBA inhibition and mitochondrial dysfunction, whereas inhibition of RAAS signaling can in part restore mitochondrial function. The finding that RAAS inhibitors are also neuroprotective in the *Drosophila pink1*-deficient model suggests that the underlying neuroprotective mechanisms are deeply conserved across evolution. Intriguingly, literature search has uncovered reports of RAAS inhibitors' neuroprotective effects in various animal models of neurodegeneration, but the mechanisms were not described in these studies [77–79]. Our findings corroborate with these reports and further demystify the actions of RAAS inhibitors, by showing that *agtr1*a and 1b act cell autonomously in DA neurons rather than their conventional actions on the vasculature systems.

Our DA neuron-specific RNA-seq has identified mitochondrial pathway genes and *trim3*, the expression of which was perturbed in the neurotoxic models and moreover restored by RAAS inhibition. While the up-regulation of mitochondrial electron transport chain gene expression or downregulation of *trim3* gene expression in the neurotoxic models may be viewed as a possible compensatory response, the observation of their restoration by AGTR1 inhibition that coincides with neuroprotection argues the contrary. Future experiments to alter the expression of these genes either individually or in combination followed by evaluating DA neuron states will help further verify the cause-effect relationships. Several lines of evidence suggest that RAAS signaling via active *agtr1* may play a direct role in promoting neurodegeneration via disrupting mitochondrial function: First, among the pathways that are commonly altered in morphologically

intact DA neurons from both neurotoxic models, those that regulate mitochondrial function have the highest significance values (e.g., oxidative phosphorylation and respiratory electron transport). The same was true when evaluating the effect of olmesartan on both neurotoxic models. The ~40 mitochondria-related genes were mostly nuclear genes that encode proteins ranging from electron transport chain subunits such as NADH ubiquinone, cytochrome-c oxidase, and ATP synthase to mitochondrial translocation machinery. Second, AGTR1 expression is detected in the mitochondria of a variety of cell types including DA neurons [80,81], lending support that it may have a direct role in regulating mitochondrial function. Indeed, transcription factors that directly activate mitochondrial electron transport chain gene expression include Nuclear Respiratory Factor (NRF-1 and NRF-2), and Peroxisome Proliferator-activated receptor-gamma Coactivator 1 (PGC-1) family of co-activators, Stimulatory Protein 1 (Sp1), Estrogen related receptor a (ERRa) and Ying Yang 1 (YY1) [82]. AGTR1 is reported to promote reactive oxygen species production and activate MAP kinase pathway that leads to the activation of transcription factors including NF-kB and AP-1, and P53 in the context of vascular senescence [83]. Intriguingly, significant upregulation of AP-1 was observed in both neurotoxic models, suggesting the following possible model: Neurotoxic insults activate AGTR1, which activates kinase signaling cascades that upregulate the expression of AP-1 among other transcription factors, in turn increasing the expression of mitochondrial electron transport chain genes. Future follow-up studies on the genes and pathways discovered in this cell type-specific RNA-seq dataset shall promise to provide deeper insights into how active *agtr1* perturbs mitochondrial function and aggravates neurodegeneration.

The evolutionarily conserved actions of RAAS inhibitors together with their prevalent use for anti-hypertension in PD patients prompted us to examine and subsequently discover their

significant effect in slowing down PD progression. Previous studies that interrogate electronic health records (EHR) data reported mixed results regarding the effect of RAAS inhibitors on the incidence of PD [84,85]. Given the diverse and complex etiology of PD, this is not surprising. In this study, rather than evaluating the incidence of PD, we focused on PD progression using the Time-to-Levodopa therapy as a criterion in addition to the commonly used UPDRS score. A significant effect of RAAS inhibitors was detected in delaying the time to levodopa therapy. This innovative marker for disease progression can also be applied to other EHR or clinical data where exam metrics are incomplete because of inadequate hospital protocols or text mining is difficult due to variations in note taking practices by healthcare workers [86,87]. Our sample size of 308 PD patients is relatively modest. It would therefore be of interest to further expand this analysis to a larger patient population. It is also worth noting that the blood-brain-barrier (BBB) permeability of RAAS inhibitors vary from compounds to compounds, with a subset showing better ability to cross the BBB than others [43,44,88]. With expanded patient population, it would be possible to evaluate and compare the BBB profile of RAAS inhibitors and their extent of neuroprotection. Given the cell autonomous mechanisms that we have discovered through animal studies, we postulate that RAAS inhibitors with better BBB penetrating ability will possibly have a higher neuroprotective effect.

## 2.6 Figures

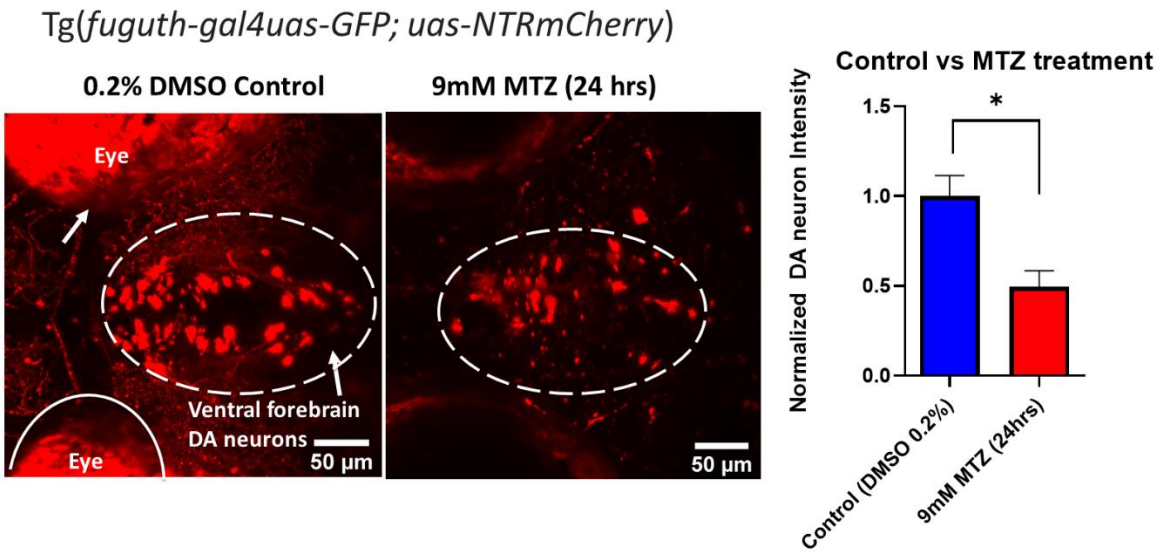


**Figure 2.1. The zebrafish NTR-MTZ chemo-genetic DA neuron ablation model causes specific damage to dopamine neurons.** Confocal images of DA neurons in 0.2% DMSO control and 9 mM MTZ-treated transgenic larval zebrafish brains show significant difference in normalized fluorescent intensity (n = 10; $P$ <0.05, unpaired t test).

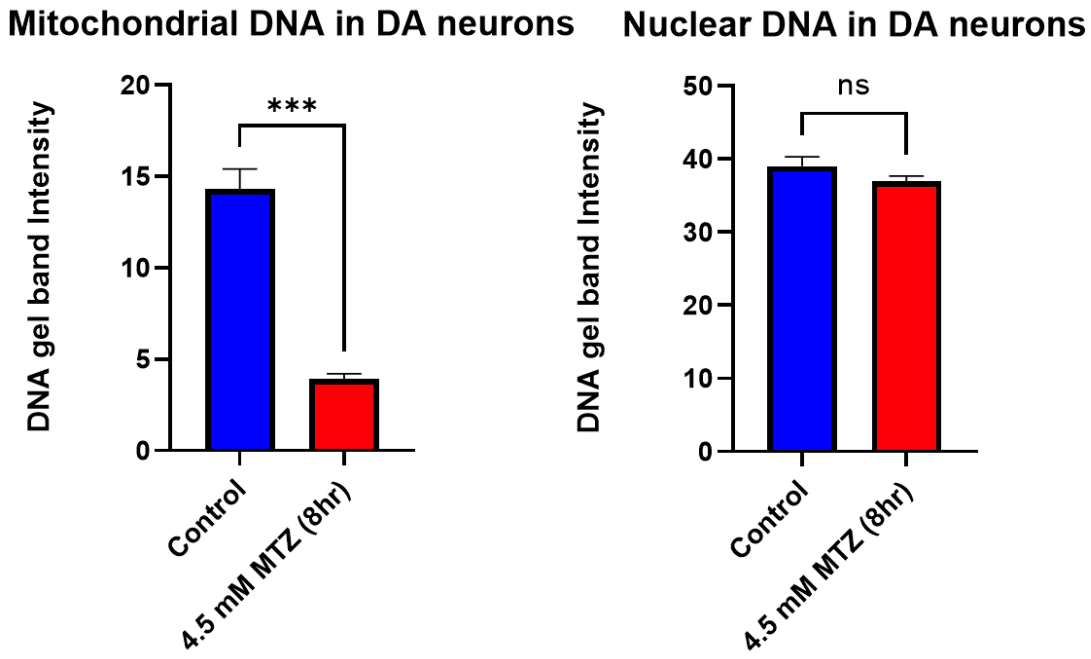


**Figure 2.2 The mitochondrial DNA shows damage in the zebrafish NTR-MTZ chemo-genetic DA neuron ablation model while nuclear DNA remains intact.** Long-range PCR of mitochondrial DNA versus nuclear DNA products using FACs-sorted DA neurons from control and MTZ-treated larval zebrafish (4.5 mM, 8 hrs) (n=4 pools of 25 larval brains per pool; *P* <0.01, unpaired t test).

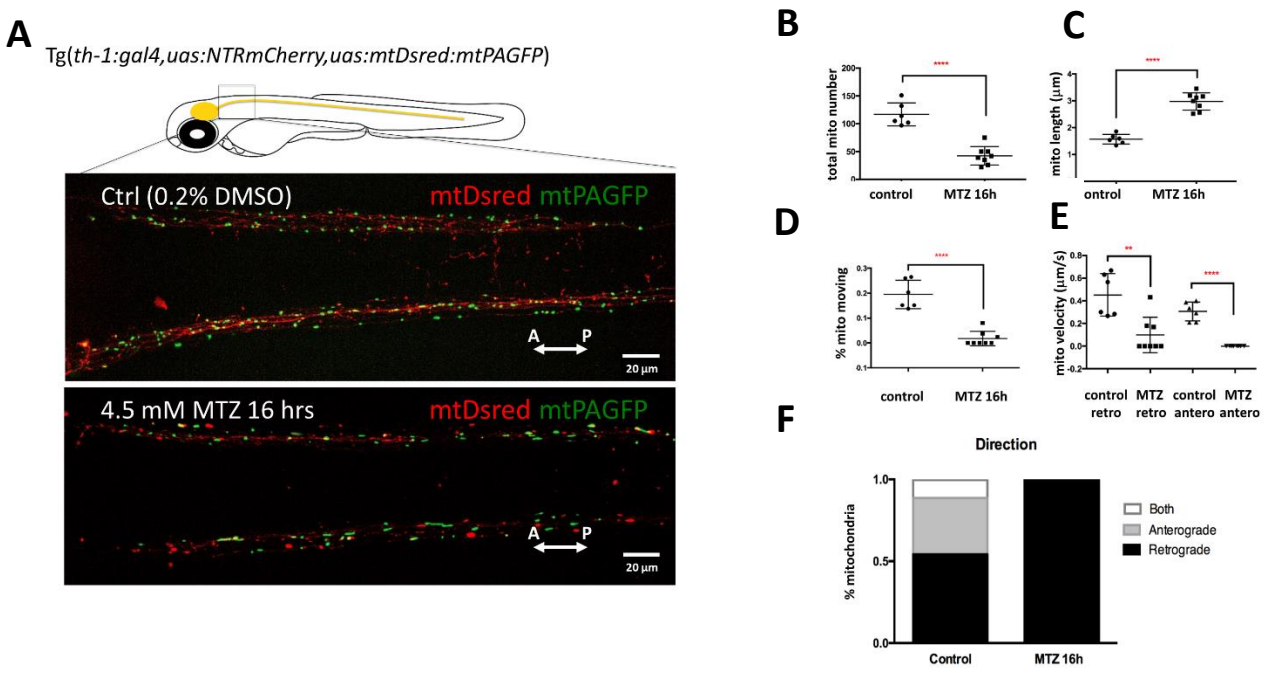


**Figure 2.3 The mitochondrial dynamics show impairment in motility, count, and reduced velocity of movement (A)** Live confocal imaging of mitochondrial dynamics with mitochondria-targeted DsRed and mitochondria-targeted photoactivatable GFP in 5dpf larvae treated with 0.2% DMSO (control) or 4.5 mM MTZ for 16 hrs. **(B-F)** Analysis of mitochondrial dynamics including total mitochondrial count, length, % moving, velocity, and direction of movement between control and MTZ-treated samples (n=8 to 10; ***P*<0.01, *****P*<0.0001, unpaired t test).

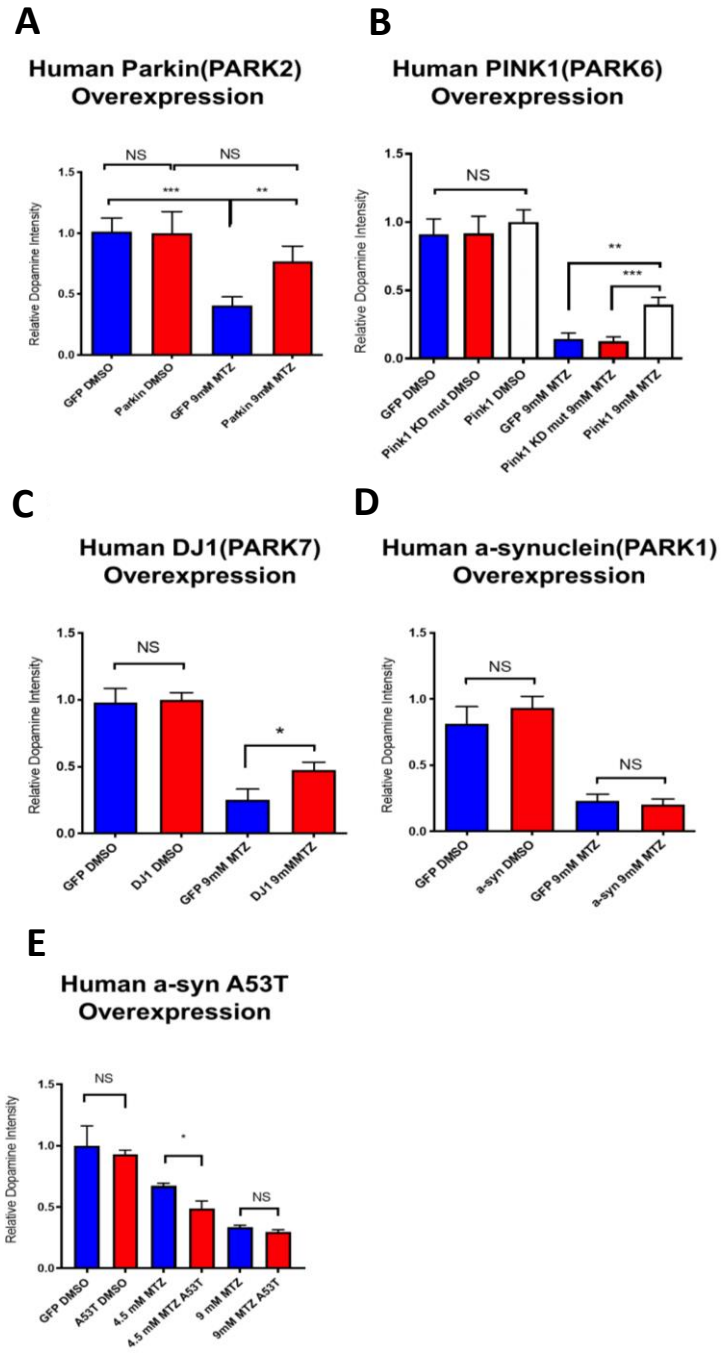


**Figure 2.4 Overexpression of PD-associated human genes including PARK2, PARK6, PARK7, PARK1, and associated mutant forms. (A-E)** mRNAs were microinjected into 1-cell stage transgenic embryos and treated with 4.5 or 9mM MTZ at 30hpf for 24hrs to determine the neuroprotective effect of experimental conditions compared to control GFP-encoding mRNA injection (n=10 to 12; **P*<0.05, ***P*<0.01, ****P*<0.001, unpaired t test).

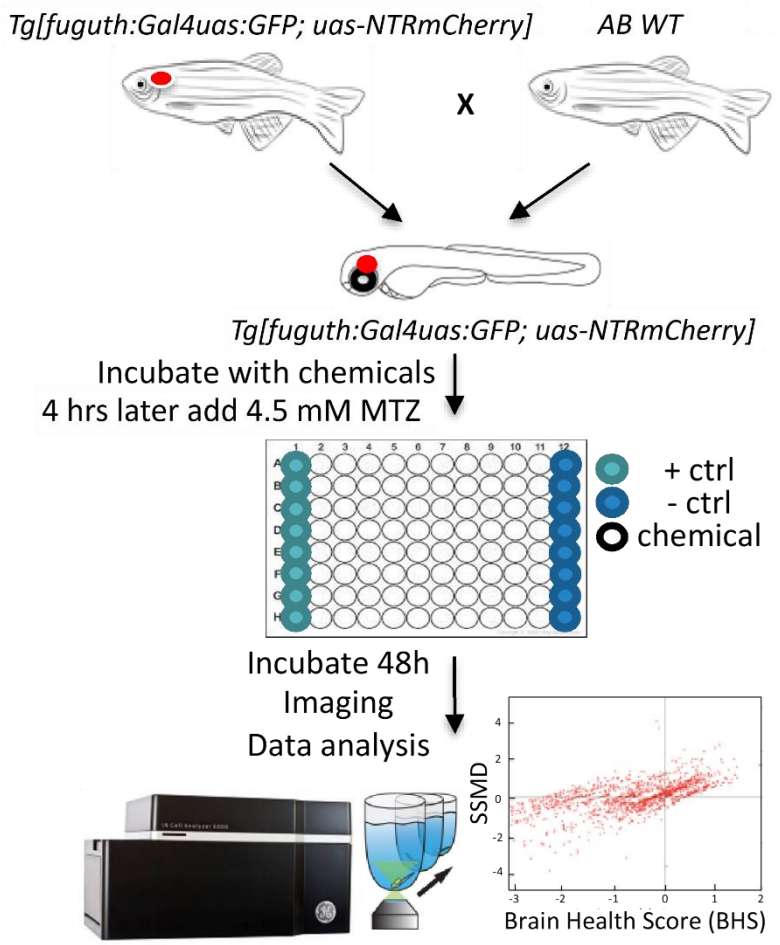


**Figure 2.5 Schematic of the high throughput in vivo imaging-based chemical screen, plate design, time point, and data analysis.** A flow chart outlining the screening pipeline. 5dpf transgenic larvae expressing *Tg[fuguth:gal4-uas:GFP;uas:NTRmCherry]* were arranged in glass bottom 96-well plates and treated with MTZ (4.5 mM, 48hrs) along with each of the 1403 bioactive compounds (n=3 per screening compound). The dual flashlight plot of Brain Health Score (BHS) and Strictly standardized mean difference (SSMD) score was used to quantify the neuroprotective effects of all compounds in the screen.

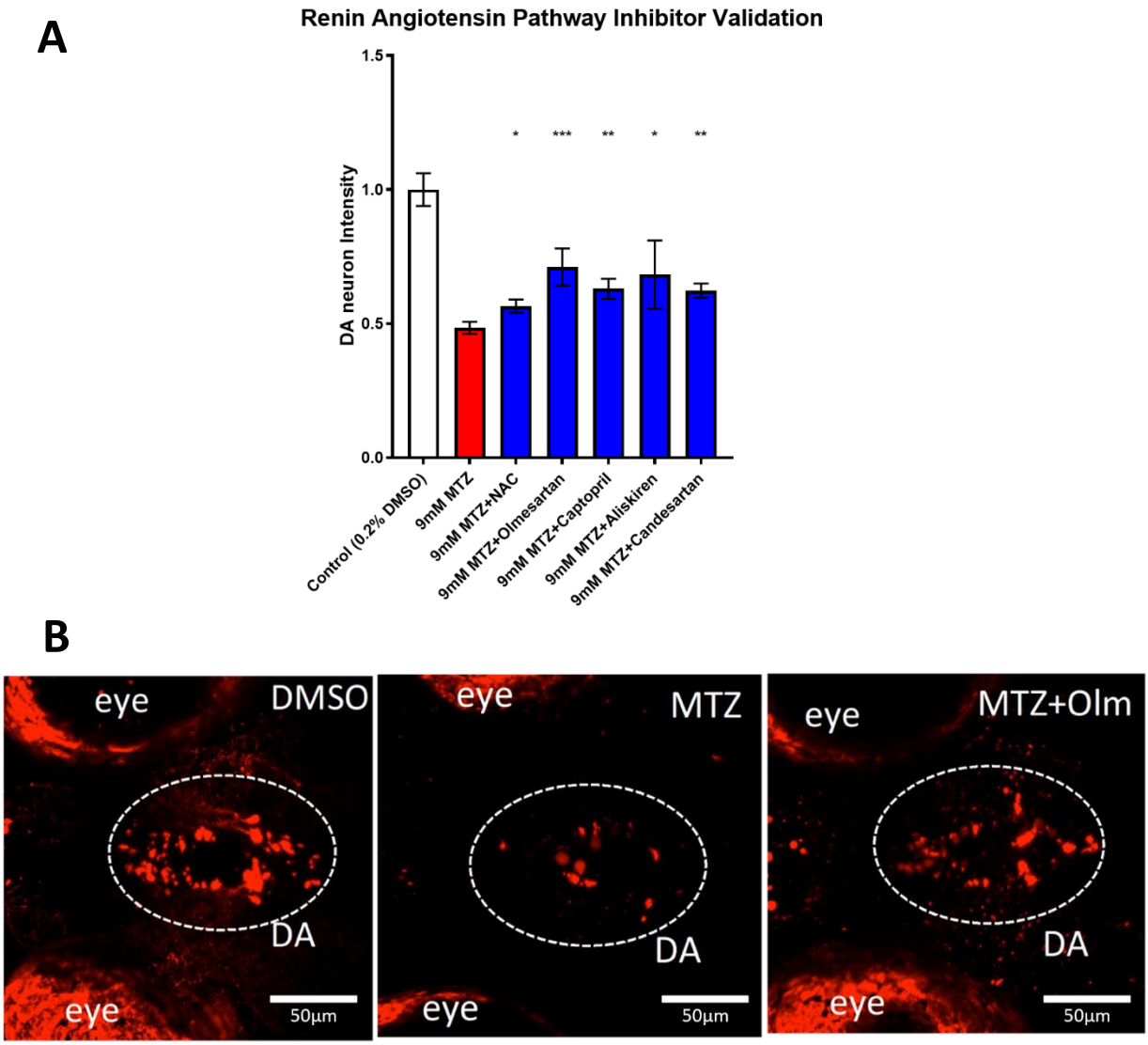


**Figure 2.6 A high throughput in vivo imaging-based chemical screen uncovers the neuroprotective effects of inhibiting the renin-angiotensin (RAAS) pathway. (A)** Secondary hit validation of RAAS inhibitors (10µM) in comparison to the N-acetyl cysteine (NAC) control compound was performed with increased sample size (n=40 per group; **P*<0.05, ***P*<0.01, ****P*<0.001, unpaired t test). **(B)** Confocal images of brain DA neurons. Positive control (0.2% DMSO), negative control (9mM MTZ), and 9mM MTZ+10µM olmesartan following 24hrs of treatment

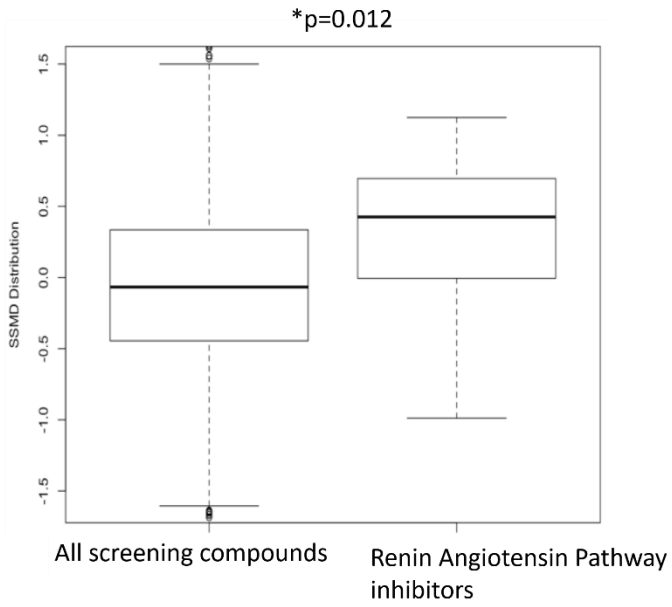


**Figure 2.7 Pathway analysis of the entire screening database shows RAAS pathway to be neuroprotective.** Wilcoxon rank sum test was performed to compare data of all 1403 compounds with those representing RAAS inhibitors (n=13) in the screened compound set, revealing a significantly higher SSMD score distribution in the RAAS inhibitor group (P=0.012, Wilcoxon rank sum test).

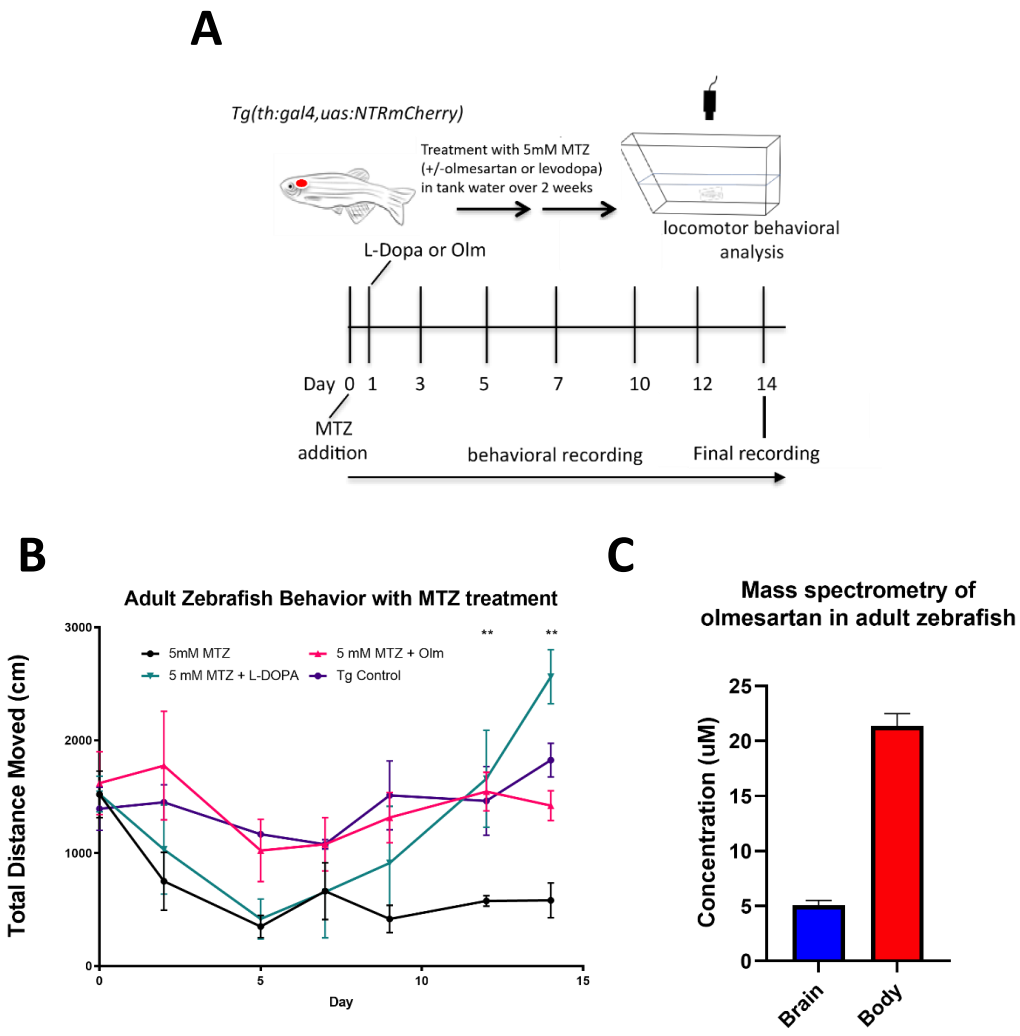


**Figure 2.8 Adult behavior test shows olmesartan improves total distance moved compared to MTZ treatment alone (A)** Schematic of the chronic drug treatment and behavior test for adult zebrafish. **(B)** Quantification of total distance traveled across 5-min recording in the home tank for adult zebrafish treated with 0.2% DMSO (positive control), 5mM MTZ (negative control), 5mM MTZ+10mM levodopa, and 5mM MTZ+10mM olmesartan (with daily change of drug solutions after behavioral recording). Distance recordings were conducted for baseline, 3d, 6d, 9d, 12d, and 14d. ANOVA and post-hoc Tukey test showed significant difference in 12d and 14d for the MTZ versus MTZ+olmesartan treated groups. [n=6 (3 males, 3 females) for MTZ and MTZ+Olm, n=4 (2 males, 2 females) for DMSO control and levodopa; $P<0.01$, one-way ANOVA post-hoc Tukey's test]. **(C)** Mass spectrometry data of adult zebrafish homogenized brain versus body samples after 14 days of chronic treatment with Olmesartan (n=6, 3 males and 3 females).

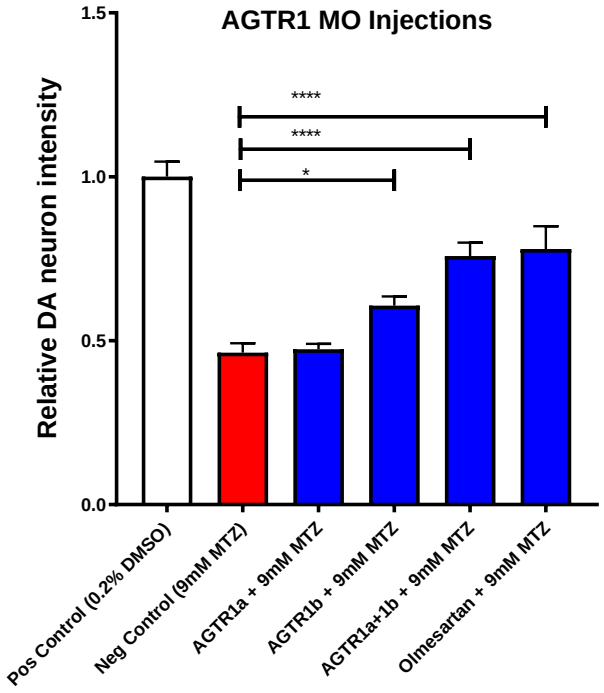


**Figure 2.9 Transient knockdown of agtr1 with morpholino oligonucleotides shows rescue of DA neurons with MTZ treatment** Quantification of relative fluorescent intensity of DA neurons at 6 dpf in positive control (0.2% DMSO), negative control (9mM MTZ, 24hrs from 5 dpf to 6 dpf), *agtr1a* morphant+9mM MTZ, *agtr1b* morphant+9mM MTZ, agtr1a/agtr1b double morphant+9mM MTZ, and 10µM olmesartan + 9mM MTZ (n=10 to 12; **P*<0.05, ****P*<0.001, unpaired t test).

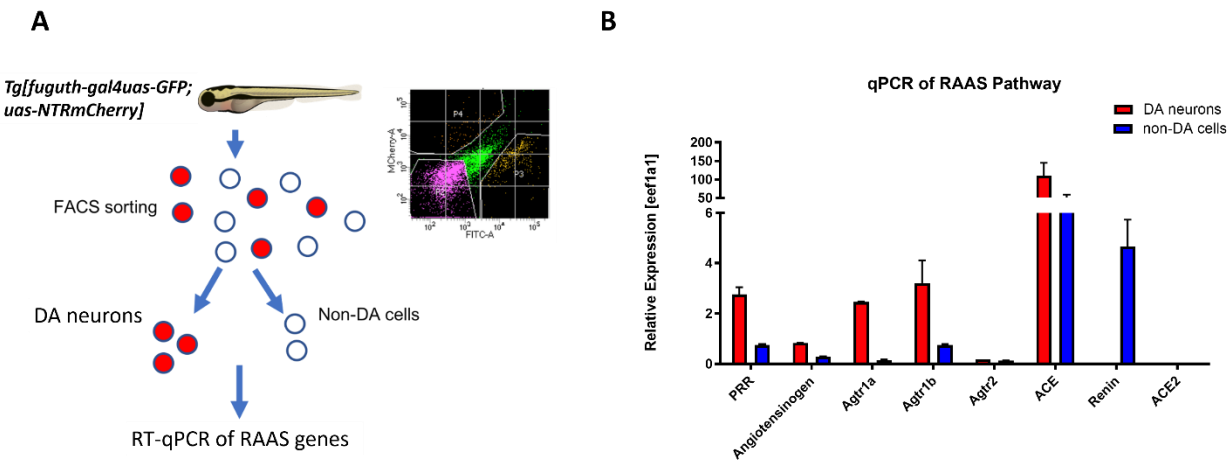


**Figure 2.10 The RAAS pathway genes are expressed in isolated DA neurons of larval zebrafish (A)** Schematic showing the procedure of FACs to isolate DA neurons for qPCR analysis of RAAS pathway gene expression. **(B)** qPCR data of 5dpf larval samples show the relative expression of RAAS pathway genes normalized to the house-keeping gene *elf1a*, in DA neurons (red bars) versus non-DA cells (blue bars). *PRR* (prorenin receptor), *agtr1a* (Angiotensin II receptor, type 1a), *agtr1b* (Angiotensin II receptor, type 1b), *agtr2* (Angiotensin II receptor, type 2), *ace* (Angiotensin I converting enzyme), *ace2* (Angiotensin I converting enzyme 2) (n=2 biological replicates, 6 technical replicates).

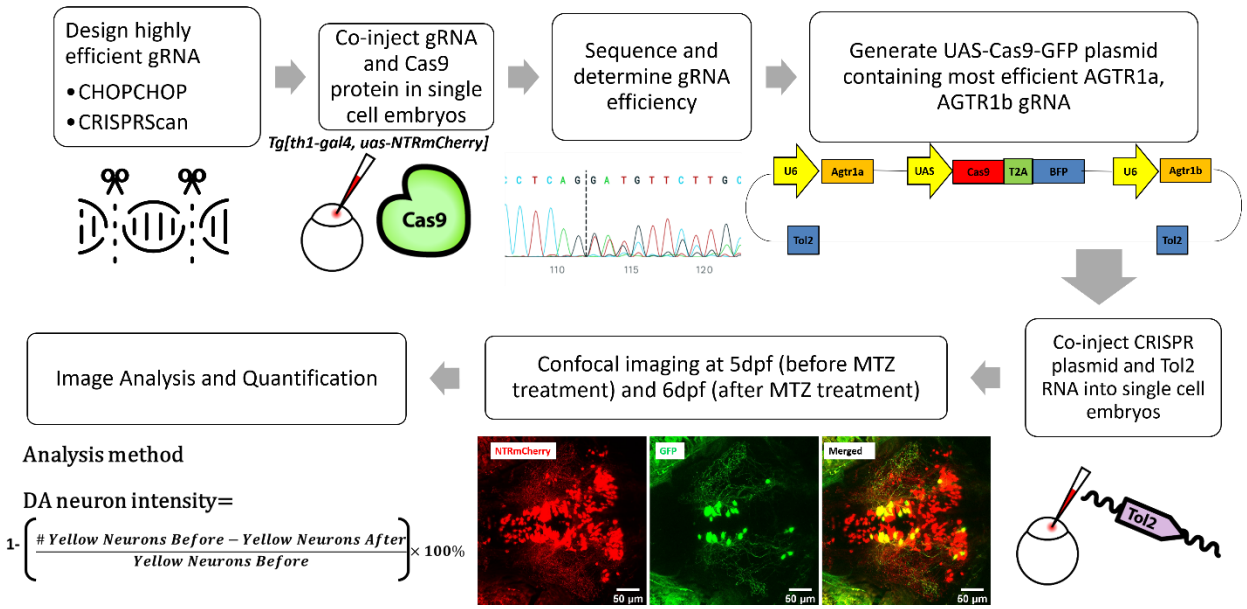


**Figure 2.11 schematic showing the conditional CRISPR design, imaging, and analysis procedure to inactivate agtr1a and agtr1b in DA neurons.** CHOPCHOP and CRISPRScan databases were used to generate highly efficient gRNA. The gRNA efficiency was initially validated by co-injecting with Cas9 protein and pooling the larvae for sequencing. The most efficient gRNA designs (agtr1a5, agtr1b6) were cloned in the UAS-Cas9-T2A-GFP plasmid with U6 promoters left and right as shown in the figure. The cloned plasmid was injected with Tol2 RNA for efficient integration during the single cell stage. The injected larvae were imaged before and after MTZ treatment. The colocalized GFP and Mcherry neurons were used for quantification.

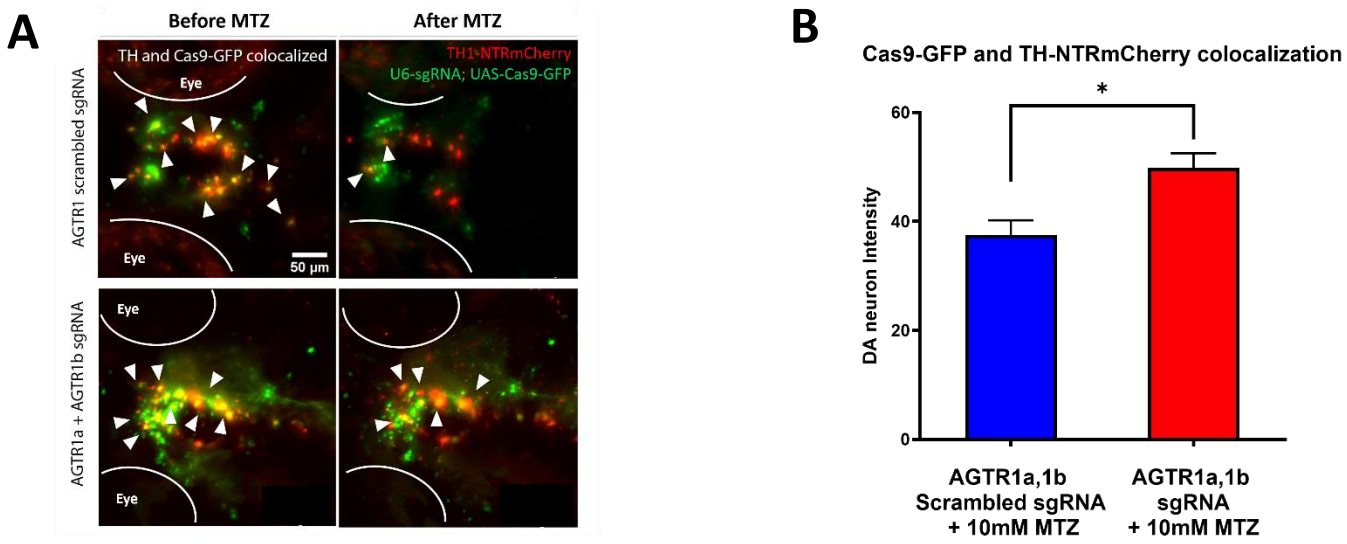


**Figure 2.12 Specific knockout of agtr1 in larval DA neurons is neuroprotective against MTZ damage. (A)** Confocal images of DA neurons in 5dpf (before MTZ treatment) and 6dpf (24hr after 10 mM MTZ treatment) larvae injected with either the scrambled control sgRNA construct (top) or the effective *agtr1a* and *agtr1b* sgRNA construct (bottom). Yellow cells express both NTR-mCherry and Cas9. **(B)** Quantification shows a significant preservation of DA neuron intensity in the *agtr1a* and *agtr1b* sgRNA construct-injected animals compared to the scrambled sgRNA control upon 10mM MTZ treatment. (n=15, $P<0.01$, unpaired t-test)

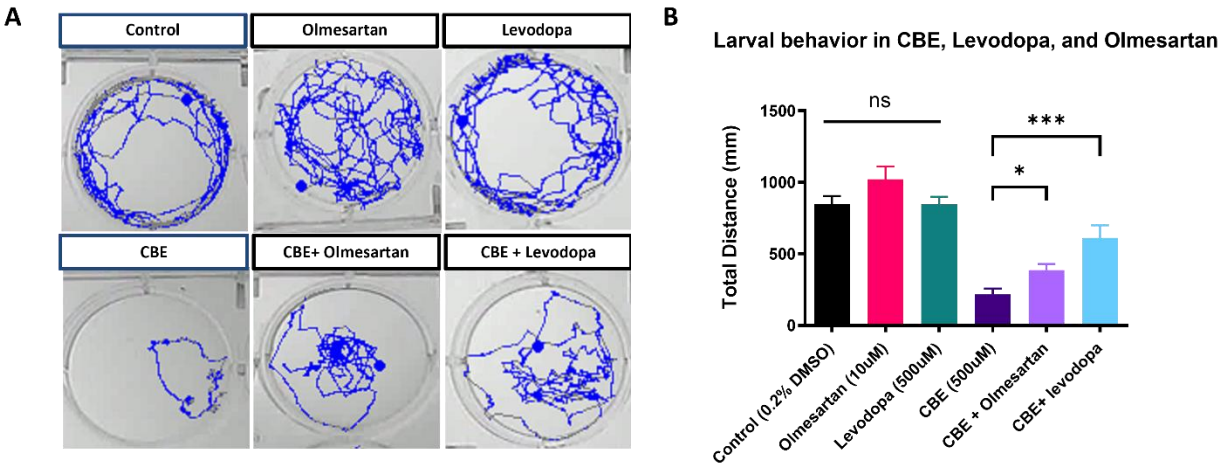


**Figure 2.13 The AGTR1 Inhibitor olmesartan shows behavioral rescue in a chemically induced Gaucher's disease model. (A)** Locomotor tracks of 5 dpf larvae treated 24hrs with 0.2% DMSO, 500µM CBE, 10µM olmesartan, and 500µM levodopa. The background subtraction method was used to identify and track movement for 5 min duration. **(B)** Quantification of total distance (in millimeters, mm) travelled during 5-min recordings for each sample group. Drugs were added at the indicated concentrations and incubated for 24hrs before behavioral recording (n=12 to 13; **P*<0.05, ****P*<0.001, unpaired t test)

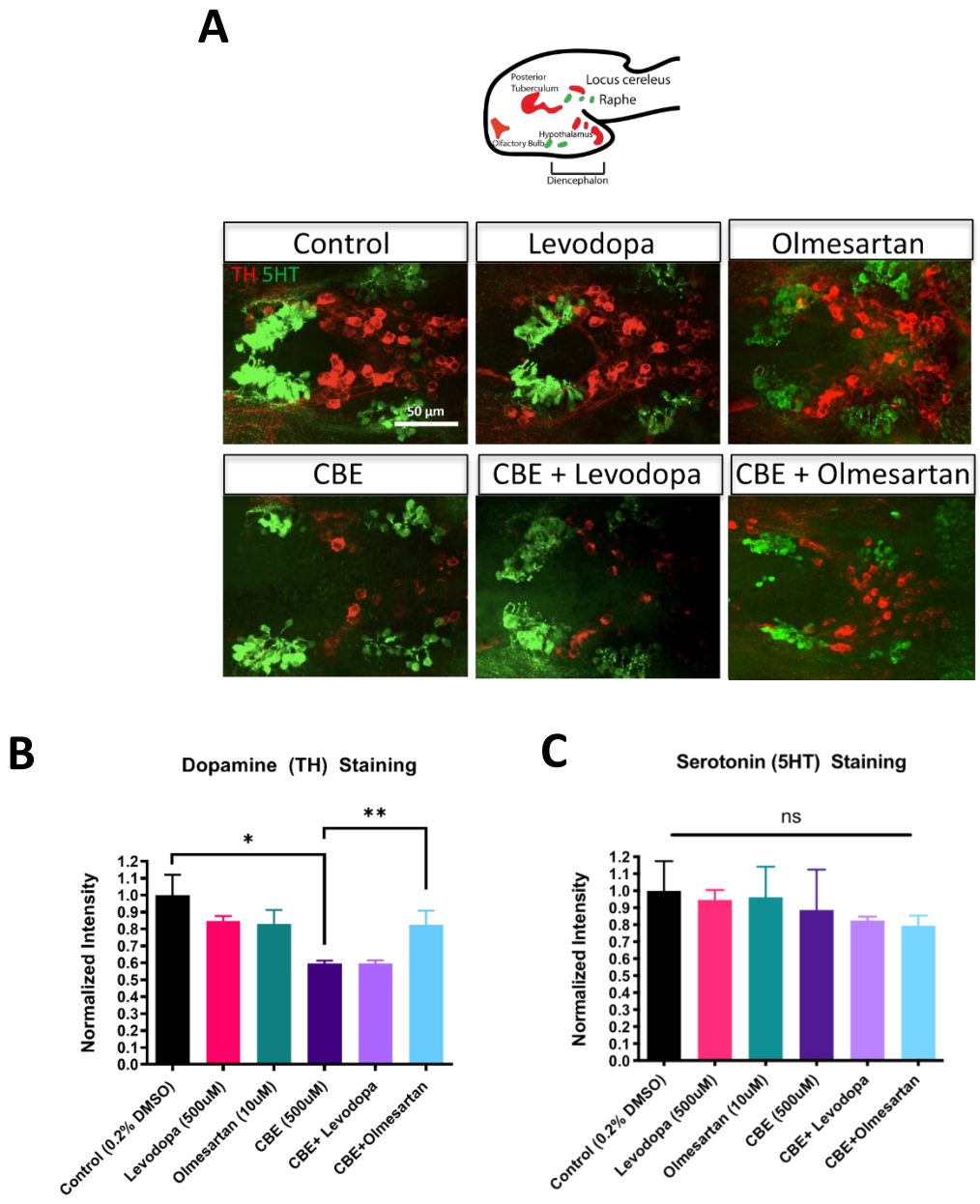


**Figure 2.14 Immunohistochemistry shows neuroprotective effects of AGTR1 Inhibitor olmesartan with CBE treatment. (A)** Confocal images of TH-immunoreactive DA neurons (red) and 5HT-immunoreactive serotonin neurons (green) in 6dpf larval zebrafish brains after treatments as indicated in Figure 2.12B. **(B-C)** Quantification for (A). Fluorescent intensity was quantified using ImageJ and normalized against the control (0.2% DMSO) (n=8; **P*<0.05, ***P*<0.01, unpaired t test).

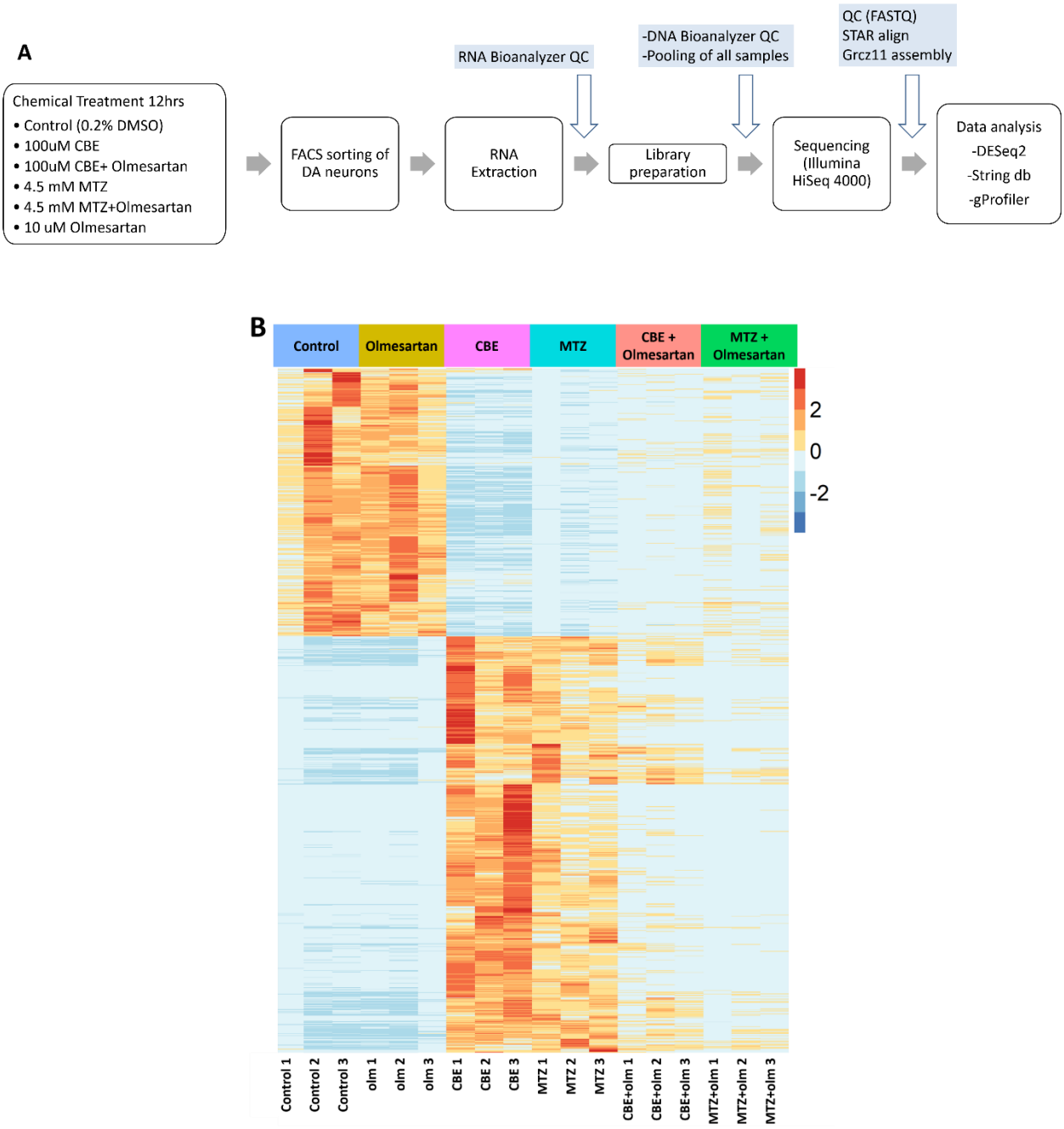


**Figure 2.15 DA neuron-specific RNA-seq uncovers neurotoxic insult-induced alterations of mitochondrial pathway gene expression that is in part restored by the AGTR1 inhibitor olmesartan. (A)** A schematic showing the RNA-seq procedure of larval samples from chemical treatment to FACs, library preparation, and differential gene expression analysis. **(B)** A heatmap of clustering analysis comparing the differential gene expression in DMSO control, olmesartan, CBE, MTZ, MTZ+olmesartan, and CBE+olmesartan treatment groups. Gene counts were normalized and analyzed with the R program DESeq2 package. All samples are numbered 1, 2 and 3 to indicate biological replicates.

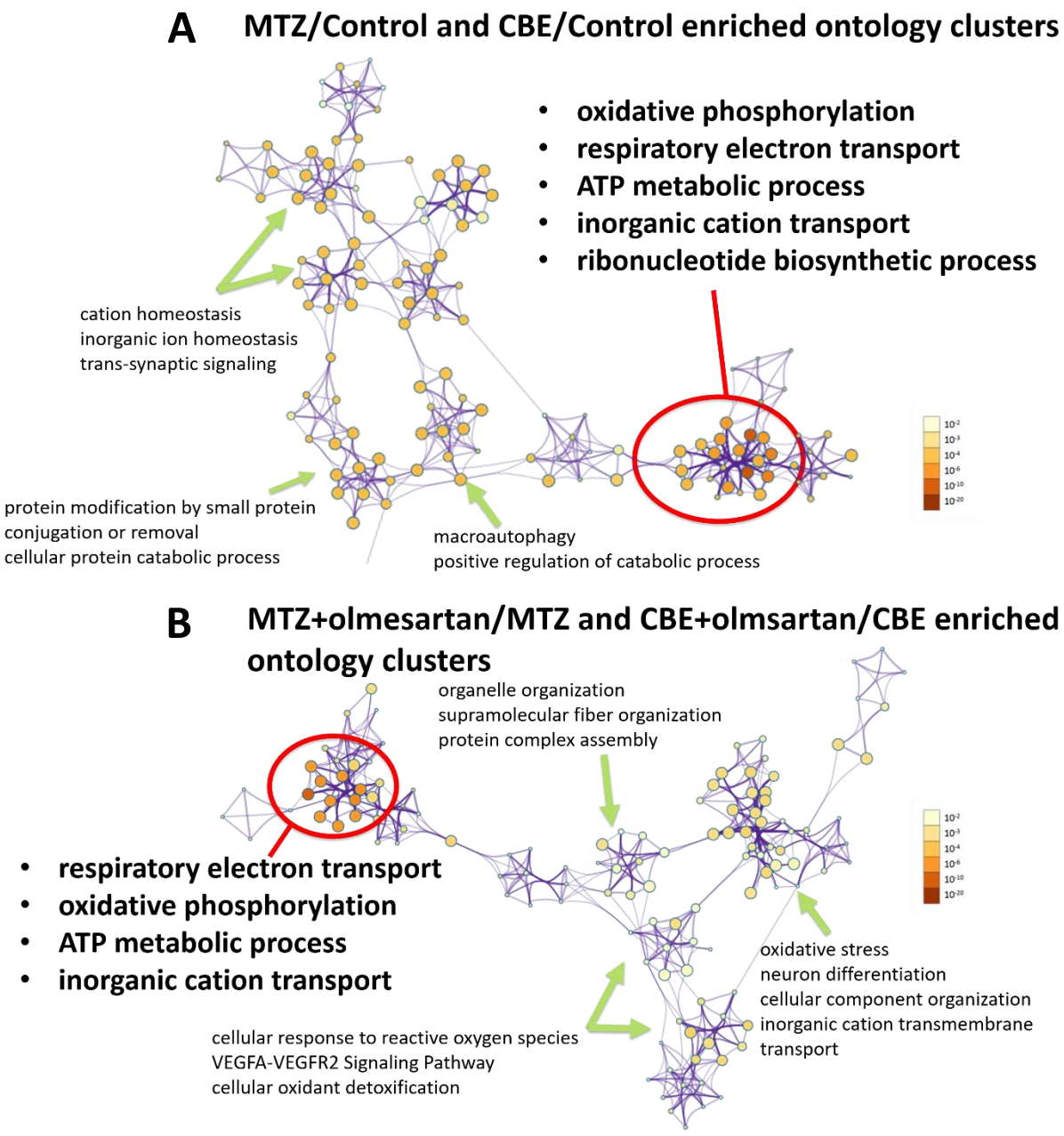


**Figure 2.16 Metascape pathway analysis shows GO enrichment relating to the mitochondrial electron transport chain for MTZ and CBE treatment (A-B)** Metascape ontology clusters highlighting the relationship of the top enriched GO terms for the overlapping differential gene expression for MTZ/Control and CBE/Control (A) and MTZ+olmesartan/MTZ and CBE+olmesartan/CBE (B). The colors of the nodes correspond to significant values. The size of the nodes is proportional to the number of input genes in the GO term.

**A**

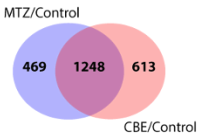


| Significantly upregulated mito-expressed genes common in MTZ/C and CBE/C | Significantly downregulated mito-expressed genes common in MTZ/C and CBE/C |
|---|---|
| ***Atp5l:*** ATP synthase, H+ transporting, mitochondrial F0 complex, subunit g **(C-V)**<br>***coa5:*** cytochrome c oxidase assembly factor 5<br>***cox5aa, cox5ab, cox6a1, cox6c, cox7a2a, cox7c, cox8a, mt-co3***: cytochrome c oxidase subunit 5Aa, 5Ab, 6A1, 6C, 7A2a, 7C, 8A, III **(C-IV)**<br>***cycsb***: cytochrome c, somatic b **(C-III)**<br>***mdh2***: malate dehydrogenase 2, NAD (mitochondrial)<br>***mrpl13, mrpl32, mrpl36***: mitochondrial ribosomal protein L13, L32, L36<br>***mrps18c, mrps21***: mitochondrial ribosomal protein s18C, S21<br>***ndufa1, ndufb2, ndufs4, ndufv2***: NADH:ubiquinone oxidoreductase subunit A1, B2, S4, core subunit V2 **(C-I)**<br>***timm9***: translocase of inner mitochondrial membrane 9<br>***tomm6, tomm20a, tomm20b***: translocase of outer mitochondrial membrane 6, 20<br>***uqcc3***: ubiquinol-cytochrome c reductase complex assembly factor 3<br>***uqcr10***: ubiquinol-cytochrome c reductase, complex III subunit X | ***atad3***: ATPase family AAA domain containing 3A<br>***bnip3la***: BCL2 interacting protein 3 like<br>***cpox***: coproporphyrinogen oxidase<br>***ctnnbip1***: catenin beta interacting protein 1<br>***kcnh3***: potassium voltage-gated channel subfamily H member 3<br>***mthfd1l***: methylenetetrahydrofolate dehydrogenase (NADP+ dependent) 1 like<br>***slc25a37***: solute carrier family 25 member 37<br>***timm17b***: translocase of inner mitochondrial membrane 17B<br>***top1mt***: DNA topoisomerase I mitochondrial<br>***trim3***: tripartite motif containing 3 |

**B**

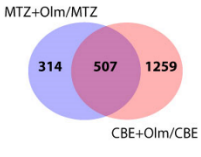


| Significantly upregulated mito-expressed genes common in MTZ+Olm/MTZ and CBE+Olm/CBE | Significantly downregulated mito-expressed genes common in MTZ+Olm/MTZ and CBE+Olm/CBE |
|---|---|
| ***trim3***: tripartite motif containing 3<br>***rims3***: regulating synaptic membrane exocytosis 3<br>***phldb1***: pleckstrin homology like domain family B member 1 | ***Atp5l:*** ATP synthase, H+ transporting, mitochondrial F0 complex, subunit g<br>***cox4i2, cox5aa, cox6a1, cox6c, cox7a2a, cox7c, cox8a:*** cytochrome c oxidase subunit 4I2, 5Aa, 6A1, 6C, 7A2a, 7C, 8A<br>***cox20***: cytochrome c oxidase assembly factor 20<br>***cyc1***: cytochrome c-1<br>***mrpl13, mrpl33, mrpl35, mrpl54:*** mitochondrial ribosomal protein L13, L33, L35, L54<br>***mrps2, mrps18c, mrps36***: mitochondrial ribosomal protein S2, S18C, S36,<br>***ndufa1, ndufb2, ndufs4, ndufv2***: NADH:ubiquinone oxidoreductase subunit A1, B2, S4, core subunit V2<br>***timm10***: translocase of inner mitochondrial membrane 10<br>***tomm6***: translocase of outer mitochondrial membrane 6 |

**Figure 2.17 MTZ and CBE treatment show high overlapping of differentially expressed genes (A-B)** Venn diagrams showing the overlapping gene expression alterations between different conditions: MTZ/control and CBE/control (A) and MTZ+Olmesartan/MTZ and CBE+Olmesartan/CBE (A) ($\alpha$=0.05, FDR = 0.1, Wald test). The table shows the mitochondrial function-related genes that are up-regulated and down-regulated in the two types of neurotoxic insults (A), and their significant changes in olmesartan-treated conditions (B). Names highlighted in blue and red indicate overlapping genes.

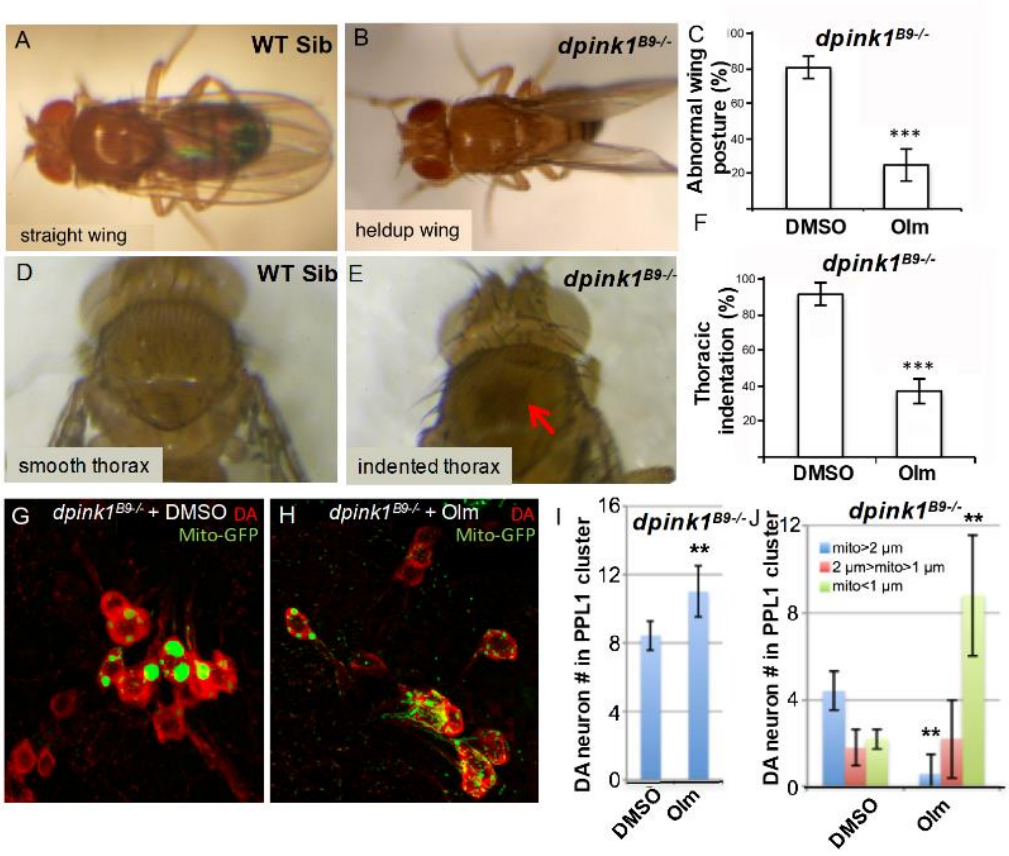


**Figure 2.18 The AGTR1 inhibitor olmesartan significantly rescues phenotypes in the Drosophila pink1 mutant model. (A-F)** images show the abnormal wing posture (B) and thoracic indentation (E) in the mutant compared to wild-type siblings (A,D). Quantification of %mutant individuals with abnormal wing posture (C) and thoracic indentation (F) showed a significant difference between vehicle- and drug (olmesartan)-treated samples. **(G-J)** Effect of olmesartan on the mitochondrial aggregation and DA neuron loss phenotypes of *pink1* mutant, in comparison to DMSO control. Mitochondria are labeled with mito-GFP reporter. Data quantification shown in I, J. (n=12; **, $P<0.01$, *** $P<0.001$, unpaired t-test).

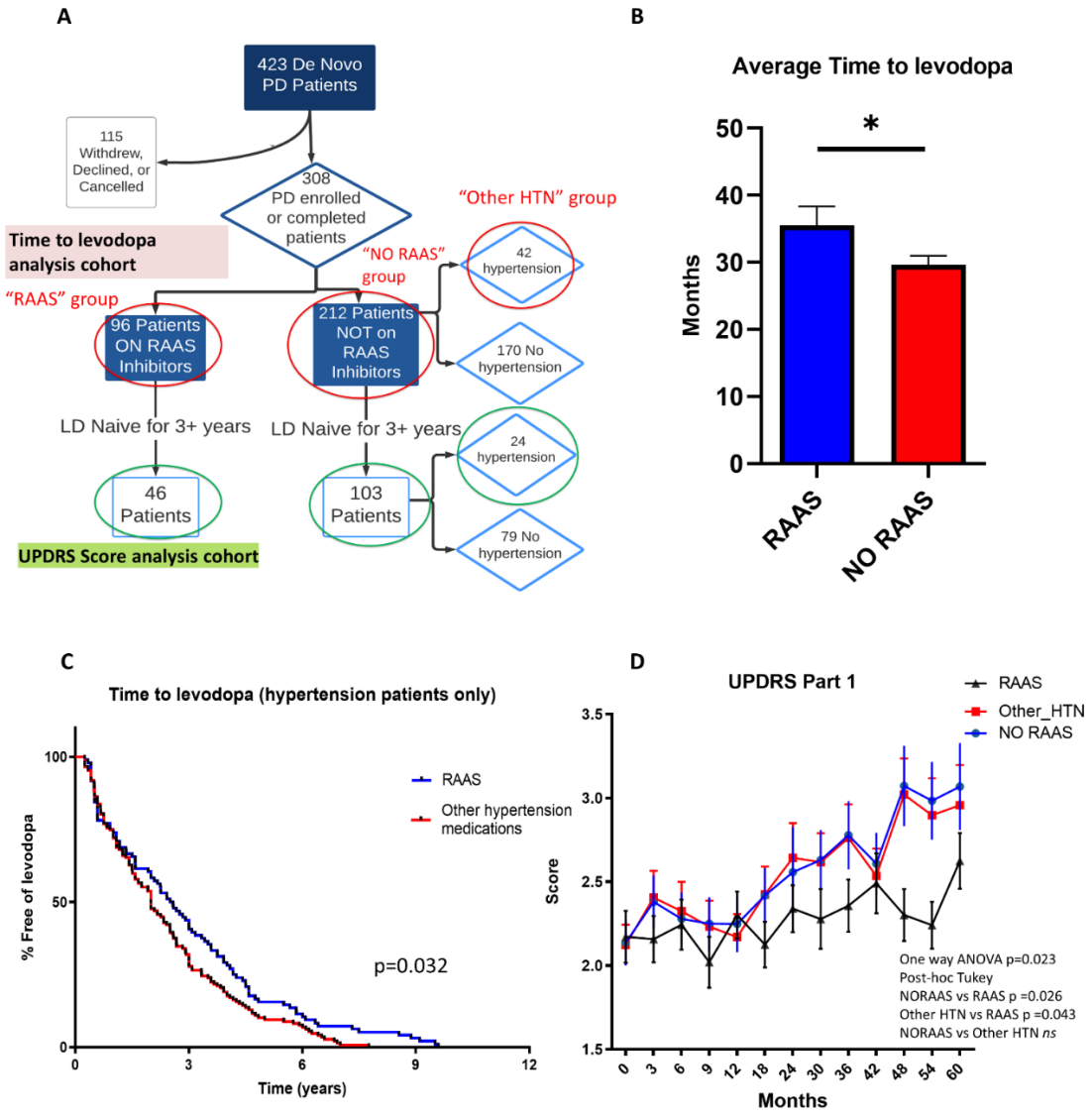


**Figure 2.19 Clinical data analysis shows delayed disease progression in PD patients on RAAS inhibitors. (A)** Flow chart showing the patient cohort studied in the PPMI data. Red circles indicate RAAS, No RAAS, and other hypertension (HTN) groups used for the time to levodopa analysis. Green circles indicate the patient cohorts not on levodopa for 3+ years that were used for the UPDRS Part 1, 2, and 3 analysis. **(B)** Average time to levodopa therapy for de novo PD patients shows significant difference in patients taking RAAS inhibitors versus patients not on RAAS inhibitors (n=96 and 212; $P<0.05$, unpaired t-test) **(C)** Kaplan Meier survival curve showing the percentage of HTN patients free of levodopa over time for those on RAAS inhibitors versus other anti-hypertensive medications. HTN patients on RAAS inhibitors showed greater percentage free of levodopa over time compared to patients on other HTN medications. (n=96 and 42; $P<0.05$, Log-rank Mantel-cox test). **(D)** UPDRS Score part 1 shows significantly worsened (higher) scores for subsequent visits in the No RAAS group and the group using other anti-hypertensives compared to the group on RAAS inhibitors (n=46, 24, and 103; $P=0.023$, one-way ANOVA, post-hoc Tukey).

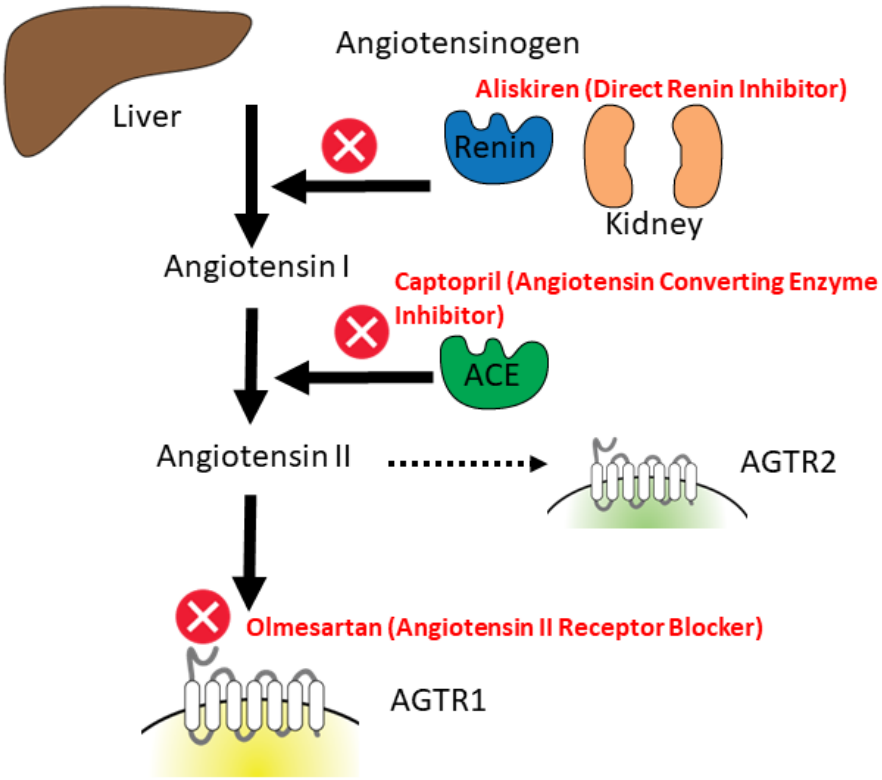


**Supplementary Figure 2.1 Overview of the classically known renin angiotensin pathway and the inhibitors identified from our high throughput screen.** Olmesartan, captopril, and aliskiren are antihypertensive medications working on the Renin-Angiotensin Signaling (RAAS) pathway by blocking the binding of angiotensin II to the receptor, inhibiting the conversion of angiotensin I to angiotensin II, and directly inhibiting the renin enzyme respectively. 10 other RAAS inhibitors also in the 1403 bioactive screen are imidapril, enalaprilat, quinapril, ramipril, moexipril, enalapril, which are angiotensin converting enzyme (ACE) inhibitors, and valsartan, telmisartan, azilsartan, and eprosartan, which are angiotensin receptor blockers (ARBs).

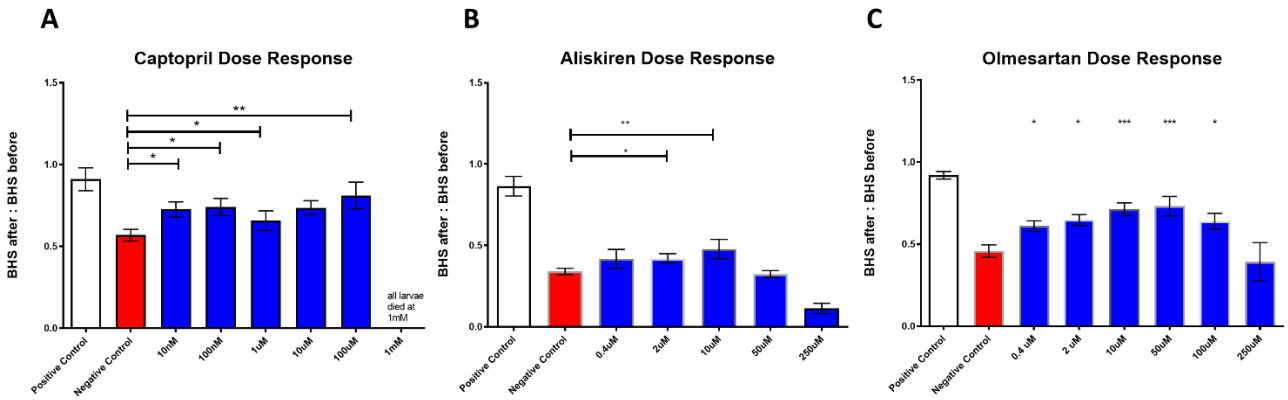


**Supplementary Figure 2.2 Dose response studies of renin angiotensin pathway inhibitors. (A-C)** Transgenic *Tg[fuguth:gal4-uas:NTRmCherry]* were imaged 5dpf (Before MTZ treatment) and 6dpf (After MTZ treatment). The Y-axis is the ratio of Brain Health Score (BHS) after vs. before MTZ treatment. The MTZ concentration for all dose response studies is 10mM. (n=12 to 24; **P*<0.05, ***P*<0.01, ****P*<0.001, unpaired t-test compared to negative control).

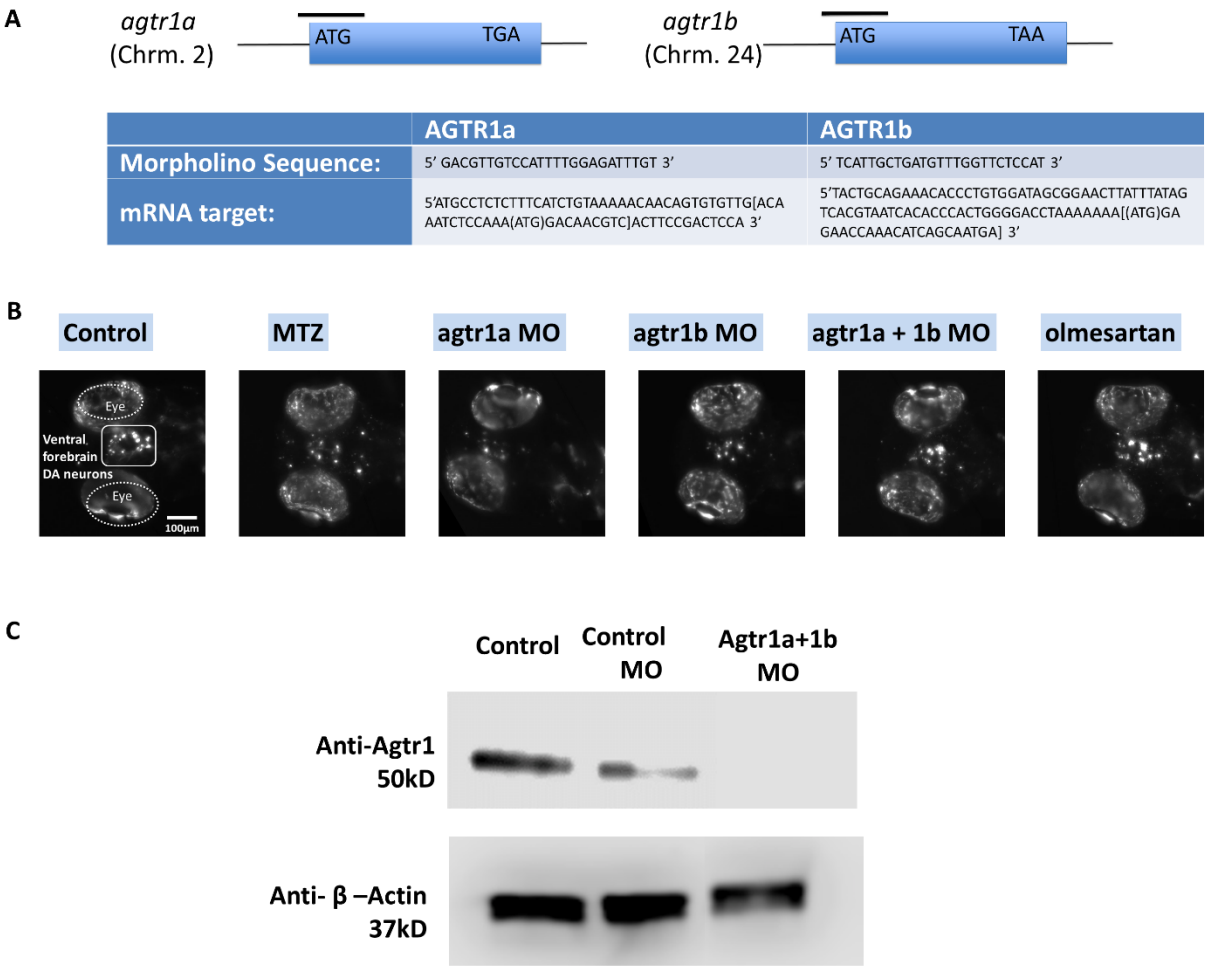


**Supplementary Figure 2.3 Agtr1a and Agtr1b morpholino phenotypes and western blot validation. (A)** Translational blocking morpholino (MO) designs for *agtr1a* and *agtr1b*. The mRNA target shows the site within the *agtr1a* and *agtr1b* transcripts that is targeted by the translational blocking MO. **(B)** Representative confocal images of DA neurons in different treatment conditions. **(C)** Western blot image showing successful knockdown of the *agtr1* protein in the *agtr1a+1b* morpholino-injected samples compared to control (β-Actin).

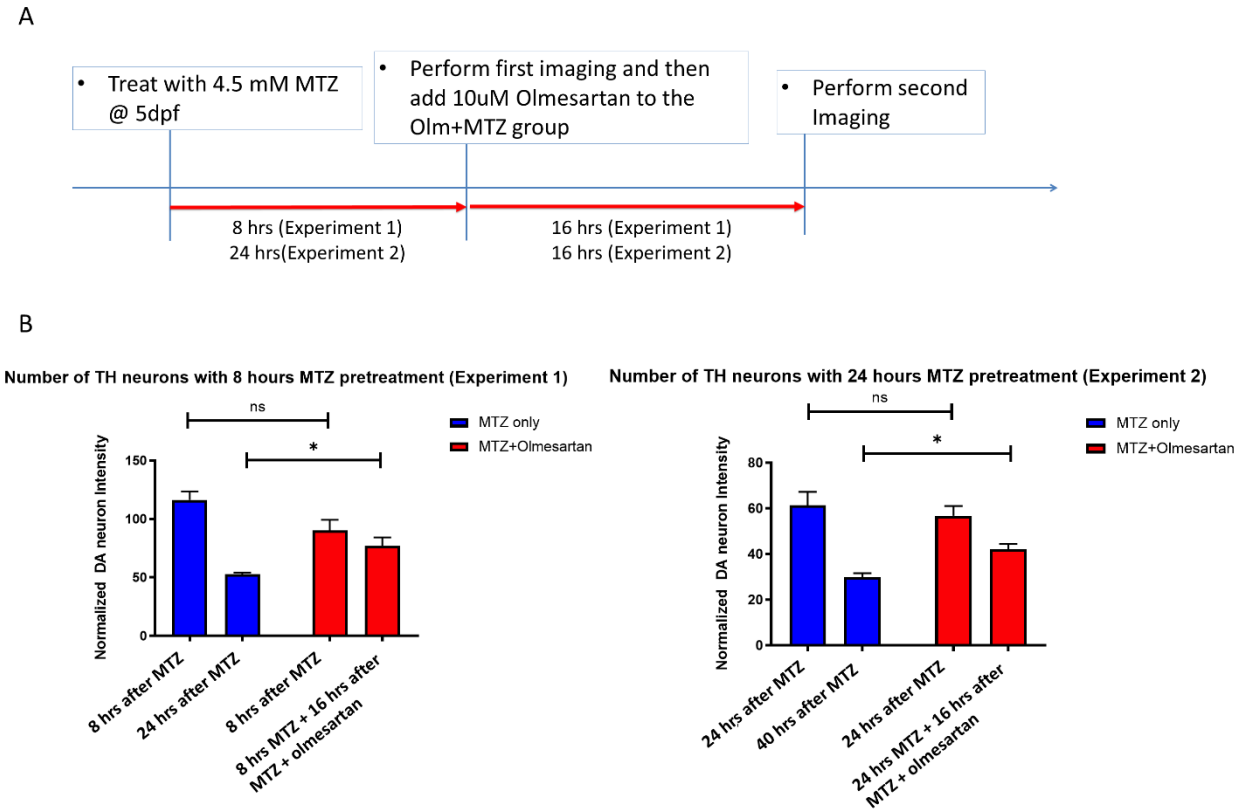


**Supplementary Figure 2.4 Olmesartan shows neuroprotective effects post neuronal injury in the NTR-MTZ DA neuron ablation model (A)** Timeline of chemical treatment for MTZ and olmesartan for experiment 1 (8 hrs MTZ pretreatment) and experiment 2 (24hrs MTZ pretreatment). After pretreating with MTZ for 8 hrs or 24 hrs, 10 mM olmesartan was added and imaged after 16 hrs (at 24 hrs and 40 hrs respectively). For both experiments 1 and 2, MTZ concentration was 4.5mM. **(B)** DA neuron intensity is significantly greater in the olmesartan-treated samples compared to MTZ alone for both 8hr (left) and 24hr MTZ pre-treatment groups (right) (n=10 to 12; $P<0.05$, unpaired t test).

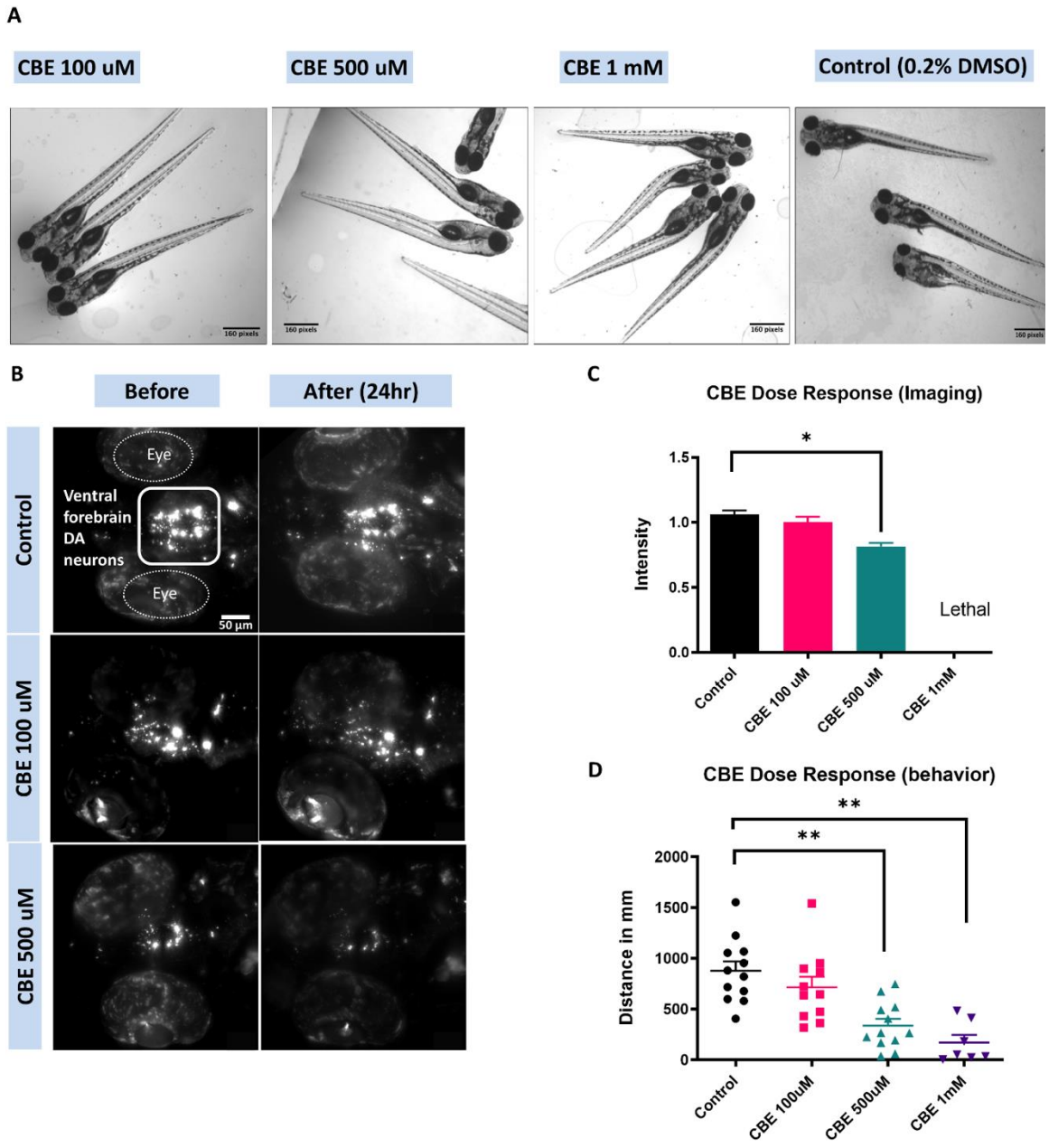


**Supplementary Figure 2.5 Dose-dependent effects of CBE on larval zebrafish. (A)** Brightfield images of 6dpf larvae treated with CBE at varying doses (100, 500, 1000 µM) for 24 hrs. No significant alterations in morphology were observed. **(B-C)** Confocal images of DA neurons after 24hrs of CBE treatment. Treatment with 500µM CBE caused a significant reduction in DA neuron fluorescent intensity. CBE 1mM was lethal to all larvae. (n=10; $P<0.05$, unpaired t test) **(D)** Total distance moved in a 5 min recording upon CBE treatment for 6dpf larvae after 24hrs of chemical treatment. (n=12, $P<0.01$, unpaired t test).

**A**

| AGTR1A versions | Target Sequence (5′ -> 3′) |
|---|---|
| AGTR1a-1 | AATCTCCAAAATGGACAACGTCACTTCCGACTC |
| AGTR1a-2 | CGACTCCAACACGGGACTTGCCCTCGCCTGTAA |
| AGTR1a-3 | TGCCCGGGTAACATGCGTTCTAGTTTGGGTGGT |
| AGTR1a-4 | CCTCACCCTTCCCATCTGGGCCATTTCCACTGC |
| AGTR1a-5 | TGCTGCCGCCCTGTCCTTTTTCCTTTGCTGGGC |
| AGTR1a-6 | CAGTTTTGTTGGAAAGAACTTCCGGAGGAACTT |
| AGTR1a-7 | CTTGCCCTCGCCTGTAACATGACAGGACACCA |
| AGTR1a-8 | TAAAACCCCTTCACTCCCTCGGGCCACATGAGA |

| AGTR1B versions | Target Sequence (5′ -> 3′) |
|---|---|
| AGTR1b-1 | CTCAACCTAGCCATATCAGACCTCACCTTCCTT |
| AGTR1b-2 | GTTGAGGAAAAGCGTTCGCTCCCGGGAGGAT |
| AGTR1b-3 | TCTTCTGGGATCCAGGGGTCTGTTGAGGAAAAG |
| AGTR1b-4 | GATTGCCGCCACCGTGCTCGCTTTCTTTGTTTG |
| AGTR1b-5 | GAGGACCTCCATGTGAACTGCAGTATGTCTGGA |
| AGTR1b-6 | ACACAACTTTCGCAAGAACCTACTGAGGTTGCT |
| AGTR1b-7 | TTGGTCGGGCTCTTCTGGGATCCAGGGGTCTGT |
| AGTR1b-8 | GGGATCATTGGCAATAGCATGGTCGTGGCTGTC |

sgRNA sequence PAM

**B**

| Versions | Forward Primer | Reverse Primer | Efficiency (%) | CRISPRScan Score |
|---|---|---|---|---|
| AGTR1a-1 | 5′ GGAAGTGACGTTGTCCATTTTGG 3′ | 5′AATTTAATACGACTCACTATAGG – CTCGGAAGTGACGTTGTCCATTT - GTTTAAGAGCTATGCT - 3′ | 2 | 60 |
| AGTR1a-2 | GGCGAGGGCAAGTCCCGTGTTGG | 5′AATTTAATACGACTCACTATAGG – CTCGGCGAGGGCAAGTCCCGTGT- GTTTAAGAGCTATGCT - 3′ | 53 | 74 |
| AGTR1a-3 | GGGTAACATGCGTTCTAGTTTGG | 5′AATTTAATACGACTCACTATAGG – CTCGGGTAACATGCGTTCTAGTT- GTTTAAGAGCTATGCT - 3′ | 2 | 70 |
| AGTR1a-4 | GGAAATGGCCCAGATGGGAAGGG | 5′AATTTAATACGACTCACTATAGG – CTCGGAAATGGCCCAGATGGGAA- GTTTAAGAGCTATGCT - 3′ | N/A | 75 |
| **AGTR1a-5** | **GCAAAGGAAAAAGGACAGGGCGG** | **5′AATTTAATACGACTCACTATAGG- CTCGCAAAGGAAAAAGGACAGGG-GTTTAAGAGCTATGCT - 3′** | **58** | 78 |
| AGTR1a-6 | TTGTTGGAAAGAACTTCCGGAGG | 5′AATTTAATACGACTCACTATAGG – CTCGTGTTGGAAAGAACTTCCGG- GTTTAAGAGCTATGCT - 3′ | 10 | 76 |
| AGTR1a-7 | TCCTGTCATGTTACAGGCGAGGG | 5′AATTTAATACGACTCACTATAGG – CTCGCCTGTCATGTTACAGGCGA- GTTTAAGAGCTATGCT - 3′ | 2 | 68 |
| AGTR1a-8 | TGTGGCCCGAGGGAGTGAAGGGG | 5′AATTTAATACGACTCACTATAGG – CTCGGTGGCCCGAGGGAGTGAAG- GTTTAAGAGCTATGCT - 3′ | 5 | 65 |
| AGTR1b-1 | AGGTGAGGTCTGATATGGCTAGG | 5′AATTTAATACGACTCACTATAGG- AGCTCGGGTGAGGTCTGATATGGCT- GTTTAAGAGCTATGCT- 3′ | N/A | 65 |
| AGTR1b-2 | GGAAAGCGTTCGCTCCCGGGAGG | 5′AATTTAATACGACTCACTATAGG- AGCTCGGAAAGCGTTCGCTCCCGGG- GTTTAAGAGCTATGCT- 3′ | 0 | 84 |
| AGTR1b-3 | TGGGATCCAGGGGTCTGTTGAGG | 5′AATTTAATACGACTCACTATAGG- AGCTCGGGGATCCAGGGGTCTGTTG- GTTTAAGAGCTATGCT- 3′ | 5 | 69 |
| AGTR1b-4 | AAAGAAAGCGAGCACGGTGGCGG | 5′AATTTAATACGACTCACTATAGG- AGCTCGAAGAAAGCGAGCACGGTGG- GTTTAAGAGCTATGCT- 3′ | N/A | 68 |
| AGTR1b-5 | ACATACTGCAGTTCACATGGAGG | 5′AATTTAATACGACTCACTATAGG- AGCTCGCATACTGCAGTTCACATGG- GTTTAAGAGCTATGCT- 3′ | 5 | 65 |
| **AGTR1b-6** | **ACTTTCGCAAGAACCTACTGAGG** | **5′AATTTAATACGACTCACTATAGG- AGCTCGCTTTCGCAAGAACCTACTG - GTTTAAGAGCTATGCT- 3′** | **65** | 65 |
| AGTR1b-7 | CGGGCTCTTCTGGGATCCAGGGG | 5′AATTTAATACGACTCACTATAGG- - AGCTCGGGGCTCTTCTGGGATCCAG - GTTTAAGAGCTATGCT- 3′ | 0 | 62 |
| AGTR1b-8 | CATTGGCAATAGCATGGTCGTGG | 5′AATTTAATACGACTCACTATAGG- - AGCTCGATTGGCAATAGCATGGTCG - GTTTAAGAGCTATGCT 3′ | 25 | 61 |

Scramble sgRNA for AGTR1a: 5′ GAAGACGACGAAAGAAAGGG 3′
Scramble sgRNA for AGTR1b: 5′ GAACTCTAAACGTACTCCGT 3′

**C**

**Isolation of DA neurons under GFP fluorescence**

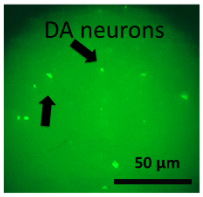


**Gel electrophoresis image of PCR products**

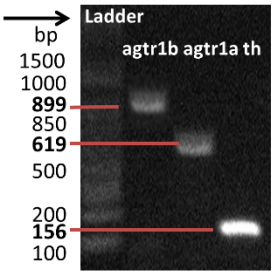


**agtr1a sgRNA**


**agtr1b sgRNA**

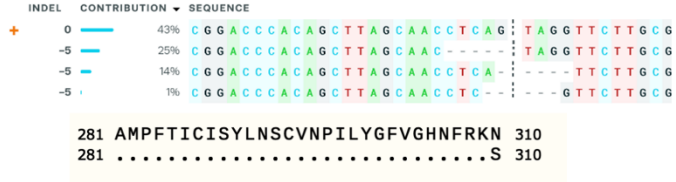


**agtr1a scramble sgRNA**


**agtr1b scramble sgRNA**

**Supplementary Figure 2.6 sgRNA design and validation for conditional CRISPR knockout of agtr1a and 1b in DA neurons. (A)** sgRNA target sequences (green) with PAM sites highlighted in yellow in the *agtr1a (left)* and *agtr1b (right)* genes. 8 different targets for each gene were examined to determine the highest sgRNA KO efficiency. **(B)** Primers used to construct template plasmids for sgRNA synthesis. sgRNA efficiency was calculated based on sequencing followed by ICE software analysis (https://ice.synthego.com/#/) comparing the knockouts to control. CRISPRScan scores with predicted efficiency is also shown in column 5. **(C)** Schematic showing the workflow for validating successful knockout of *agtr1a* and *agtr1b* in DA neurons. After DA neuron imaging, larval zebrafish brains were dissociated and DA neurons expressing Cas9-GFP and NTR-mCherry were collected via mouth-pipetting and pooled. PCR was performed to amplify genomic DNA regions targeted by *agtr1a* and agtr1b sgRNAs followed by sequencing. The samples were also amplified with *th* primers for QC. Sequencing results were analyzed with the Synthego ICE software. In this example dataset, at least 50% or 40% of sequenced reads carry open reading frame-shifting deletions in *agtr1a* and *agtr1b* genes respectively. The scrambled sgRNA for agtr1a and agtr1b showed no indel mutations when compared to controls.

**A**

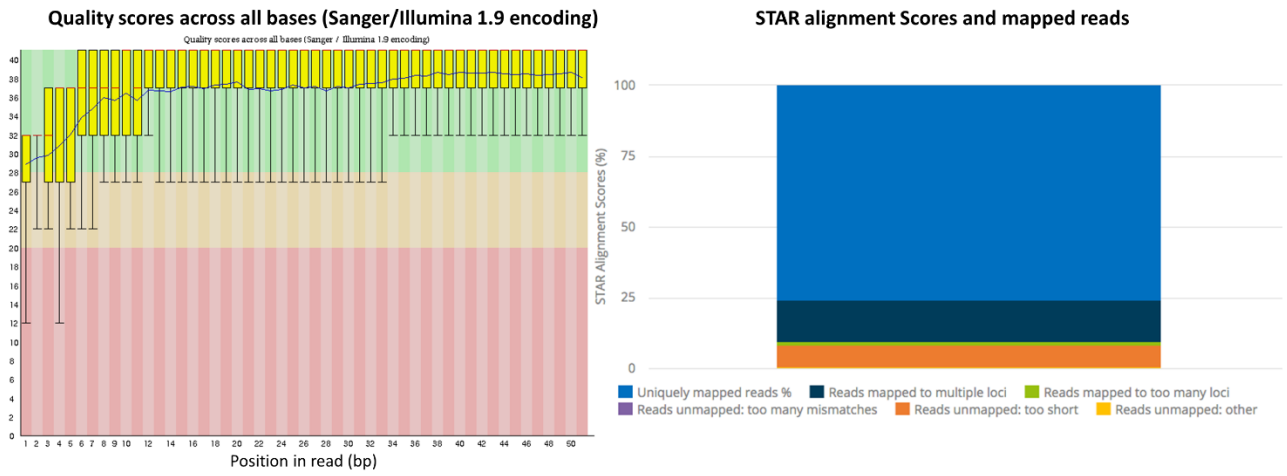


**B**

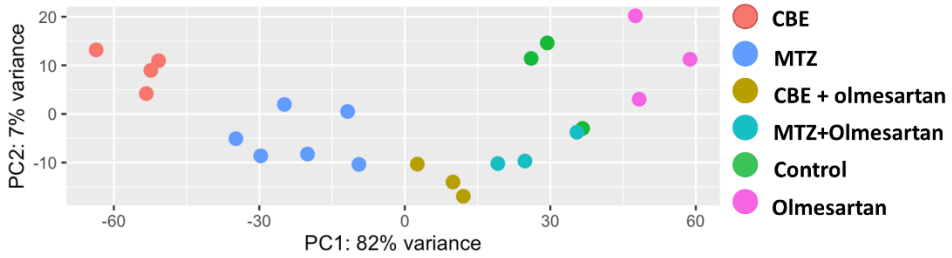


**C**

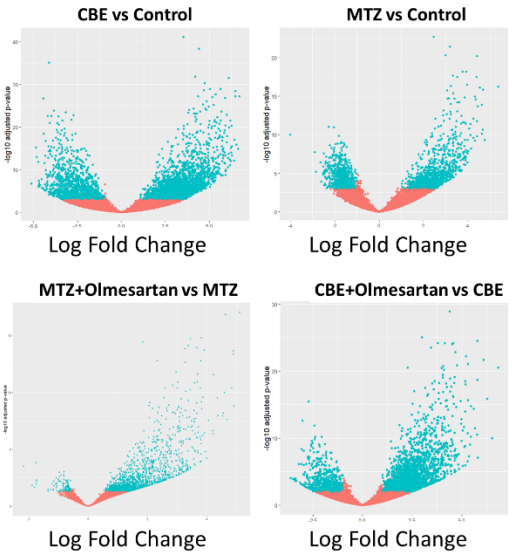


**D**

GO enrichment analysis of Olmesartan/Control differential gene expression

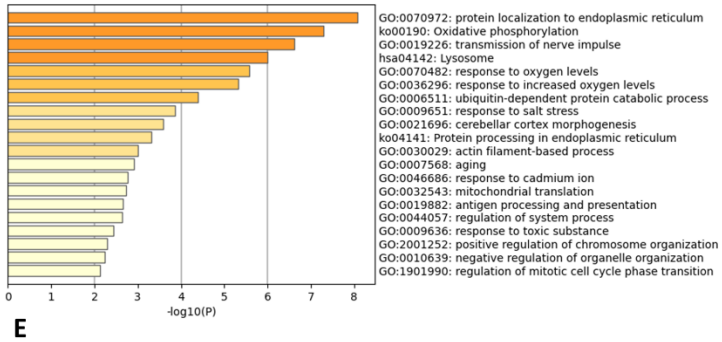


**E**

| Differential Gene Expression | Top 10 Upregulated Genes | Top 10 Downregulated Genes |
|---|---|---|
| MTZ vs Control | *rpl27, cox8a, rack1, crygm2d4, atp5mc3b, rps13, mycbp, camlg, ndufa1, jpt2* | *cant1b, zbtb22b, noto, fam102aa, faxcb, timm17b, tmem175, kcnc3b, dnajb9a, top1mt* |
| CBE vs Control | *rpl27, ak2, rack1, cox8a, lim2.3, vdac2, rnaset2, mmgt1, crygm2d6, cebpb* | *drc3, tab1, SNORD21, kbtbd7, kcnc3b, GRIN2B, ndr2, unc5c, tmem175, gabrr1* |
| MTZ+olmesartan vs MTZ | *epn3b, drd3, mpp3b, FRMD7, arl5c, mier2, tbc1d20, slc25a23b, ldlrap1a, rtel1* | *atp5l, rps26, cox8a, crygm2d15, cox6a1, atp5mc3b, rbp4l, fkbp1aa, crygm2d2, atp5f1d* |
| CBE+olmesartan vs CBE | *crygmx, romo1, sdhc, mmgt1, prrg2, mat2b, mmp13a, emc6, proza, ndrg3* | *gabrr1, unc5c, ndr2, dqx1, prickle2a, GRIN2B, fam161a, tmem67, tab1, SNORD21* |

**Supplementary Figure 2.7 Quality control (QC) and pathway analysis of the DA neuron-specific RNA-seq data. (A)** Representative FastQC output of a CBE-treated sample. All samples underwent FastQC (https://www.bioinformatics.babraham.ac.uk/projects/fastqc/) for quality control. Mappings were aligned with the GRCz11 genome assembly and all samples showed greater than 75% uniquely mapped reads as the example. **(B)** The Principal Component Analysis (PCA) plot of the RNA-seq sample replicates shows that each sample group forms distinct clusters. **(C)** Volcano plots showing the differential gene expression comparing CBE vs control, MTZ vs control, MTZ+olmesartan vs MTZ, and CBE+olmesartan vs CBE. Log transformed adjusted p-values are plotted on the y-axis and log2 fold change values are plotted on the x-axis. ($\alpha = 0.05$, FDR=0.1; Wald test) **(D)** Pathway enrichment analysis of the differential gene set for olmesartan treatment compared to control using gProfiler. The top 20 pathways are shown. 13 additional pathways (not shown) also showed significance with *Padj*<0.05. (E) List of top 10 upregulated genes and down regulated genes for the differential gene compared between sample group types listed in the first column.

**A**

**Baseline Characteristics of RAAS and No_RAAS cohort**

| COHORT | AGE (yr) | GENDER | RACE | SMOKING | CAFFEINE | ALCOHOL | HEAD INJURY |
|---|---|---|---|---|---|---|---|
| NO RAAS | 59.5[31-92] | 61.3% M | 96.1% White | 36.3% | 75.5% | 83.78% | 40.8% |
| RAAS | 64.4[47-96] | 75 % M | 94.25% White | 34.5% | 75.7% | 87.01% | 31.81% |

**B**

**Propensity Score matching of RAAS and No_RAAS cohort**

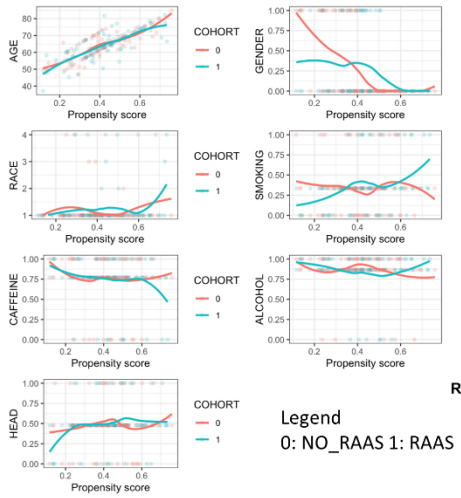


**C**

Correlation matrix heatmap

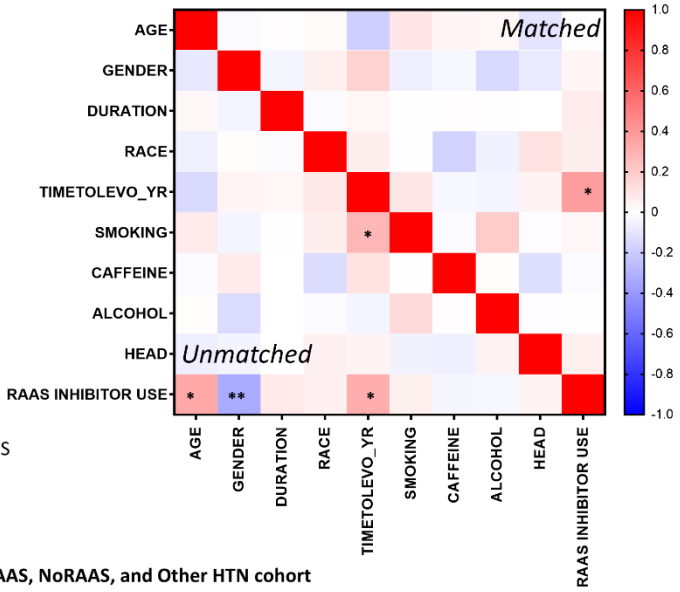


**D**

**Summary of UPDRS scores Part 1, 2 and 3 for RAAS, NoRAAS, and Other HTN cohort**

| | Baseline | | | Month 12 (v4) | | | Month 24 (v6) | | |
|---|---|---|---|---|---|---|---|---|---|
| | RAAS N=46 | NORAAS N=103 | NORAAS_HTN N= 24 | RAAS N=46 | NORAAS N=103 | NORAAS_HTN N= 24 | RAAS N=42 | NORAAS N=97 | NORAAS_HTN N= 24 |
| **Age** | 62.96± 8.04 | 57.27± 9.03 | 56.72± 8.26 | Mean ± SD | | | | | |
| **Sex (m)** | 79.30% | 65.30% | 65.76% | | | | | | |
| **UPDRS Score** | | | | | | | | | |
| *Part 1* | 2.17 ± 0.20 | 2.13 ± 0.12 | 2.12 ± 0.12 | 2.30 ± 0.19 | 2.24 ± 0.15 | 2.17 ± 0.13 | 2.33 ± 0.19 | 2.55 ± 0.17 | 2.64 ± 0.20 |
| *Part 2* | 5.00 ± 0.37 | 6.17 0.32 | 6.01 ± 0.33 | 6.62 ± 0.45 | 8.00 ± 0.42 | 7.67 ± 0.41 | 8.07 ± 0.58 | 8.85 ± 0.46 | 8.54 ± 0.50 |
| *Part 3* | 18.24 ± 1.04 | 19.23 ± 0.65 | 18.70 ± 0.70 | 19.48 ± 1.16 | 22.35 ± 0.81 | 21.8230 ± 0.87 | 25.39 ± 1.50 | 24.73± 0.83 | 23.69 ± 0.90 |

| | Month 36 (v8) | | | Month 48 (v10) | | | Month 60 (v12) | | |
|---|---|---|---|---|---|---|---|---|---|
| | RAAS N=46 | NORAAS N=103 | NORAAS_HTN N= 24 | RAAS N=46 | NORAAS N=103 | NORAAS_HTN N= 24 | RAAS N=39 | NORAAS N=92 | NORAAS_HTN N= 21 |
| *Part 1* | 2.35 ± 0.20 | 2.77 ± 0.18 | 2.76 ± 0.20 | 2.30 ± 0.21 | 3.07 ± 0.21 | 3.02 ± 0.21 | 2.625 ± 0.22 | 3.06± 0.23 | 2.95 ± 0.24 |
| *Part 2* | 8.33 ± 0.55 | 9.54 ± 0.45 | 9.39±0.49 | 8.96 ± 0.66 | 10.63 ± 0.58 | 9.87 ± 0.60 | 9.39± 0.62 | 10.55 ± 0.59 | 9.78 ± 0.64 |
| *Part 3* | 25.94 ± 1.29 | 25.68 ± 0.81 | 25.37 ± 0.90 | 27.21± 1.11 | 26.30 ± 1.03 | 25.41 ± 0.92 | 27.27 ± 1.16 | 25.62 ± 0.85 | 24.49 ± 0.95 |

**E**

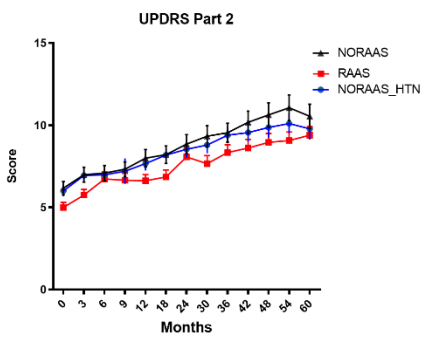


**F**

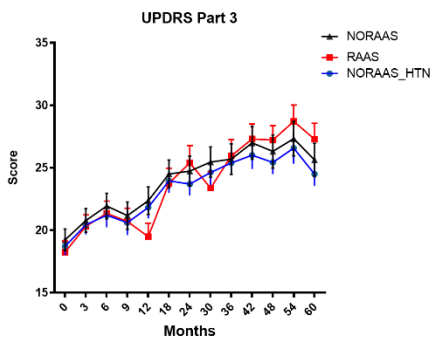

**Supplementary Figure 2.8 Patient cohorts from PPMI data, propensity score matching, and UPDRS Part2, Part3 analysis. (A)** Baseline characteristics of the *de novo* PD patients on RAAS inhibitors and not on RAAS inhibitors. Patients on RAAS inhibitors had a greater mean age and similar male to female gender distribution compared to patients not on RAAS inhibitors. **(B)** Plots of the covariates against the estimated propensity score, separately by patients on RAAS inhibitors verses patients not on RAAS inhibitors. There was no significant difference in means upon matching (Welch two sample t-test; Age $P$=0.98, Race $P$=0.93, Gender $P$=0.93, Caffeine intake $P$=0.52, History of head injury $P$= 0.81, Smoking $P$=0.84, Alcohol intake $P$=0.91) **(C)** Pairwise Pearson correlation of the covariables including age, gender, duration of PD, race, time to levodopa, smoking status, caffeine, alcohol consumption, history of head injury, and RAAS inhibitor use. The lower left panel shows the correlation without matching and the upper right panel shows the correlation upon matching. Prior to matching, the RAAS inhibitor cohort was significantly different for gender, age, and time to levodopa compared to the No RAAS group (*$P$<0.05, **$P$<0.01). Upon matching, the RAAS inhibitor use was significantly correlated with time to levodopa (*$P$<0.05). **(D)** Mean UPDRS scores and standard deviation progression for the RAAS inhibitor, Non-RAAS, and other hypertension medication cohort starting from baseline to visit 12. **(E)** UPDRS part 2 and **(F)** part 3 progression showed no significant difference across the RAAS inhibitor, Non-RAAS, and other hypertension cohort. (n=39 to 46 for RAAS cohort, n=92 to 103 for No RAAS cohort, n=21 to 24 for No RAAS_HTN cohort; Part 2 $P$=0.53; Part 3 $P$=0.85, one-way ANOVA)

## 2.7 Tables

**Table 2.1 Primer design sequences for genes related to the RAAS pathway used for the QPCR of larval DA neurons.** Transcript sequences were obtained from the Ensembl genome browser for zebrafish (GRCz11; https://uswest.ensembl.org/Danio_rerio/Info/Index) as shown in column 6. The primers were designed with NCBI primer blast (https://www.ncbi.nlm.nih.gov/tools/primer-blast/) spanning a product length between 70bp to 200 bp while minimizing self 3' complementary score. All primers were validated with gel electrophoresis prior to the QPCR (data not shown).

| Gene Name | Gene symbol | Function | Primer Sequences (5'->3') | bp | Transcript ID |
|---|---|---|---|---|---|
| **Angiotensin II receptor, type 1a** | agtr1a | G protein-coupled receptor for angiotensin II | F: CTTCTCACTGCTCTCAGCGT<br>R: CATCCGTGGGACCCATTTCA | 163 | ENSDART00000021528.7 |
| **Angiotensin II receptor, type 1b** | agtr1b | G protein-coupled receptor for angiotensin II | F: TCCAGGGGTCTGTTGAGGAA<br>R: CAGTTTTCCACCACGCCAAG | 155 | ENSDART00000066834.5 |
| **Angiotensin I converting enzyme** | ace1 | Metallopeptidase involved in the conversion of angiotensin I to angiotensin II | F: CGCTCTACCTCAGCGTTCAT<br>R: GCCCACATGTTTCCAAGCAG | 115 | ENSDART00000114637.4 |
| **Angiotensin I converting enzyme 2** | ace2 | Transmembrane protein catalyzing angiotensin II hydrolysis. Main entry point for coronavirus. | F: CTGATGCCTGTCTTCCAGCA<br>R: TTTCATCCCAACCCTGCTCC | 141 | ENSDART00000003712.8 |
| **Angiotensinogen** | agt | Precursor molecule for angiotensin I and the substrate for renin produced in the liver. | F: GGCTTCGACACCTCAAGGAA<br>R:ACACCACCTTGTTGAGTACCTTA | 192 | ENSDART00000010918.5 |
| **Angiotensin II receptor, type 2** | at2 | G protein-coupled receptor. Regulation of aldosterone secretion | F: GTTCACGAACATCAGAACTCCC<br>R: TGAGGCTGTAAAAGGCAGGG | 187 | ENSDART00000051532.5 |
| **Renin** | ren | Enzyme cleaving angiotensinogen to form angiotensin I | F: CGGTGTACTACAGCAGGGAC<br>R: GTGTCGGTTGGGGCAGATAT | 160 | ENSDARG00000041858 |
| **Prorenin receptor** | atp6ap2 | Renin and prorenin receptor involved in the assembly of the ATPase protein pump | F: GTCTCTCTCAGCCGCAACAA<br>R: CTGCAACTGTAGCAAACGAACA | 184 | ENSDART00000178882.2 |
| **Elongation factor 1-alpha** | eef1a1 | Housekeeping gene; promote the GTP-dependent binding of aa-tRNA to the A-site of ribosomes | F: TTTTTGGGGTTTTGCAGGTCG<br>R: TTGGCCTTCTGGGCTTTCTG | 138 | ENSDART00000164533.2 |

**Table 2.2 Differential gene expression of mitochondria related genes for Olmesartan + CBE- or MTZ-treated samples compared to controls.** 15 mitochondria related genes enriched in CBE- or MTZ-treated samples are shown in the first column. The differential gene expression analysis was performed on CBE+olmesartan and MTZ+olmesartan samples against the control samples (α=0.05, FDR=0.1). Many of the genes were not expressed for the olmesartan + CBE- or MTZ-treated samples compared to the controls which indicates the olmesartan treatment restoring these mitochondra genes back to normal. *ns*= not significant.

| | **CBE+olmesartan/control** | **MTZ+olmseartan/control** |
|---|---|---|
| Atp5l | ns (p-value; not significant) | 0.031 |
| Cox5aa | ns | ns |
| Cox6a1 | ns | ns |
| Cox6c | ns | 0.012 |
| Cox7a2a | ns | ns |
| Cox7c | ns | ns |
| Cox8a | 0.0083 | ns |
| Mrpl13 | 0.019 | ns |
| Mrps18c | ns | ns |
| Ndufa1 | 0.02484 | ns |
| Ndufb2 | ns | ns |
| Ndufs4 | ns | ns |
| Ndufv2 | ns | ns |
| Tomm6 | ns | ns |
| Trim3 | ns | ns |

## 2.8 References


1. Rizek, P., Kumar, N. & Jog, M. S. An update on the diagnosis and treatment of Parkinson disease. *CMAJ* **188**, 1157–1165 (2016).
2. Massano, J. & Bhatia, K. P. Clinical approach to Parkinson's disease: Features, diagnosis, and principles of management. *Cold Spring Harb. Perspect. Med.* **2**, 1–15 (2012).
3. Opara, J. A., Małecki, A., Małecka, E. & Socha, T. Motor assessment in parkinson's disease. *Ann. Agric. Environ. Med.* **24**, 411–415 (2017).
4. Tysnes, O. B. & Storstein, A. Epidemiology of Parkinson's disease. *J. Neural Transm.* **124**, 901–905 (2017).
5. Kowal, S. L., Dall, T. M., Chakrabarti, R., Storm, M. V & Jain, A. The current and projected economic burden of Parkinson's disease in the United States. *Mov. Disord.* **28**, 311–318 (2013).
6. Armstrong, M. J. & Okun, M. S. Diagnosis and Treatment of Parkinson Disease: A Review. *JAMA - J. Am. Med. Assoc.* **323**, 548–560 (2020).
7. Haddad, F., Sawalha, M., Khawaja, Y., Najjar, A. & Karaman, R. Dopamine and Levodopa Prodrugs for the Treatment of Parkinson's Disease. *Molecules* **23**, 40 (2017).
8. Masato, A., Plotegher, N., Boassa, D. & Bubacco, L. Impaired dopamine metabolism in Parkinson's disease pathogenesis. *Mol. Neurodegener.* **14**, 1–21 (2019).
9. Brooks, D. J. Optimizing levodopa therapy for Parkinson's disease with levodopa/carbidopa/entacapone: implications from a clinical and patient perspective. *Neuropsychiatr. Dis. Treat.* **4**, 39–47 (2008).
10. Verschuur, C. V. M. *et al.* Randomized Delayed-Start Trial of Levodopa in Parkinson's Disease. *N. Engl. J. Med.* **380**, 315–324 (2019).

11. Wong, C. H., Siah, K. W. & Lo, A. W. Estimation of clinical trial success rates and related parameters. *Biostatistics* **20**, 273–286 (2019).

12. Pankevich, D. E., Altevogt, B. M., Dunlop, J., Gage, F. H. & Hyman, S. E. Improving and accelerating drug development for nervous system disorders. *Neuron* **84**, 546–553 (2014).

13. O'Donnell, P. *et al.* Strategies to Address Challenges in Neuroscience Drug Discovery and Development. *Int. J. Neuropsychopharmacol.* **22**, 445–448 (2019).

14. Moffat, J. G., Vincent, F., Lee, J. A., Eder, J. & Prunotto, M. Opportunities and challenges in phenotypic drug discovery: An industry perspective. *Nat. Rev. Drug Discov.* **16**, 531–543 (2017).

15. Bespalov, A. *et al.* Failed trials for central nervous system disorders do not necessarily invalidate preclinical models and drug targets. *Nat. Rev. Drug Discov.* **15**, 516 (2016).

16. Guo, S. Using zebrafish to assess the impact of drugs on neural development and function. *Expert Opin. Drug Discov.* **4**, 715–726 (2009).

17. Pieper, A. A. *et al.* Discovery of a proneurogenic, neuroprotective chemical. *Cell* **142**, 39–51 (2010).

18. Szabo, M. *et al.* Cell and small animal models for phenotypic drug discovery. *Drug Des. Devel. Ther.* **11**, 1957–1967 (2017).

19. Denny, P. W. Yeast: bridging the gap between phenotypic and biochemical assays for high-throughput screening. *Expert Opin. Drug Discov.* **13**, 1153–1160 (2018).

20. Zon, L. I. & Peterson, R. T. In vivo drug discovery in the zebrafish. *Nature Reviews Drug Discovery* vol. 4 35–44 (2005).

21. MacRae, C. A. & Peterson, R. T. Zebrafish as tools for drug discovery. *Nat. Rev. Drug Discov.* **14**, 721–731 (2015).

22. Lavoie, J. L. & Sigmund, C. D. Minireview: Overview of the Renin-Angiotensin System—An Endocrine and Paracrine System. *Endocrinology* **144**, 2179–2183 (2003).

23. Riboldi, G. M. & Di Fonzo, A. B. GBA, Gaucher Disease, and Parkinson's Disease: From Genetic to Clinic to New Therapeutic Approaches. *Cells* **8**, (2019).

24. Yang, Y. *et al.* Mitochondrial pathology and muscle and dopaminergic neuron degeneration caused by inactivation of Drosophila Pink1 is rescued by Parkin. *Proc. Natl. Acad. Sci. U. S. A.* **103**, 10793–10798 (2006).

25. Marek, K. *et al.* The Parkinson's progression markers initiative (PPMI) – establishing a PD biomarker cohort. *Ann. Clin. Transl. Neurol.* **5**, 1460–1477 (2018).

26. Dawson, T. M., Ko, H. S. & Dawson, V. L. Genetic animal models of Parkinson's disease. *Neuron* **66**, 646–661 (2010).

27. Williams, E. M. *et al.* Nitroreductase gene-directed enzyme prodrug therapy: insights and advances toward clinical utility. *Biochem. J.* **471**, 131–153 (2015).

28. Pisharath, H. & Parsons, M. J. Nitroreductase-mediated cell ablation in transgenic zebrafish embryos. *Methods Mol. Biol.* **546**, 133–143 (2009).

29. Curado, S. *et al.* Conditional targeted cell ablation in zebrafish: A new tool for regeneration studies. *Dev. Dyn.* **236**, 1025–1035 (2007).

30. Rink, E. & Wullimann, M. F. The teleostean (zebrafish) dopaminergic system ascending to the subpallium (striatum) is located in the basal diencephalon (posterior tuberculum). *Brain Res.* **889**, 316–330 (2001).

31. Chen, C.-F. *et al.* Establishment of a transgenic zebrafish line for superficial skin ablation and functional validation of apoptosis modulators in vivo. *PLoS One* **6**, e20654 (2011).

32. Edwards, D. I. Mechanism of antimicrobial action of metronidazole. *J. Antimicrob.*

*Chemother.* **5**, 499–502 (1979).

33. Furda, A. M., Bess, A. S., Meyer, J. N. & Van Houten, B. Analysis of DNA damage and repair in nuclear and mitochondrial DNA of animal cells using quantitative PCR. *Methods Mol. Biol.* **920**, 111–132 (2012).

34. Yakes, F. M. & Van Houten, B. Mitochondrial DNA damage is more extensive and persists longer than nuclear DNA damage in human cells following oxidative stress. *Proc. Natl. Acad. Sci. U. S. A.* **94**, 514–519 (1997).

35. Kitada, T. *et al.* Mutations in the parkin gene cause autosomal recessive juvenile parkinsonism. *Nature* **392**, 605–608 (1998).

36. Pickrell, A. M. & Youle, R. J. The roles of PINK1, parkin, and mitochondrial fidelity in Parkinson's disease. *Neuron* **85**, 257–273 (2015).

37. Han, J.-Y., Kim, J.-S. & Son, J. H. Mitochondrial homeostasis molecules: regulation by a trio of recessive Parkinson's disease genes. *Exp. Neurobiol.* **23**, 345–351 (2014).

38. Liu, H. *et al.* A high-content larval zebrafish brain imaging method for small molecule drug discovery. *PLoS One* **11**, 1–14 (2016).

39. Monti, D. A. *et al.* N-Acetyl Cysteine Is Associated With Dopaminergic Improvement in Parkinson's Disease. *Clin. Pharmacol. Ther.* **106**, 884–890 (2019).

40. Gellhaar, S., Marcellino, D., Abrams, M. B. & Galter, D. Chronic L-DOPA induces hyperactivity, normalization of gait and dyskinetic behavior in MitoPark mice. *Genes. Brain. Behav.* **14**, 260–270 (2015).

41. Nicholas, A. P. Levodopa-induced hyperactivity in mice treated with 1-methyl-4-phenyl-1,2,3,6-tetrahydropyridine. *Mov. Disord.* **22**, 99–104 (2007).

42. Pandey, S. & Srivanitchapoom, P. Levodopa-induced Dyskinesia: Clinical Features,

Pathophysiology, and Medical Management. *Ann. Indian Acad. Neurol.* **20**, 190–198 (2017).

43. Gao, Y. *et al.* Effects of centrally acting ACE inhibitors on the rate of cognitive decline in dementia. *BMJ Open* **3**, 1–8 (2013).

44. O'Caoimh, R. *et al.* Effects of centrally acting angiotensin converting enzyme inhibitors on functional decline in patients with alzheimer's disease. *J. Alzheimer's Dis.* **40**, 595–603 (2014).

45. Sparks, M. A., Crowley, S. D., Gurley, S. B., Mirotsou, M. & Coffman, T. M. Classical Renin-Angiotensin system in kidney physiology. *Compr. Physiol.* **4**, 1201–1228 (2014).

46. Kawarazaki, W. & Fujita, T. The Role of Aldosterone in Obesity-Related Hypertension. *Am. J. Hypertens.* **29**, 415–423 (2016).

47. Xue, B. *et al.* Central Renin-Angiotensin System Activation and Inflammation Induced by High-Fat Diet Sensitize Angiotensin II-Elicited Hypertension. *Hypertension* **67**, 163–170 (2016).

48. Rocha, N. P. *et al.* RAS in the Central Nervous System: Potential Role in Neuropsychiatric Disorders. *Curr. Med. Chem.* **25**, 3333–3352 (2018).

49. Di Donato, V. *et al.* 2C-Cas9: a versatile tool for clonal analysis of gene function. *Genome Res.* **26**, 681–692 (2016).

50. Ablain, J., Durand, E. M., Yang, S., Zhou, Y. & Zon, L. I. A CRISPR/Cas9 vector system for tissue-specific gene disruption in zebrafish. *Dev. Cell* **32**, 756–764 (2015).

51. Vardi, A. *et al.* Delineating pathological pathways in a chemically induced mouse model of Gaucher disease. *J. Pathol.* **239**, 496–509 (2016).

52. Artola, M. *et al.* Functionalized Cyclophellitols Are Selective Glucocerebrosidase

Inhibitors and Induce a Bona Fide Neuropathic Gaucher Model in Zebrafish. *J. Am. Chem. Soc.* **141**, 4214–4218 (2019).

53. Keatinge, M. *et al.* Glucocerebrosidase 1 deficient Danio rerio mirror key pathological aspects of human Gaucher disease and provide evidence of early microglial activation preceding alpha-synuclein-independent neuronal cell death. *Hum. Mol. Genet.* **24**, 6640–6652 (2015).

54. Huang, D. W., Sherman, B. T. & Lempicki, R. A. Systematic and integrative analysis of large gene lists using DAVID bioinformatics resources. *Nat. Protoc.* **4**, 44–57 (2009).

55. Zhou, Y. *et al.* Metascape provides a biologist-oriented resource for the analysis of systems-level datasets. *Nat. Commun.* **10**, 1523 (2019).

56. Saffari, A., Kölker, S., Hoffmann, G. F. & Ebrahimi-Fakhari, D. Linking mitochondrial dysfunction to neurodegeneration in lysosomal storage diseases. *J. Inherit. Metab. Dis.* **40**, 631–640 (2017).

57. Dong, W. *et al.* Proteomics and bioinformatics approaches for the identification of plasma biomarkers to detect Parkinson's disease. *Exp. Ther. Med.* **18**, 2833–2842 (2019).

58. Dong, W. *et al.* TRIM3 attenuates apoptosis in Parkinson's disease via activating PI3K/AKT signal pathway. *Aging (Albany. NY).* **13**, 735–749 (2020).

59. West, R. J. H., Furmston, R., Williams, C. A. C. & Elliott, C. J. H. Neurophysiology of Drosophila models of Parkinson's disease. *Parkinsons. Dis.* **2015**, 381281 (2015).

60. Lu, B. & Vogel, H. Drosophila models of neurodegenerative diseases. *Annu. Rev. Pathol.* **4**, 315–342 (2009).

61. Yang, Y., Nishimura, I., Imai, Y., Takahashi, R. & Lu, B. Parkin suppresses dopaminergic neuron-selective neurotoxicity induced by Pael-R in Drosophila. *Neuron* **37**, 911–924

(2003).

62. Greene, J. C. *et al.* Mitochondrial pathology and apoptotic muscle degeneration in Drosophila parkin mutants. *Proc. Natl. Acad. Sci. U. S. A.* **100**, 4078–4083 (2003).

63. Park, J. *et al.* Mitochondrial dysfunction in Drosophila PINK1 mutants is complemented by parkin. *Nature* vol. 441 1157–1161 (2006).

64. Clark, I. E. *et al.* Drosophila pink1 is required for mitochondrial function and interacts genetically with parkin. *Nature* vol. 441 1162–1166 (2006).

65. Wang, D. *et al.* Antioxidants protect PINK1-dependent dopaminergic neurons in Drosophila. *Proc. Natl. Acad. Sci. U. S. A.* **103**, 13520–13525 (2006).

66. Coates, D. *et al.* Functional conservation of the active sites of human and Drosophila angiotensin I-converting enzyme. *Biochemistry* **39**, 8963–8969 (2000).

67. Lee, S.-H., Gomes, S. M., Ghalayini, J., Iliadi, K. G. & Boulianne, G. L. Angiotensin Converting Enzyme Inhibitors and Angiotensin Receptor Blockers Rescue Memory Defects in Drosophila-Expressing Alzheimer's Disease-Related Transgenes Independently of the Canonical Renin Angiotensin System. *eNeuro* **7**, (2020).

68. Espay, A. J. *et al.* Biomarker-driven phenotyping in Parkinson's disease: A translational missing link in disease-modifying clinical trials. *Mov. Disord.* **32**, 319–324 (2017).

69. The Unified Parkinson's Disease Rating Scale (UPDRS): status and recommendations. *Mov. Disord.* **18**, 738–750 (2003).

70. Müller, T. & Möhr, J.-D. Long-term management of Parkinson's disease using levodopa combinations. *Expert Opin. Pharmacother.* **19**, 1003–1011 (2018).

71. Marsden, C. D. Problems with long-term levodopa therapy for Parkinson's disease. *Clin. Neuropharmacol.* **17 Suppl 2**, S32-44 (1994).

72. Chung, S. J. *et al.* Does Late Levodopa Administration Delay the Development of Dyskinesia in Patients with De Novo Parkinson's Disease? *CNS Drugs* **32**, 971–979 (2018).

73. Cummings, J. Disease modification and Neuroprotection in neurodegenerative disorders. *Transl. Neurodegener.* **6**, 25 (2017).

74. Paul, M., Poyan Mehr, A. & Kreutz, R. Physiology of local renin-angiotensin systems. *Physiol. Rev.* **86**, 747–803 (2006).

75. Godoy, R. *et al.* Dopaminergic neurons regenerate following chemogenetic ablation in the olfactory bulb of adult Zebrafish (Danio rerio). *Sci. Rep.* **10**, 1–12 (2020).

76. Curado, S., Stainier, D. Y. R. & Anderson, R. M. Nitroreductase-mediated cell/tissue ablation in zebrafish: a spatially and temporally controlled ablation method with applications in developmental and regeneration studies. *Nat. Protoc.* **3**, 948–954 (2008).

77. Muñoz, A. *et al.* Reduction of dopaminergic degeneration and oxidative stress by inhibition of angiotensin converting enzyme in a MPTP model of parkinsonism. *Neuropharmacology* **51**, 112–120 (2006).

78. Lopez-Real, A., Rey, P., Soto-Otero, R., Mendez-Alvarez, E. & Labandeira-Garcia, J. L. Angiotensin-converting enzyme inhibition reduces oxidative stress and protects dopaminergic neurons in a 6-hydroxydopamine rat model of Parkinsonism. *J. Neurosci. Res.* **81**, 865–873 (2005).

79. Ongali, B. *et al.* Angiotensin II type 1 receptor blocker losartan prevents and rescues cerebrovascular, neuropathological and cognitive deficits in an Alzheimer's disease model. *Neurobiol. Dis.* **68**, 126–136 (2014).

80. Valenzuela, R. *et al.* Mitochondrial angiotensin receptors in dopaminergic neurons. Role

in cell protection and aging-related vulnerability to neurodegeneration. *Cell Death Dis.* **7**, e2427 (2016).

81. Abadir, P. M. *et al.* Identification and characterization of a functional mitochondrial angiotensin system. *Proc. Natl. Acad. Sci. U. S. A.* **108**, 14849–14854 (2011).

82. Scarpulla, R. C. Nuclear control of respiratory chain expression by nuclear respiratory factors and PGC-1-related coactivator. *Ann. N. Y. Acad. Sci.* **1147**, 321–334 (2008).

83. Min, L.-J., Mogi, M., Iwai, M. & Horiuchi, M. Signaling mechanisms of angiotensin II in regulating vascular senescence. *Ageing Res. Rev.* **8**, 113–121 (2009).

84. Lee, Y. C. *et al.* Antihypertensive agents and risk of Parkinson's disease: A nationwide cohort study. *PLoS One* **9**, 17–21 (2014).

85. Laudisio, A. *et al.* Use of ACE-inhibitors and falls in patients with Parkinson's disease. *Gait Posture* **54**, 39–44 (2017).

86. Moacdieh, N., Ganje, T. & Sarter, N. Electronic health records: effects of clutter and stress on physicians' information search and noticing performance. *Proc. Hum. Factors Ergon. Soc. Annu. Meet.* **58**, 718–722 (2014).

87. Haneuse, S. *et al.* Learning About Missing Data Mechanisms in Electronic Health Records-based Research: A Survey-based Approach. *Epidemiology* **27**, 82–90 (2016).

88. Fazal, K., Perera, G., Khondoker, M., Howard, R. & Stewart, R. Associations of centrally acting ACE inhibitors with cognitive decline and survival in Alzheimer's disease. *BJPsych Open* **3**, 158–164 (2017).

89. Dukes, A. A. *et al.* Live imaging of mitochondrial dynamics in CNS dopaminergic neurons in vivo demonstrates early reversal of mitochondrial transport following MPP(+) exposure. *Neurobiol. Dis.* **95**, 238–249 (2016).

90. Yao, Y. *et al.* Visual Cue-Discriminative Dopaminergic Control of Visuomotor Transformation and Behavior Selection. *Neuron* **89**, 598–612 (2016).

91. Jones, T. R. *et al.* CellProfiler Analyst: data exploration and analysis software for complex image-based screens. *BMC Bioinformatics* **9**, 482 (2008).

92. Li, X., Cooper, N. G. F., O'Toole, T. E. & Rouchka, E. C. Choice of library size normalization and statistical methods for differential gene expression analysis in balanced two-group comparisons for RNA-seq studies. *BMC Genomics* **21**, 75 (2020).

93. Bullard, J. H., Purdom, E., Hansen, K. D. & Dudoit, S. Evaluation of statistical methods for normalization and differential expression in mRNA-Seq experiments. *BMC Bioinformatics* **11**, 94 (2010).

# CHAPTER 3: The effect of renin-angiotensin-aldosterone system inhibitors on organ-specific *ace2* expression in zebrafish and its implications for COVID-19

## 3.1 Abstract

As a global pandemic, the Coronavirus disease 2019 (COVID-19) caused by severe acute respiratory syndrome coronavirus 2 (SARS-CoV-2) has affected more than 140 million people and leading to more than 3 million deaths worldwide. Among cases that develop into serious conditions or mortality, many are associated with hypertension and cardiovascular disorders as a comorbidity. Furthermore, the virus itself also poses risk of developing heart conditions and cardiac injury after hospitalization. The SARS-CoV-2 enters cells by binding its spike protein to the angiotensin-converting enzyme 2 (ACE2) receptor and this has generated attention on the best practices for the management of patients with hypertension as angiotensin-converting enzyme inhibitors and angiotensin II receptor blockers are commonly prescribed medications. To understand the expression profile of RAAS pathway genes, we treated AB wild type adult zebrafish with aliskiren, olmesartan, and captopril which inhibit the RAAS pathway signaling for 7 consecutive days and performed RT-qPCR of RAAS pathway genes in the brain, gill, heart, intestine, kidney, and liver. Both olmesartan and captopril treatment showed an increase in *ace2* expression in the heart, gill, and kidney. Additionally, olmesartan also increased *ace2* expression in the intestine. Conversely, aliskiren treatment showed significant decrease in *ace2* expression in the heart. A second group of adult zebrafish were discontinued from the compounds for 7 days to determine whether *ace2* expression would be altered. Except for captopril and amlodipine

treatment group showing an increase in *ace2* expression 7 days after discontinuation in the heart, all other gene-organ-drug combination showed no expression differences upon discontinuation. With the uncertainties on the potential risk and benefits on the use of antihypertensives in the setting of COVID-19, this study provides how RAAS inhibitors modulate the gene level expression to contribute to the scientific evidence behind the decision-making process.

## 3.2 Introduction

The severe acute respiratory syndrome coronavirus 2 (SARS-CoV-2) is an RNA virus that has been spreading rapidly affecting millions of people worldwide in more than 200 countries. Although continued safety guidance and vaccination efforts have played an immense role in controlling the disease, it remains as a global pandemic. The clinical manifestations of SARS-CoV-2 are predominantly respiratory symptoms but some hospitalized patients also suffer from other cardiac injuries including myocardial injury, heart failure, and dysrhythmias[1]. Furthermore, studies have shown that hypertension is associated with increased risk of developing COVID-19 complications and increased mortality from COVID-19[2].

The angiotensin-converting enzyme 2 (ACE2) receptor is known to be a coreceptor for the entry of SARS-CoV2-2 by binding of the spike protein to the enzyme[3]. Reports have shown that 30% of patients admitted to the hospital due to COVID-19 had hypertension making it one of the most common comorbidies[4]. As many patients with hypertension and cardiovascular comorbidities are commonly prescribed angiotensin-converting enzyme inhibitors (ACE-I) and angiotensin II receptor blockers (ARBs), whether these compounds should be continued or

discontinued for the management of COVID-19 has been the subject of considerable debate. The angiotensin-converting enzyme 2(ACE2) negatively regulates the renin angiotensin system (RAAS) and exert protective effects on the lungs [5,6]. Preclinical studies have shown that ACE2 expression can be upregulated by RAAS inhibitors[7]. ACE-I and ARBs are therapeutic because they block angiotensin II signaling, but this could induce higher expression of ACE2 resulting in an increased viral entry[8].

Interest has grown on understanding whether the use of ACE-I and ARBs in patients can provide potential benefits or harm to the patient. The general guidelines from cohort studies and metanalysis have shown that RAAS inhibitors can safely be continued[9,10]. However, the pharmacological effects of treatment and discontinuation of RAAS inhibitors at the molecular and organ level remains unclear. A recent clinical trial has shown that routine discontinuation of ACE-I or ARBs are not recommended for mild to moderate COVID-19[10]. Metanalysis on the electronic health records of over a million hypertension patients have shown that there is no clinically significant increased risk of COVID-19 diagnosis or hospital admission-related outcomes associated with ACE-I or ARB use[9]. In this study we wanted to determine the organ-specific expression profile changes upon the administration of a panel of antihypertensive drugs (Table 3.1) and the effects on the expression profile upon discontinuation**.**

In the adult zebrafish, all the RAAS signaling components including ACE2 are present, allowing us to understand the different expression profiles upon RAAS inhibitor treatment. The zebrafish possess a high degree of genetic, physiological and morphological similarity with humans sharing nearly 71.4% homology with the human genome [11] and 58% sequence match for the *ace2* gene[12]. As the ACE2 enzyme is known to be expressed in various organs including the

lung, nasopharyngeal tissue, vascular tissue, kidney, heart, intestine, as well as the nervous tissue for potential viral entry, the organ system homology of zebrafish can be utilized for understanding the RAAS signaling genes at the organ level.

## 3.3 Methods

### 3.3.1 Zebrafish Husbandry

For experiments, the wild type of the AB strain adult zebrafish was used in this study. The zebrafish were raised on a 14:10 hr light/dark cycle and maintained in the zebrafish facility according to the University of California San Francisco Institutional Animal Care and Use Committee standards.

### 3.3.2 Sample setup, drug treatment, and discontinuation

The adult zebrafish were housed in 1-liter tanks separated based on what compound they receive and the treatment group (group 1) and treatment plus discontinuation group (group 2). For each group, three males and three females between 2-3 years old were selected to control for gender and age distribution per compound (or vehicle control). Each tank was filled with 500mL of system water along with the dissolved compounds. All samples were treated with a concentration of 10μM olmesartan medoxomil, captopril, aliskiren hemifumarate, or amlodipine besylate. The vehicle control was treated with 0.2% DMSO. The tanks were changed to fresh system water and compounds daily. The compounds olmesartan medoxomil, captopril, aliskiren hemifumarate,

amlodipine besylate were obtained from Sigma-Aldrich (cat #144689-63-4, 62571-86-2, 173334-58-2, A5605).

### 3.3.3 Extraction of Total RNA and cDNA synthesis from adult zebrafish organs

The adult zebrafish were treated with 2µg/mL of tricaine for sedation and the brain, kidney, heart, intestine, liver, and gill were dissected. Total RNAs were prepared from isolated adult tissues of zebrafish using Trizol reagent (Invitrogen cat no 15596026) by homogenization and purified using RNeasy Mini Kit (Qiagen cat no 74104). cDNAs were synthesized from 1 µg of purified RNA using SuperScript® IV First-Strand Synthesis System for RT-PCR (Invitrogen cat no 18091050) and used as templates.

### 3.3.4 Quantitative polymerase chain reaction (qPCR) analysis

The primers for the qPCR were designed with the NCBI primer blast. The primer sequences and the ensemble ID for each gene were listed in Table 3.2. The PCR product size was designed to span 120 to 200 bp with low self 3'-complementarity score. Different primer designs were initially validated with gel electrophoresis to determine the optimal forward and reverse pair with specific amplification of the desired sized products. qPCR was performed using Applied Biosystems SYBR Green PCR Master Mix (Thermofisher cat no 4367659) and the ABI7900HT (Applied Biosystems machine cat no 4329001). Cycling conditions were 95 °C for 10 min, [95 °C for 15 s, 60 °C for 1 min 40 cycles], 20°C for 2 min. Each sample was run with triplicates along with the positive control (elf1a1) in the top row of the MicroAmp Optical 384-Well Reaction Plate (Applied Biosystems cat no 4309849). The Ct values were exported and ΔCt values were calculated to compare relative expression of the genes of interest to the *elf1a1* control.

### 3.3.5 Statistical Analysis

The mRNA expression from the qRT-PCR was processed by the $2^{-\Delta\Delta ct}$ method in comparison to the *elf1a1* housekeeping gene. The histograms in the study are represented as means ± SEM. The box and whisker plot are represented as medians with first and third quartile ranges. The gene-organ-drug interaction was examined with the R 'interactions' package and multiple regression model. The comparison between drug treatment and discontinuation was compared with an unpaired t-test. The confidence interval plot of the gene-drug-organ interaction was generated with R program at a 95% interval and represented as the estimated mean.

## 3.4 Results

### 3.4.1Quantitative analysis of RAAS pathway gene expression in six organs reveals tissue-specific enrichment of ace2 transcripts

Major genes of the RAAS pathway and available small molecules that inhibit RAAS signaling are schematized (Figure 3.1). The adult zebrafish organs including the brain, gill, heart, intestine, kidney, and liver were extracted from the AB wildtype fish (Figure 3.2). After tissue homogenization and isolation of RNA, qRT-PCR was performed for angiotensinogen (*agt*), angiotensin II receptor type 1a (*agtr1a)*, angiotensin II receptor type 1b (*agtr1b)*, angiotensin II receptor type 2 (*agtr2)*, angiotensin I converting enzyme (*ace1)*, and Angiotensin I converting enzyme 2 (*ace2)* (Figure 3.3). The elongation factor 1 alpha (*elf1a1*) was used as the control housekeeping gene to quantify the relative expression of RAAS genes. There was no significant difference in RAAS gene expression levels between gender for all the different organs

(Supplemental Figure 3.1). For *ace2*, the gill, heart, intestine showed higher expression levels of nearly 1.5-fold relative *to elf1a1*. The kidney, brain, and liver also showed *ace2* expression but at lower levels compared to elf1a1. The liver showed high expression of *agt* and the angiotensin receptors *agtr1a* and *agtr1b*. Trace amounts of *agtr2* expression was detected across all organs but showed lower levels relative to *elf1a1*. Together, while *ace2* expression is detected in all organs examined, it appears to be enriched in the gill (fish equivalent of the lung), heart, and intestine.

### 3.4.2 Treatment with RAAS inhibitors increases ace2 expression in a drug- and organ-specific manner

The transcript levels of the aforementioned RAAS pathway genes were examined after 7 days of RAAS inhibitor or vehicle (0.2% DMSO) treatment (group 1). Data were normalized to vehicle control for each gene-organ combination (Figure 3.4). In addition to RAAS inhibitors, we also used amlodipine (a non-RAAS antihypertensive) as a comparison. Olmesartan treatment significantly increased *ace2* expression in the gill, heart, intestine, and kidney ($p<0.001$ for gill, $p=0.012$ for heart, $p=0.043$ for intestine, $p<0.001$ for kidney). Captopril increased *ace2* expression in the gill, heart, and kidney ($p=0.0087$ for gill, $p=0.026$ for heart, $p<0.001$ for kidney). Conversely, aliskiren treatment significantly decreased *ace2* expression in the heart ($p=0.021$). In addition, captopril decreased *ace1* expression in the heart, intestine, and kidney ($p=0.012$ for heart, $p=0.037$ for intestine, $p=0.026$ for kidney). The confidence interval plot of the three-way interaction between drug treatment, gene, and organ identified a total of 11 significant combinations (Supplemental Figure 3.2). Thus, RAAS inhibitors increase *ace2*

expression in a drug- and organ-specific manner: the ARB Olmesartan and ACE-I captopril commonly increase *ace2* expression in the gill, heart, and kidney. Olmesartan also increases *ace2* expression in the intestine. However, the renin inhibitor aliskiren decreases ace2 expression in the heart.

### 3.4.3 The expression of ace2 shows no significant change upon discontinuation of RAAS inhibitors for seven days

For a second group of zebrafish (group 2), the fish were treated with 7 days of RAAS inhibitors, amlodipine, or vehicle control. The compounds were then discontinued for 7 days, followed by organ dissection and qRT-PCR analysis (Figure 3.2) to determine whether discontinuation would have an effect on gene expression levels. When comparing the *ace2* expression between treatment (group 1) and treatment plus discontinuation (group 2), we found no significant *ace2* expression differences in the brain, gill, intestine, kidney, and liver. The elevated *ace2* expression in the gill, kidney, and the heart following 7-day olmesartan and captopril treatment were not significantly altered after 7-day discontinuation of these compounds. In contrast, discontinuing captopril and amlodipine treatment for 7 days significantly elevated *ace2* expression in the heart compared to 7-day treatment with these compounds ($p=0.0013$ for captopril, $p=0.0419$ for amlodipine) (Figure 3.5). The decrease in *ace2* expression with 7-day aliskiren treatment in the heart did not change following 7-day discontinuation. Together, 7-day discontinuation of RAAS inhibitors does not significantly alter ace2 transcript levels.

## 3.5 Discussion

In this study, we have determined that different RAAS inhibitors have varying effects on the *ace2* mRNA expression across different organs. We have also shown that adult zebrafish express all the major components of RAAS pathway genes that have been used in this study. Many of these gene expression profiles across zebrafish organs closely resembled that of the human organs. For instance, the angiotensin receptor type 1 (*agtr1*) RNA in humans are predominantly expressed in the liver, kidney, adrenal glands, and adipose tissues[13]. For the zebrafish, the liver showed the highest expression for both *agtr1a* and *agtr1b* followed by kidney, heart, and intestine. The zebrafish kidney showed the highest *ace2* expression which is also the case of humans[13].

The gill, kidney, heart, and intestine showed significantly higher *ace2* expression when treated with an ACE-I and an ARB. It is known that ACE-Is such as captopril activate the ACE2/angiotensin-(1–7) /Mas receptor axis which could lead to the increase of *ace2* expression at the transcript level[7,14]. In a study conducted on Lewis rats it was shown that lisinopril, another commonly used ACE-I, caused an increase in plasma Ang-(1-7), and increased cardiac *ace2* mRNA but did not affect the ACE2 protein expression[15]. Interestingly, *ace2* expression was decreased in the heart with 7-day aliskiren treatment. As a direct renin inhibitor, the pharmacological action of aliskiren is known to affect the AngII/ Ang1-7 signal axis[16]. In a diabetic neuropathy model of Sprague Dawley rats, it was shown that chronic administration of aliskiren decreased ACE2 expression in the kidneys and this decreased expression was also observed in another hypertension rat model[16,17]. As many patients who experience COVID symptoms have pre-existing cardiovascular comorbidities, it is more often that these patients have been using RAAS inhibitors chronically. In our zebrafish model we have observed that the

7-day discontinuation did not significantly alter the *ace2* expression compared to the 7-day treatment groups. In this case, an abrupt discontinuation of RAAS inhibitors, particularly if already being used for other indications, would not be beneficial.

One side of the ongoing debate on use of RAAS inhibitors in the COVID-19 setting is toward continuing the medication based on the large cohort studies that find no association between the use of RAAS inhibitors and susceptibility to SARS-CoV-2 infection[18–20]. Studies are also trying to understand whether the increase in *ace2* can potentially be linked to protective benefits. Clinical trials have been conducted on initiating losartan, another commonly used ARB, for COVID-19 hospitalized patients (NCT04312009). The downregulation of ACE2 with COVID-19 could lead to an increase in ACE activity resulting in damage to the alveolus and lead to acute respiratory failure which could warrant the use of RAAS inhibitors[21]. A meta-analysis of evaluating patients with COVID-19 showed a significantly lower risk of severe adverse events among patients who received ACE-Is or ARBs with implications on the protective benefits[19]. In another study it has been shown that the RAAS imbalance through angiotensin II or ACE2 blockage shows clinical manifestations closely resembling COVID-19[22].

Although we have chosen three compounds with mechanism of actions that target different parts of the RAAS pathway, the *ace2* expression could also be different based on the chemical structure, pharmacokinetics, and receptor affinities. Olmesartan medoxomil is a prodrug that requires hydrolysis to the active form while valsartan, another commonly used ARB is an active drug. Losartan, another ARB, has nearly 10-fold greater selectivity compared to olmesartan[23]. Whether these differences in molecular effects have implications in the clinical setting is not clear. As we have tried to mimic the study to be a chronic treatment model, the treatment and

discontinuation duration was chosen as 7 days based on other studies that involved continued drug treatment for pharmacological studies in zebrafish[24,25]. While this is certainly not a direct comparison to the long duration that many hypertension patients have been taking chronically for years, based on the pharmacokinetic properties of the RAAS inhibitors used in the study, the direct uptake of the drugs in the water bath should reach steady state at the target tissues during the treatment duration.

In conclusion, our study uncovers that RAAS inhibitors can influence the RAAS pathway gene expression in an organ-specific manner in zebrafish. The organs that were most sensitive to changes in *ace2* expression include the gill, heart, intestine, and kidney, which are all known target sites of COVID-19 leading to clinical manifestations. Furthermore, the expression levels after 7 days of discontinuation did not show remarkable changes in gene expression. Although more studies need to be done to understand how these gene expression profiles translate at the protein level, our study provides new insights into the transcript level modulation of RAAS pathway genes with RAAS inhibitor treatment. This basic knowledge lays foundation for deciding the use of RAAS inhibitors in the context of COVID-19.

## 3.6 Figures

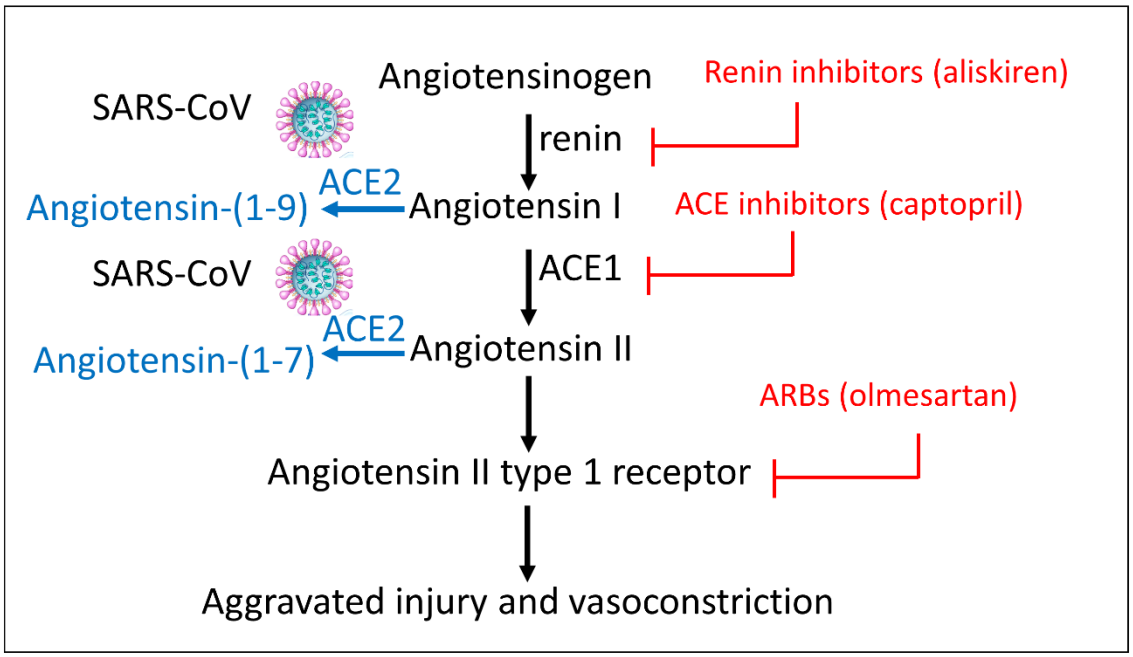


**Figure 3.1 The RAAS pathway and its relationship to SARS-CoV(1 and 2) viruses.** Upon entry to cells, the SARS-CoV is known to bind to its functional receptor, angiotensin converting enzyme 2 (ACE2). In normal physiology, renin cleaves angiotensinogen, produced by the liver which yields angiotensin I. The angiotensin converting enzyme (ACE) converts angiotensin I to angiotensin II and the angiotensin II binds to the angiotensin II type 1 receptor which leads to vasoconstriction and other injury and hormonal production. ACE2 cleaves angiotensin II into angiotensin (1-7) to attenuate the effects of vasoconstriction. Another function of ACE2 involves cleaving angiotensin I to angiotensin-(1–9) for the hydrolysis of peptides such as apelin-1. Aliskiren is a direct renin inhibitor that blocks the conversion of angiotensinogen to angiotensin I. Captopril is an ACE-I that blocks the conversion of angiotensin I to angiotensin II. Olmesartan is an ARB ACE-I: Angiotensin Converting Enzyme Inhibitor, ARB: Angiotensin Receptor Blocker, ACE1: Angiotensin Converting Enzyme-1, ACE2: Angiotensin Converting Enzyme-2

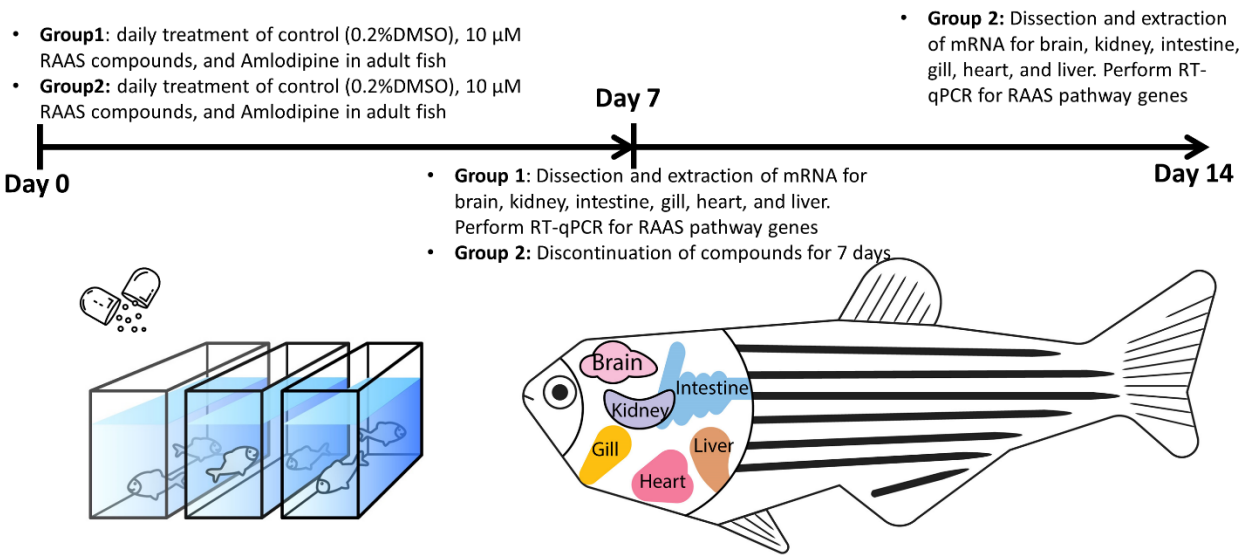


**Figure 3.2 A schematic diagram for the experimental design.** Group 1 included zebrafish that were treated with 0.2% DMSO (control), aliskiren, olmesartan, captopril, and amlodipine daily for 7 days and dissected for qRT-PCR analysis. Group 2 included zebrafish that were treated with the compounds (or vehicle control) daily for 7 days, discontinued for 7 days, and then dissected for the qRT-PCR analysis. The extracted organs include the brain, kidney, intestine, gill, liver, and heart. Six biological replicates (3 males and 3 females) were used for each compound (or vehicle) in each group.

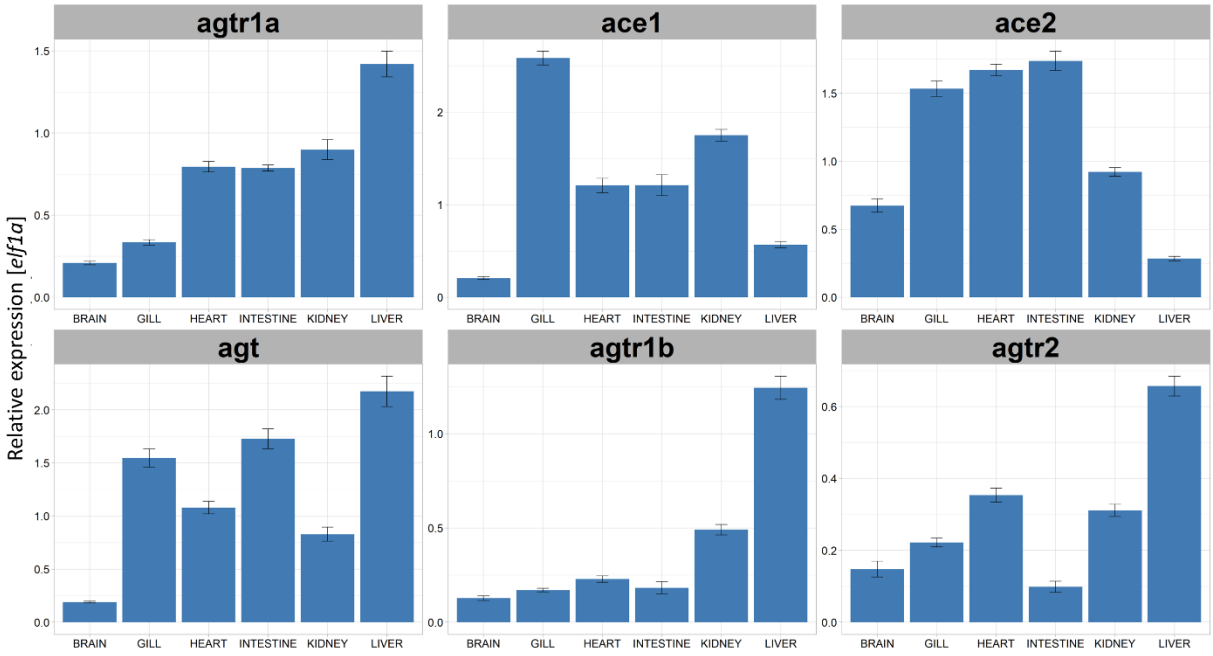


**Figure 3.3 RAAS pathway gene expression displays tissue-specific enrichment.** The relative expression levels of *agtr1a*, *ace1*, *ace2*, *agt*, *agtr1b*, and *agtr2* to *elf1a1* for different organs in wild type adult zebrafish (n=6). *agt*: Angiotensinogen, *agtr1b*: Type-1B angiotensin II receptor, *agtr2*: Type-2 Angiotensin II Receptor, *agtr1a*: Type-1A angiotensin II receptor, *ace1*: Angiotensin-converting enzyme 1, *ace2*: Angiotensin-converting enzyme 2.

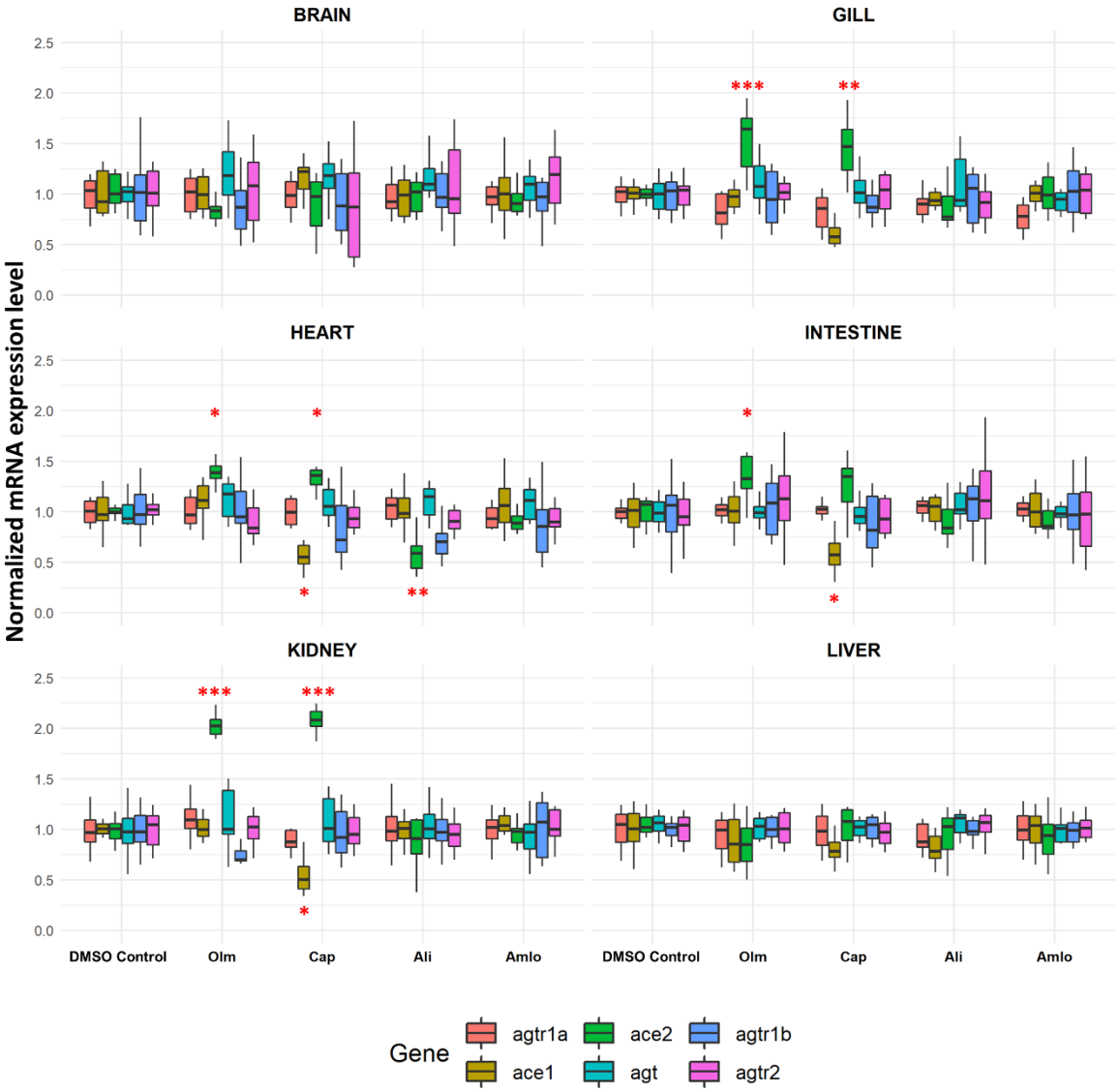


**Figure 3.4 Tissue-specific up-regulation of ace2 expression by RAAS inhibitors.** The *ace2* expression was significantly increased in captopril and olmesartan treated groups compared to the DMSO control in the gill, heart, and kidney (n=6 per gene-organ-drug combination, *P<0.05, **P<0.01, ***P<0.001 unpaired t test). Olmesartan also increased *ace2* expression in the intestine (n=6, P<0.05, unpaired t test). Aliskiren treatment significantly decreased the *ace2* expression in the heart; captopril treatment decreased *ace1* expression in the heart, intestine, and the kidney (n=6, P<0.05, unpaired t test).

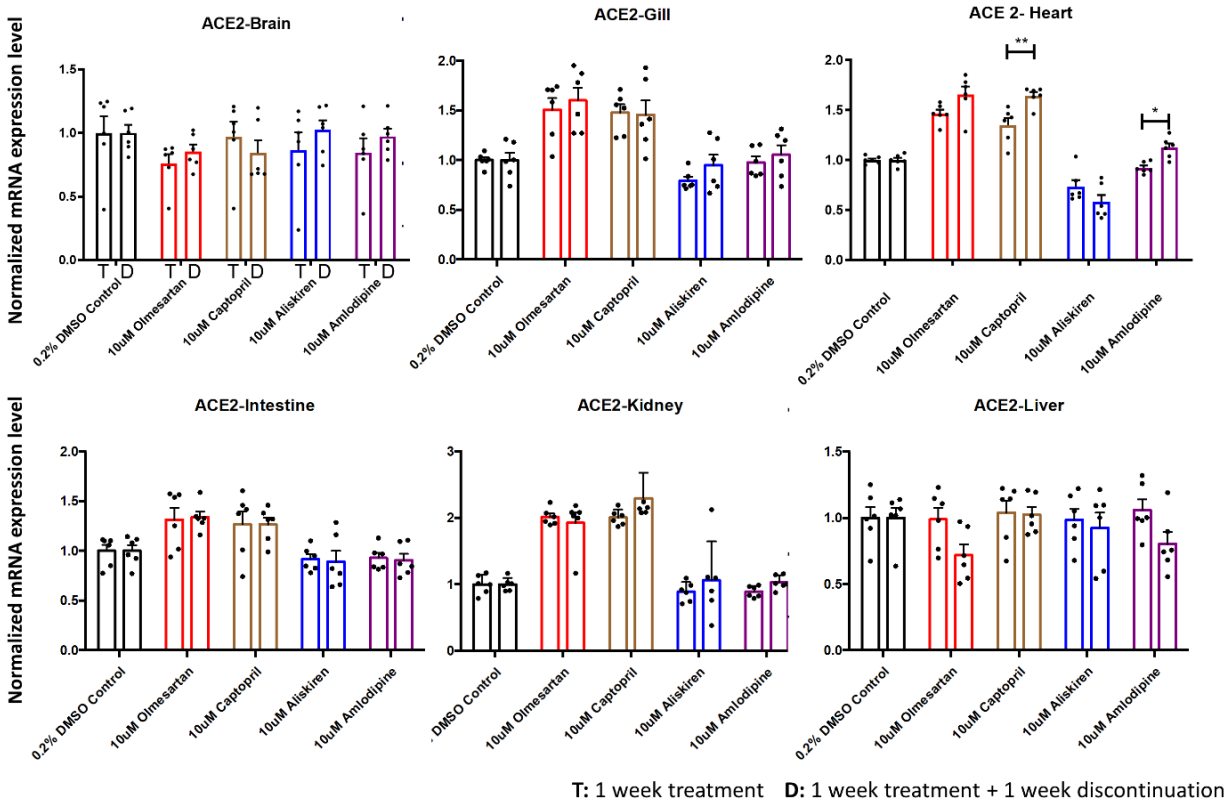


**Figure 3.5 Comparison of ace2 expression levels between treatment and discontinuation.** The expression levels were compaired between the 1-week treatment group and 1-week treatment plus 1week discontinuation group for different organs. The captopril and amlodipine treatment increased *ace2* mRNA expression in the heart 7 days after discontinuation compared to 7-day treatment (n=6 per group; *P<0.05, **P<0.01, unpaired t test). Other organs showed no significant difference between treatment and discontinuation. T: 1 week treatment D: 1 week treatment + 1 week discontinuatoin

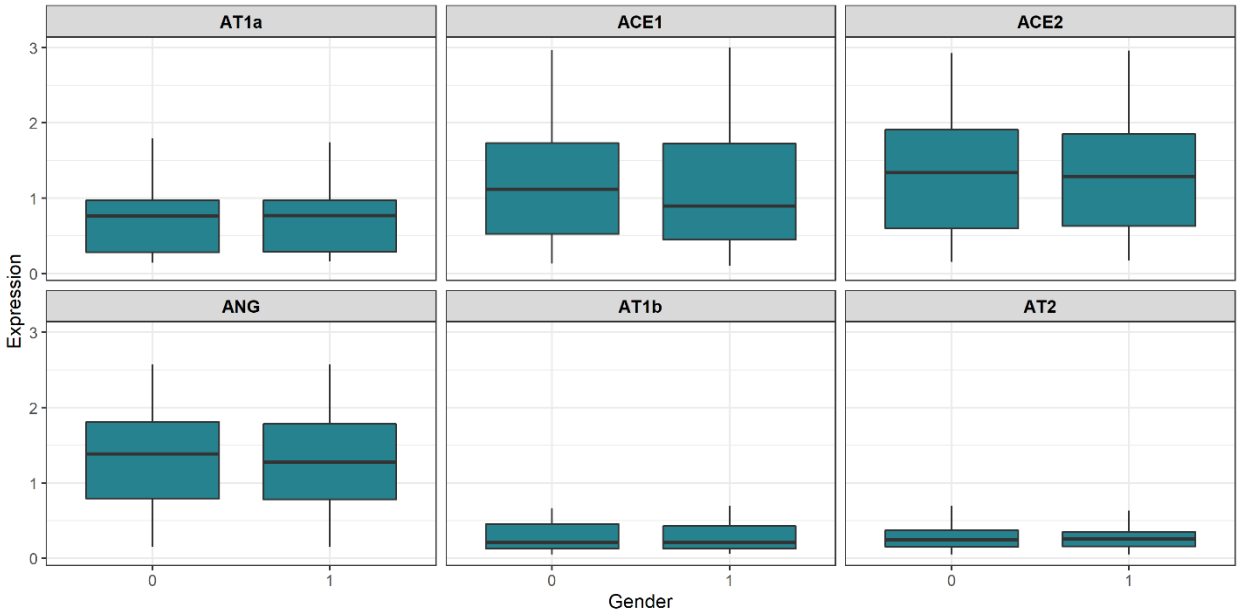


**Supplemental Figure 3.1 Wildtype zebrafish shows no differences in gender for mRNA expression.** The expression levels of *agtr1a*, *ace1*, *ace2*, *agt*, *agtr1b*, *agtr2* for the wildtype showed no significant difference between the genders. 0: male 1: female (n=6 per gene-gender combination; unpaired t test)

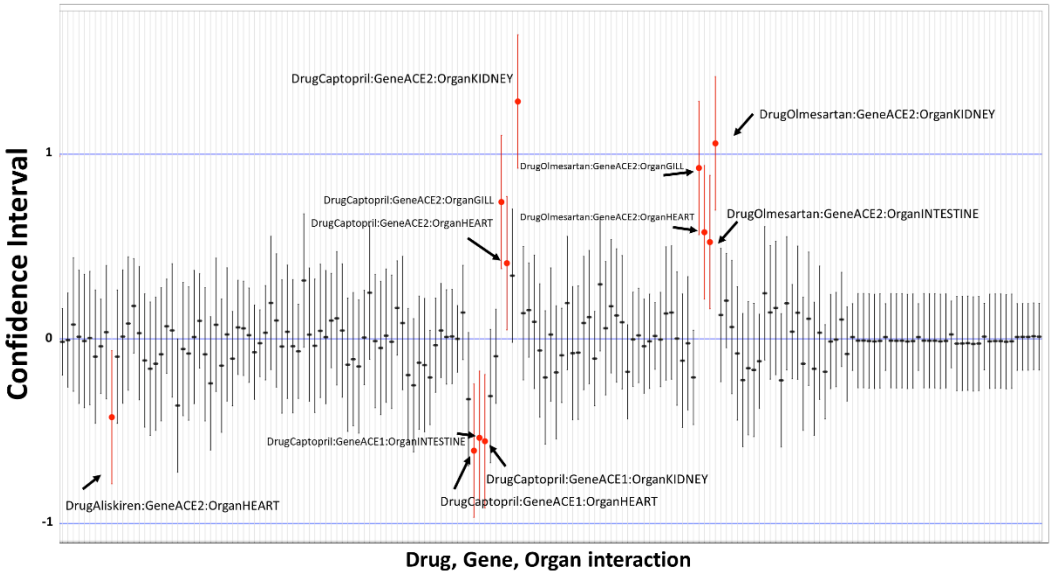


**Supplemental Figure 3.2 Confidence interval plot of gene organ drug interaction.** A total of 11 drug-gene-organ combinations showed significant difference at the 95% CI.

## 3.7 Tables

### Table 4.1 Description of the anti-hypertensive drugs evaluated in this study

| Drug | Pharmaceutical Class | Mechanism of Action | IC50 | MW (g/mol) | Therapeutic Indication |
|---|---|---|---|---|---|
| **Aliskiren** | Direct Renin Inhibitor | Renin inhibitor blocking the conversion of angiotensinogen to angiotensin I | 1.5 nM | 609.79 | Hypertension |
| **Captopril** | Angiotensin Converting Enzyme Inhibitor | Blocks the conversion of angiotensin I to angiotensin II | 6 nM | 217.29 | Hypertension, Congestive Heart Failure, Diabetic Nepropathy |
| **Olmesartan Medoxomil** | Angiotensin II Receptor Antagonist | Selective binding to angiotensin I receptor for competitive blocking of angiotensin II | 66.2 μM | 558.59 | Hypertension, Heart Failure |
| **Amlodipine besylate** | Calcium Channel Blocker | Block the voltage-dependent L-type calcium channels to inhibit the influx of calcium | 1.9 nM | 567.05 | Angina, Coronary artery disease, Hypertension |

**Table 4.2. Summary of RAAS pathway genes, RT-qPCR primer sequence, and Ensembl ID used for the RT-qPCR analysis.**

| Gene Name | Gene symbol | Function | Primer Sequences (5'->3') | Transcript ID | Product length |
|---|---|---|---|---|---|
| Angiotensin II receptor, type 1a | *agtr1a* | G protein-coupled receptor for angiotensin II | F: CATCCGTGGGACCCATTTCA<br>R: GCAGTAGCACGTGAGGATGA | ENSDART00000021528.7 | 154 |
| Angiotensin II receptor, type 1b | *agtr1b* | G protein-coupled receptor for angiotensin II | F: TTCATGCCGTTTGGCTCAGA<br>R: GGTCCTCGCTCATTGCTGAT | ENSDART00000066834.5 | 200 |
| Angiotensin I converting enzyme | *ace1* | Metallopeptidase involved in the conversion of angiotensin I to angiotensin II | F: GAGCCAATCCTGGCTTCCAT<br>R: CCGATGACGCTGAGAGTGAC | ENSDART00000114637.4 | 133 |
| Angiotensin I converting enzyme 2 | *ace2* | Transmembrane protein catalyzing angiotensin II hydrolysis. Main entry point for coronavirus. | F: CTGATGCCTGTCTTCCAGCA<br>R: TTTCATCCCAACCCTGCTCC | ENSDART00000003712.8 | 141 |
| Angiotensinogen | *agt* | Precursor molecule for angiotensin I and the substrate for renin produced in the liver. | F: GGCTTCGACACCTCAAGGAA<br>R:ACACCACCTTGTTGAGTACCTTA | ENSDART00000010918.5 | 192 |
| Angiotensin II receptor, type 2 | *at2* | G protein-coupled receptor. Regulation of aldosterone secretion | F: GTTCACGAACATCAGAACTCCC<br>R: TGAGGCTGTAAAAGGCAGGG | ENSDART00000051532.5 | 188 |
| Elongation factor 1 alpha 1 | *elf1a1* | Housekeeping gene for RT-qCPR | F: CTTCTCAGGCTGACTGTGC<br>R: CCGCTAGCATTACCCTCC | adopted from McCurley et al[25] | - |

## 3.8 References


1. Long, B., Brady, W. J., Koyfman, A. & Gottlieb, M. Cardiovascular complications in COVID-19. *Am. J. Emerg. Med.* **38**, 1504–1507 (2020).

2. Du, Y., Zhou, N., Zha, W. & Lv, Y. Hypertension is a clinically important risk factor for critical illness and mortality in COVID-19: A meta-analysis. *Nutr. Metab. Cardiovasc. Dis.* **31**, 745–755 (2021).

3. Zamorano Cuervo, N. & Grandvaux, N. ACE2: Evidence of role as entry receptor for SARS-CoV-2 and implications in comorbidities. *Elife* **9**, e61390 (2020).

4. Zhou, F. *et al.* Clinical course and risk factors for mortality of adult inpatients with COVID-19 in Wuhan, China: a retrospective cohort study. *Lancet (London, England)* **395**, 1054–1062 (2020).

5. Patel, V. B., Zhong, J.-C., Grant, M. B. & Oudit, G. Y. Role of the ACE2/Angiotensin 1-7 Axis of the Renin-Angiotensin System in Heart Failure. *Circ. Res.* **118**, 1313–1326 (2016).

6. Rice, G. I., Thomas, D. A., Grant, P. J., Turner, A. J. & Hooper, N. M. Evaluation of angiotensin-converting enzyme (ACE), its homologue ACE2 and neprilysin in angiotensin peptide metabolism. *Biochem. J.* **383**, 45–51 (2004).

7. Wysocki, J., Lores, E., Ye, M., Soler, M. J. & Batlle, D. Kidney and Lung ACE2 Expression after an ACE Inhibitor or an Ang II Receptor Blocker: Implications for COVID-19. *J. Am. Soc. Nephrol.* **31**, 1941–1943 (2020).

8. Singh, A. K., Gupta, R. & Misra, A. Comorbidities in COVID-19: Outcomes in

hypertensive cohort and controversies with renin angiotensin system blockers. *Diabetes Metab. Syndr.* **14**, 283–287 (2020).

9. Morales, D. R. *et al.* Renin–angiotensin system blockers and susceptibility to COVID-19: an international, open science, cohort analysis. *Lancet Digit. Heal.* **3**, e98–e114 (2021).

10. Lopes, R. D. *et al.* Effect of Discontinuing vs Continuing Angiotensin-Converting Enzyme Inhibitors and Angiotensin II Receptor Blockers on Days Alive and out of the Hospital in Patients Admitted with COVID-19: A Randomized Clinical Trial. *JAMA - J. Am. Med. Assoc.* **325**, 254–264 (2021).

11. Howe, K. *et al.* The zebrafish reference genome sequence and its relationship to the human genome. *Nature* **496**, 498–503 (2013).

12. Hunt, S. E. *et al.* Ensembl variation resources. *Database* **2018**, (2018).

13. Consortium, Gte. The Genotype-Tissue Expression (GTEx) project. *Nat. Genet.* **45**, 580–585 (2013).

14. Simões e Silva, A. C., Silveira, K. D., Ferreira, A. J. & Teixeira, M. M. ACE2, angiotensin-(1-7) and Mas receptor axis in inflammation and fibrosis. *Br. J. Pharmacol.* **169**, 477–492 (2013).

15. Ferrario, C. M. *et al.* Effect of angiotensin-converting enzyme inhibition and angiotensin II receptor blockers on cardiac angiotensin-converting enzyme 2. *Circulation* **111**, 2605–2610 (2005).

16. Ding, W. *et al.* [Aliskiren inhibits angiotensin II/angiotensin 1-7(Ang II/Ang1-7) signal

pathway in rats with diabetic nephropathy]. *Xi bao yu fen zi mian yi xue za zhi = Chinese J. Cell. Mol. Immunol.* **34**, 891–895 (2018).

17. Hsu, C.-N. *et al.* Aliskiren Administration during Early Postnatal Life Sex-Specifically Alleviates Hypertension Programmed by Maternal High Fructose Consumption. *Front. Physiol.* **7**, 299 (2016).

18. Mehta, N. *et al.* Association of Use of Angiotensin-Converting Enzyme Inhibitors and Angiotensin II Receptor Blockers With Testing Positive for Coronavirus Disease 2019 (COVID-19). *JAMA Cardiol.* **5**, 1020–1026 (2020).

19. Baral, R. *et al.* Association Between Renin-Angiotensin-Aldosterone System Inhibitors and Clinical Outcomes in Patients With COVID-19: A Systematic Review and Meta-analysis. *JAMA Netw. Open* **4**, e213594–e213594 (2021).

20. Mancia, G., Rea, F., Ludergnani, M., Apolone, G. & Corrao, G. Renin–Angiotensin–Aldosterone System Blockers and the Risk of Covid-19. *N. Engl. J. Med.* **382**, 2431–2440 (2020).

21. Chaudhry, F. *et al.* Manipulation of ACE2 expression in COVID-19. *Open Hear.* **7**, (2020).

22. Rysz, S. *et al.* COVID-19 pathophysiology may be driven by an imbalance in the renin-angiotensin-aldosterone system. *Nat. Commun.* **12**, 2417 (2021).

23. Miura, S., Karnik, S. S. & Saku, K. Review: angiotensin II type 1 receptor blockers: class effects versus molecular effects. *J. Renin. Angiotensin. Aldosterone. Syst.* **12**, 1–7 (2011).

24. Petrunich-Rutherford, M. L. Chronic fluoxetine treatment of juvenile zebrafish (Danio

rerio) does not elicit changes in basal cortisol levels and anxiety-like behavior in adulthood. *PeerJ* **7**, e6407–e6407 (2019).

25. Dang, M., Henderson, R. E., Garraway, L. A. & Zon, L. I. Long-term drug administration in the adult zebrafish using oral gavage for cancer preclinical studies. *Dis. Model. Mech.* **9**, 811–820 (2016).

**Publishing Agreement**

It is the policy of the University to encourage open access and broad distribution of all theses, dissertations, and manuscripts. The Graduate Division will facilitate the distribution of UCSF theses, dissertations, and manuscripts to the UCSF Library for open access and distribution. UCSF will make such theses, dissertations, and manuscripts accessible to the public and will take reasonable steps to preserve these works in perpetuity.

I hereby grant the non-exclusive, perpetual right to The Regents of the University of California to reproduce, publicly display, distribute, preserve, and publish copies of my thesis, dissertation, or manuscript in any form or media, now existing or later derived, including access online for teaching, research, and public service purposes.

DocuSigned by:
Jeffrey Kim
DC85A819BE7F4DA...
Author Signature

5/17/2021
Date